University of Windsor
Scholarship at UWindsor

Electronic Theses and Dissertations | Theses, Dissertations, and Major Papers

2019

Corrosion Behavior of AM60 Magnesium Alloy Based Composites with and without Plasma Electrolytic Oxidation Coating

Xinyu Geng
University of Windsor

Follow this and additional works at: https://scholar.uwindsor.ca/etd

Part of the Materials Science and Engineering Commons

Recommended Citation

Geng, Xinyu, "Corrosion Behavior of AM60 Magnesium Alloy Based Composites with and without Plasma Electrolytic Oxidation Coating" (2019). *Electronic Theses and Dissertations*. 7676.
https://scholar.uwindsor.ca/etd/7676

This online database contains the full-text of PhD dissertations and Masters' theses of University of Windsor students from 1954 forward. These documents are made available for personal study and research purposes only, in accordance with the Canadian Copyright Act and the Creative Commons license—CC BY-NC-ND (Attribution, Non-Commercial, No Derivative Works). Under this license, works must always be attributed to the copyright holder (original author), cannot be used for any commercial purposes, and may not be altered. Any other use would require the permission of the copyright holder. Students may inquire about withdrawing their dissertation and/or thesis from this database. For additional inquiries, please contact the repository administrator via email (scholarship@uwindsor.ca) or by telephone at 519-253-3000ext. 3208.

Corrosion Behavior of AM60 Magnesium Alloy Based Composites with and without Plasma Electrolytic Oxidation Coating

By

Xinyu Geng

A Thesis

Submitted to the Faculty of Graduate Studies
through the Department of Mechanical, Automotive and Materials Engineering
in Partial Fulfillment of the Requirements for
the Degree of Master of Applied Science
at the University of Windsor

Windsor, Ontario, Canada

2019

© 2019 Xinyu Geng

Corrosion Behavior of AM60 Magnesium Alloy Based Composites with and without Plasma Electrolytic Oxidation coating

by

Xinyu Geng

APPROVED BY:

_____

N. Zamani
Department of Mechanical, Automotive and Materials Engineering

_____

X. Nie
Department of Mechanical, Automotive and Materials Engineering

_____

H. Hu, Advisor
Department of Mechanical, Automotive and Materials Engineering

April 2, 2019

DECLARATION OF CO-AUTHORSHIP / PREVIOUS PUBLICATION

I. Co-Authorship

I hereby declare that this thesis incorporates material that is result of joint research, as follows:

In all cases, the key ideas, primary contributions, experimental designs, data analysis and interpretation, were performed by the author, Dr. H. Hu as advisor and Dr. X. Nie as co-advisor. Chapter 3 and 4 were co-authored with Zixi Sun and Luyang Ren. Zixi Sun and Luyang Ren contributed in bulk samples preparations. I certify that, with the above qualification, this dissertation, and the research to which it refers, is the product of my own work.

I am aware of the University of Windsor Senate Policy on Authorship and I certify that I have properly acknowledged the contribution of other researchers to my thesis and have obtained written permission from each of the co-author(s) to include the above material(s) in my thesis.

I certify that, with the above qualification, this thesis, and the research to which it refers, is the product of my own work.

II. Previous Publication

This thesis includes 2 original papers that have been previously published/submitted for publication in peer reviewed journals, as follows:

Thesis Chapter	Publication title/full citation	Publication status*
Chapter [3]	*Xinyu Geng, Luyang Ren, Zixi Sun, Henry Hu and Xueyuan Nie, Corrosion and Microstructure of As-Cast Magnesium Alloy AM60-based Hybrid Nanocomposite, Advances in Materials and Processing Technologies, August, 2018*	*Journal of Advanced Materials and Processing Technology* *Under Review*
Chapter [4]	*Xinyu Geng, Luyang Ren, Zixi Sun, Henry Hu and Xueyuan Nie, Enhanced corrosion resistance of as-cast magnesium alloy AM60-based hybrid nanocomposite by plasma electrolytic oxidation (PEO) coating*	*22nd International Conference on Advances in Materials and Processing Technology (AMPT 2019), Taiwan.* *Submitted*

I certify that I have obtained a written permission from the copyright owner(s) to include the above published material(s) in my thesis. I certify that the above material describes work completed during my registration as a graduate student at the University of Windsor.

III. General

I declare that, to the best of my knowledge, my thesis does not infringe upon anyone's copyright nor violate any proprietary rights and that any ideas, techniques, quotations, or any other material from the work of other people included in my thesis, published or otherwise, are fully acknowledged in accordance with the standard referencing practices. Furthermore, to the extent that I have included copyrighted material that surpasses the bounds of fair dealing within the meaning of

the Canada Copyright Act, I certify that I have obtained a written permission from the copyright owner(s) to include such material(s) in my thesis.

I declare that this is a true copy of my thesis, including any final revisions, as approved by my thesis committee and the Graduate Studies office, and that this thesis has not been submitted for a higher degree to any other University or Institution.

ABSTRACT

7 vol.% Fibre/ AM60, and (7 vol.% Fibre + 3 vol.% nano-Particle)/AM60 composites, named 7FC and MHNC-7F3NP, respectively, and the unreinforced matrix alloy AM60 were prepared by using the preform-squeeze casting technique. The corrosion behaviors of the 7FC and MHNC-7F3NP composites and the matrix alloy were investigated by using the potential-dynamic polarization test in 3.5 wt.% NaCl aqueous solution. Compared with the matrix alloy, the introduction of micron-sized alumina fibres decreased the corrosion resistance of the matrix alloy AM60, however the addition of the nano-sized particles led to almost no further reduction in the corrosion resistance of the MHNC-7F3NP. To enhance the corrosion resistance of as-cast magnesium alloy AM60-based composite, the plasma electrolytic oxidation (PEO) coatings with $NaAlO_2$ and KOH electrolytes were applied on the surfaces of as-cast AM60 (PEO-AM60), 7 vol.% Al_2O_3 fibres/AM60 (PEO-7FC) and 7 vol.% Al_2O_3 fibres +3 vol.% Al_2O_3 nano-sized particles/AM60 (PEO-MHNC-7F3NP). By comparing the corrosion test results of the coated AM60 and the composites with those of the uncoated counterparts, it was found that the PEO coating significantly improved the corrosion resistances by up to 154 times. The corrosion rates of the coated composites were higher than the coated AM60, although the PEO coating reduced the corrosion rates of the composites by two orders of magnitudes. The addition of nano-sized particles barely increased the corrosion rate of the composite. The microstructure of each uncoated and coated material was observed and analysed by scanning electron microscopy (SEM) and X-ray energy dispersive spectroscopy (EDS).

DEDICATION

To My Parents,

Zhanying Geng and Qingli Zhang

To My Love

Xinhui Zhang

For their endless love and devotion

ACKNOWLEDGEMENTS

I would like to express to Dr. Henry Hu, for providing me with the opportunity to work on this project in the engineering materials graduate program of the University of Windsor, and for his kindly suggestion, encouragement and excellent supervision of this research work.

Great thanks to Dr. Nader Zamani and Dr. Xueyuan Nie for the time given for my research thesis and presentations as my committee members and providing valuable suggestions for this project.

I am very grateful to Mr. Andy Jenner, Mr. Steve Budinsky, Ms. Sharon Lackie, and other technicians for the technical support, Dr. Xuezhi Zhang, Dr. Li Fang, and all other group members for their technical assistance in the experimental analysis, tests, informative and valuable discussion in this research.

Most of all I would like to express my deepest gratitude to my family: my parents and my girlfriend for their love, understanding, encouragement and support.

TABLE OF CONTENTS

DECLARATION OF CO-AUTHORSHIP / PREVIOUS PUBLICATION iii

ABSTRACT vi

DEDICATION vii

ACKNOWLEDGEMENTS viii

LIST OF TABLES xii

LIST OF FIGURES xiv

CHAPTER 1 Introduction 1

1.1. Background 1

1.2. Objectives of this study 2

1.3. Organization of the thesis 3

CHAPTER 2 Literature review 4

2.1. Introduction 4

2.2. Magnesium-based MMCs Fabrication Process 5

2.3. Corrosion Mechanism 6

2.4. Analysis of the Experimental Investigations 9

2.4.1 Electrochemical experimentation of fibre reinforced magnesium alloys 9

2.4.1.1 Potential dynamic polarization test of alumina fibre reinforced magnesium alloys 9

2.4.1.2 Potential dynamic polarization test of carbon fibre reinforced magnesium alloys 15

2.4.2 Electrochemical experimentation of micro-sized particle reinforced magnesium alloys 18

2.4.3 Electrochemical experimentation of Nano-sized particle Reinforced Magnesium Alloys 25

2.4.4 Electrochemical experimentation of Magnesium based hybrid composites 30

2.4.5 Electrochemical experimentation of Magnesium based metal matrix composites with PEO coating 35

2.5. Micro Galvanic Corrosion of Magnesium-based Metal Matrix Composites 40

2.6. Summary and conclusions 43

2.7. References 44

CHAPTER 3 Corrosion and Microstructure of As-Cast Magnesium Alloy AM60-based Hybrid Nanocomposite 46

3.1. Introduction 46

3.2. Experimental Procedure 49

3.2.1. Composites Preparation 49

3.2.2. Electrochemical Experimentation 50

3.2.3. Microstructure Analysis 51

3.3. Results and Discussion 51

3.3.1. Microstructure Analysis 51

3.3.2. Electrochemical Tests 60

3.3.3. Corroded Surfaces and Corrosion Mechanisms 64

3.4. Conclusions 71

3.5. Acknowledgements 73

3.6. Disclosure statement 73

3.7. Funding 73

3.8. References 73

CHAPTER 4 Enhanced corrosion resistance of as-cast magnesium alloy AM60-based hybrid nanocomposite by plasma electrolytic oxidation (PEO) coating 76

4.1. Introduction 76

4.2. Experimental procedure 78

4.2.1. Composites Preparation 78

4.2.2. Plasma electrolytic oxidation (PEO) process 79

4.2.3. Electrochemical experimentation 80

4.2.4. Microstructure analysis 81

4.3. Results and discussion 82

4.3.1. Surface morphology of PEO coating 82

4.3.2. Electrochemical tests 92

4.3.3. Surface appearance of corrosion 97

4.4. Conclusions 100

4.5. References 102

CHAPTER 5 Conclusions 106

CHAPTER 6 Future works 110

APPENDICES 111

Appendix A 111

Appendix B 115

VITA AUCTORIS 128

LIST OF TABLES

Table 2.1. Typical chemical composition (wt. %) of both magnesium matrix alloy (AS41) and alumina (Saffil) fibres [2] 10
Table 2.2. Electrochemical parameters obtained from polarization curves for Al_2O_3/AS41 Mg composite and the matrix alloy in pH 12 sodium hydroxide solution [2] 11
Table 2.3. Electrochemical parameters obtained from polarization curves for Al_2O_3/AS41 Mg composite and its pure matrix alloy in neutral NaCl solutions [2]. 14
Table 2.4. Corrosion rate determination by Tafel extrapolation and linear polarization (LP) experiments [6]. 20
Table 2.5. Corrosion potential, polarization resistance and corrosion rate of tested materials after immersion in 3.5 wt.% NaCl for 1 h [3]. 21
Table 2.6. Corrosion potentials and currents of synthesized materials in 3.5 wt % NaCl solutions [4]. 27
Table 2.7. Results from polarization plots using Tafel extrapolation method for case of AZ31B and AZ31B-1.5 Al_2O_3 in NaCl solution [8]. 30
Table 2.8. Abbreviated nomenclatures used for the composites [10] 31

Table 3.1 Measured grain sizes of the unreinforced matrix alloy, and the 7FC and MHNC-7F3NP composites 53
Table 3.2. Elements in analyzed phases shown in Figure 3.2..... 55
Table 3.3. Elements in analyzed phases shown in Figure 3.4..... 57
Table 3.4. Elements in analyzed phases shown in Figure 3.5..... 60
Table 3.5. Electrochemical parameters of the unreinforced alloy AM60, and the 7FC and MHNC-7F3NP composites..... 63

Table 4.1. PEO process parameters of the unreinforced alloy AM60, and the 7FC and MHNC-7F3NP composites..... 80
Table 4.2. Elements in analyzed phases of the substrate and PEO coating shown in Figure 4.4 88

Table 4.3. Elements in analyzed phases respectively in the substrate and PEO coating shown in Figure 5 90
Table 4.4. Elements in analyzed phases respectively in the substrate and PEO coating shown in Figure 4.6 91
Table 4.5. Electrochemical parameters of the PEO coated and uncoated AM60 alloy, and the 7FC and MHNC-7F3NP composites 94

LIST OF FIGURES

Fig. 2.1. Schematic illustration of the squeeze casting process [2]. 5
Fig. 2.2. Schematic representative model showing the corrosion mechanism of Al_2O_3/Mg MMC [2]..... 8
Fig. 2.3. Potential dynamic polarization diagrams for alloy and composite specimens in pH 12 sodium hydroxide solution: (a) with 100 ppm NaCl, (b) chloride-free [2]..... 10
Fig. 2.4. SEM micrograph of corroded surface after 3 h polarization at 1050 mV in pH 12 sodium hydroxide solution containing 100 ppm NaCl, showing the pitting sites represented by arrows [2]. 12
Fig. 2.5. SEM micrograph of composite surface polarized for 3 h at 1050 mV in chloride-free pH 12 sodium hydroxide solution [2]. 12
Fig. 2.6. Potential dynamic polarization diagrams for alloy and composite specimens in neutral 0.03, 0.3, 1.0 and 3.0wt% NaCl solutions [2]..... 13
Fig. 2.7. Potential dynamic polarisation diagrams for monolithic AS41 and AS41 (0.5%Ca) Mg alloys in 100ppm NaCl solution; pH 12 [5]. 16
Fig. 2.8. Potential dynamic polarisation diagrams for both C/AS41 and C/AS41(0.5% Ca) Mg MMCs in 100ppm NaCl solution; pH 12 [5].... 16
Fig. 2.9. Potentiodynamic polarisation diagrams of the matrix alloy and composite specimens in neutral 0.03, 0.3 and 1.0 wt.% NaCl solutions [5]. 17
Fig. 2.10. Typical SEM micrographs of (a) Mg and (b) Mg-6SiC surfaces obtained after immersion in 1M NaCl for 5 min [6]..... 19
Fig. 2.11. Typical SEM micrograph of (a) Mg, (b) Mg–6SiC and (c) Mg–16SiC surfaces obtained after immersion in 1M NaCl for 1 h [6]. 20
Fig. 2.12. Tafel plots for the magnesium, Mg-6SiC and Mg-16SiC in 1M NaCl [6]. 20
Fig. 2.13. Linear polarization plots for magnesium, Mg-6SiC and Mg-16SiC in 1M NaCl [6]. 21
Fig. 2.14. Polarization curves of tested materials after immersion in 3.5 wt.% NaCl for 1 h at room temperature [3]. 22

Fig. 2.15. Thickness of the corrosion layer for the tested materials exposed to salt fog (21 days) and high humidity (28 days) environments [3]..... 22
Fig. 2.16 SEM cross-section micrograph and X-ray elemental maps of Mg and O of AZ92/SiC/5p composite after exposure to salt fog atmosphere for 21 days [3]..... 23
Fig. 2.17 SEM cross-section micrograph and X-ray elemental maps of Mg and O of AZ92/SiC/5p composite after 28 days of exposure to high humidity environment (98% RH at 50°C) [3]..... 24
Fig. 2.18. Potential verses current density curves of as-extruded (a) AZ31 alloy and its composites; (b) AZ61 alloy and its composite samples [4]. 26
Fig. 2.19. SEM micrographs of extruded AZ31 alloy and its composites before and after corrosion tests: (a) AZ31 alloy, (b) AZ31-1.5GNP, and (c) AZ31-3.0GNP composites [4]..... 27
Fig. 2.20. SEM micrographs of extruded AZ61 alloy and its composites before and after corrosion tests: (a) AZ61 alloy, and (b) AZ61-3.0GNP composite [4]..... 28
Fig. 2.21. Typical Tafel plots for monolithic AZ31B and AZ31B-1.5% Al_2O_3 in 3.5 wt% NaCl [8]. 29
Fig. 2.22. Potential dynamic polarization curves corresponding to the AE42 alloy and its composites [10]. 31
Fig. 2.23. Comparison of the corrosion rate of the AE42 alloy and its composites [10]..... 32
Fig. 2.24. SEM micrographs of the surfaces before removal of the corrosion products corresponding to the (a) AE42 alloy; (b) 20% Saffil composite and (c) 1010 HC [10]..... 33
Fig. 2.25. SEM micrographs of the surfaces after removal of the corrosion products corresponding to the (a) AE42 alloy; (b) 20% Saffil composite and (c) 1010 HC (representative picture for the hybrid composites) [10]..... 34
Fig. 2.26. Potential dynamic curves after 1 h of immersion in NaCl 3.5 wt.% for (a) AZ91/SiC/0-10p and (b) AZ91/SiC/0-10p-PEO. (c) Corrosion current

density as a function of SiCp vol% for AZ91/SiC/0-10p and AZ91/SiC/0-10p-PEO [11]. 37
Fig. 2. 27. Scanning electron micrographs of the cross sections after 8 days of exposure in NaCl 3.5 wt.% aqueous solution (a) AZ91 and (b, c) AZ91/SiC/5p [11]. 38
Fig. 2.28. Optical micrographs of the cross sections after 8 days of exposure in NaCl 3.5 wt.% aqueous solution AZ91/SiC/5p-PEO [11]. 39
Fig. 2.29. Scanning electron micrograph showing the surface of the MMC before exposure to saline solution: the surface was originally in contact with lacquer during preparation of the MMC [13]. 41
Fig. 2.30. Scanning electron micrograph revealing the interface between a silicon carbide particle and the magnesium film [13]. 41
Fig. 2.31. Scanning electron micrographs of the surface of the MMC following exposure to 3.5 wt. % NaCl solution, of pH 6.5, for: (a) 1 h; and (b) 36 h [13]. 42

Fig. 3.1. Optical micrographs showing grain structures of etched (a) unreinforced matrix alloy AM60, (b) 7FC, and (c) MHNC-7F3NP. 53
Fig. 3.2. SEM micrographs in BSE mode showing constituent phases in microstructure of etched unreinforced matrix alloy AM60. 54
Fig. 3.3. EDS spectra (a), (b) and (c) for the areas containing α-Mg grains (dark contrast), and β-$Mg_{17}Al_{12}$ phases (bright contrast), and Al-Mn intermetallic (white spots) as shown in Figure 2, respectively. 55
Fig. 3.4. (a) SEM micrographs in BSE mode showing constituent phases in microstructure of the 7FC composite; EDS spectra (b), (c) and (d) for the areas containing α-Mg grains (dark contrast), and β-$Mg_{17}Al_{12}$ phases (bright contrast), and Al-Mn intermetallic (white spots) as shown in (a), respectively; EDS spectrum (e) for the Al_2O_3 fibre. 57
Fig. 3.5. (a) SEM micrographs in BSE mode showing constituent phases in microstructure of the MHNC-7F3NP composite; EDS spectra (b), (c) and (d) for the areas containing α-Mg grains (dark contrast), and β-$Mg_{17}Al_{12}$

phases (bright contrast), and Al-Mn intermetallic (white spots) as shown in (a), respectively; EDS spectrum (e) for the Al_2O_3 fibre. 59
Fig. 3.6. Polarization curves of the as-cast AM60, 7FC and MHNC-7F3NP composites. 63
Fig. 3.7. Corrosion current densities and potentials of the as-cast AM60, and the 7FC and MHNC-7F3NP composites..... 63
Fig. 3.8. Corrosion resistances and rates of the as-cast AM60, and the 7FC and MHNC-7F3NP composites. 64
Fig. 3.9. SEM micrographs in SE mode showing corroded surfaces of (a) the unreinforced alloy AM60, and the (b) 7FC and (c) MHNC-7F3NP composites. 69
Fig. 3.10. EDS spectra identifying oxygen and chlorine for the (a) unreinforced alloy AM60, and (b) 7FC and (c) MHNC-7F3NP composites respectively, which corresponds the SEM graphs in Figure 3.9..... 70
Fig. 3.11. SEM micrographs in SE mode showing corroded sub surfaces in the cross-section of (a) the unreinforced alloy AM60, and the (b) 7FC and (c) MHNC-7F3NP composites. 71

Fig. 4.1. SEM micrographs in SE mode showing PEO coating surfaces of (a) PEO-AM60, (b) PEO-7FC and (c) PEO-MHNC-7F3NP, respectively. 84
Fig. 4.2. SEM micrograph in SE mode showing the PEO coating cross-sections of PEO coatings for (a) PEO-AM60, (b) PEO-7FC and (c) PEO-MHNC-7F3NP, respectively. 85
Fig. 4.3. PEO coating thicknesses of PEO-AM60, PEO-7FC and PEO-MHNC-7F3NP. 86
Fig. 4.4. (a) SEM micrograph in SE mode showing constituent phases in microstructure of the PEO-AM60; EDS spectra (b), (c) and (d) for the areas containing α-Mg grains (dark contrast), and β-$Mg_{17}Al_{12}$ phases (bright contrast strip), and Al-Mn intermetallic (white spots) in the substrate of AM60 and (e) for the PEO coating. 87

Fig. 4.5. (a) SEM micrograph in SE mode showing constituent phases in the microstructure of the PEO-7FC; and EDS spectra (b), (c) and (d) for the areas containing α-Mg grains (dark contrast), and β-$Mg_{17}Al_{12}$ phases (bright contrast strip), and Al-Mn intermetallic (white spots); (e) for the Al_2O_3 fiber in the composite and (f) for PEO coating. 89

Fig. 4.6. (a) SEM micrograph in SE mode showing constituent phases in the microstructure of the PEO-MHNC-7F3NP; and EDS spectra (b), (c) and (d) for the areas containing α-Mg grains (dark contrast), and β-$Mg_{17}Al_{12}$ phases (bright contrast strip), and Al-Mn intermetallic (white spots); (e) for the Al_2O_3 fiber in the composite and (f) for PEO coating. 91

Fig. 4.7. Polarization curves of the PEO coated and uncoated AM60 alloy, 7FC and MHNC-7F3NP composites. 95

Fig. 4.8. Corrosion current densities and potentials of the PEO coated samples PEO-AM60, PEO-7FC and PEO-MHNC-7F3NP composites. 95

Fig. 4.9. Corrosion current densities and potentials of the uncoated samples AM60, 7FC and MHNC-7F3NP composites. 96

Fig. 4.10. Corrosion resistances and rates of the uncoated AM60, 7FC and MHNC-7F3NP composites and the PEO coated PEO-AM60, PEO-7FC and PEO-MHNC-7F3NP. 96

Fig. 4.11. SEM micrographs in SE mode showing corroded surfaces of (a) AM60, (b)PEO-AM60, (c) 7FC, (d) PEO-7FC, (e) MHNC-7F3NP and (f) PEO-MHNC-7F3NP composites. 98

Fig. 4.12. SEM micrographs in SE mode showing corroded surfaces of (a) PEO-AM60, and the (b) PEO-7FC and (c) PEO-MHNC-7F3NP composites. 99

Fig. 4.13. EDS spectra identifying oxygen, aluminum and chlorine for the (a) PEO-AM60, and the (b) PEO-7FC and (c) PEO-MHNC-7F3NP composites respectively, which corresponds the SEM graphs in Figure 4.12. 100

CHAPTER 1
Introduction

1.1. Background

Light weight metals have become one of the most desirable and necessary materials in automotive and manufacture industries, because they possess high strength-to-weight ratios, good ductility, low density and excellent corrosion resistance. Magnesium alloys are the significant members in the light weight metals family, and in particular magnesium alloy-based metal matrix composites (MMCs) have also been investigated and studied for decades due to the improved mechanical properties of the MMCs. However, the high cost of reinforcement materials and fabrication process and the lower corrosion resistance have limited the application of MMCs in the real industries. Thus, the cost-effective fabrication method and reinforcement materials have been massively investigated in research, and studies on corrosion behavior of MMCs are still in progress.

In the past, the magnesium alloy-based composites were generally built by introducing two kinds of reinforcements which were the micron-sized fibres and micron/nano-sized particles into matrix materials. The composites can be made by adding single or multi-types of reinforcement materials. The composite with two or more types of reinforcements, called hybrid composite, commonly possesses combined advantages of all reinforcements and provides enormous probabilities of reinforcements combination. Therefore, a great potential of magnesium alloy-based composites for structural applications in the automotive and aerospace industries can be seen by investigating the optimized engineering materials. The preform-squeeze casting is the method of fabricating the magnesium alloy-based composite in this research. Low cost raw materials and wide

volume percentage range of reinforcements can be achieved by employing the preform-squeeze casting method.

The primary limitation of the magnesium alloy-based composites applications is their poor corrosion resistance. The addition of reinforcement is the main factor which might cause the deterioration of the corrosion behavior of composites due to the combined effect of galvanic corrosion and pitting corrosion. However, a protecting coat can be applied on the surface of composites to improve the corrosion resistance by employing plasma electrolytic oxidation (PEO) process. PEO process is an emerging, environmentally friendly surface technique to deposit ceramic coatings on material surface. This technique can be distinguished from conventional anodizing by using voltages above the dielectric breakdown potential and leading to the local formation of plasmas with releasing gases. Recently, the development of PEO process allows to produce dense, uniform and well adhered coating laying on massive of material surfaces which create a huge potential for the originally low corrosion resistance materials to be used in many applications.

1.2. Objectives of this study

The magnesium alloy-based composites possess better mechanical properties such as higher yield strength and tensile strength. However, their corrosion resistance significantly affected by adding different reinforcements into the magnesium matrix is still unclear. The effect of the different combination of reinforcements on the corrosion behavior of the composites should be investigated, and the method of enhancing the corrosion resistance by plasma electrolytic oxidation process need to be more developed.

The objectives of this study were to:

- Analyze the microstructures of the developed magnesium-based hybrid composite containing micron sized fibres and nano sized particles in comparison with the only micron sized fibres reinforced composite.
- Evaluate the corrosion resistance of magnesium alloy-based micron sized fibre reinforced composite and micron sized fibre and nano sized particle reinforced hybrid composite in comparison with the unreinforced magnesium matrix alloy.
- Determine the corrosion mechanisms of the magnesium alloy-based composites.
- Investigate the plasma electrolytic oxidation process for improving the corrosion resistance of magnesium alloy-based composites.
- Evaluate the corrosion resistance of PEO coated magnesium alloy and its composites, and compare the corrosion resistance between the PEO coated materials and uncoated materials.

1.3. Organization of the thesis

This thesis is divided into five main chapters. The introduction of the thesis is given in Chapter 1 which shows the background information, objective of the study and the thesis organization. Chapter 2 presents the literature review which are related with the corrosion behavior of the magnesium alloys and the magnesium alloy-based composites, and the corrosion resistance of PEO coated magnesium alloys. Chapter 3 shows the result of the microstructure and corrosion behavior of the AM60 alloys and its composites. The corrosion behavior of the PEO coated AM60 alloys and its composites is discussed in Chapter 4. Chapter 5 summarizes the present study and gives a conclusion for the whole thesis. The future work is proposed in Chapter 6.

CHAPTER 2

Literature review

2.1. Introduction

Magnesium alloys are the light weight metals which have been desired hugely in the automotive related manufacturing industry, because they possess high strength-to-weight ratios, good ductility, low density and excellent corrosion resistance. At the same time, magnesium-based metal matrix composites (MMCs) have been investigated by massive researchers for decades, due to the fact that MMCs has even better mechanical properties than magnesium alloys. Thus, magnesium-based metal matrix composite can be a good candidate for applications which the unreinforced magnesium alloys are unsuitable. Massive different mechanical property tests on magnesium-based metal matrix composite have already been carried out, meanwhile the relationship between the engineering performance and microstructure has been analyzed. Micro-sized particle, nano-sized particle and fibre have been commonly used for fabricating the magnesium-based metal matrix composites.

In addition, the corrosion behavior of the MMCs also have been studied by worldwide researchers. The reinforcements in the MMCs is not only increase the strength of material, but the ductility and corrosion resistance are also substantially reduced because of the particle cracking and void formation at particle-matrix interface [1]. Therefore, plasma electrolytic oxidation (PEO) coating and other surface treatments are reported to be used for increasing the corrosion resistance of MMCs. Nonetheless, the study on PEO coating and other surface treatments debase the corrosion rate is still limited due to economic and technical reasons.

2.2. Magnesium-based MMCs Fabrication Process

One of the most commonly used methods to produce the fibre reinforced Magnesium MMCs is squeeze casting with pressure infiltration. The fibre reinforcement preform is usually prepared firstly, of which the shape can be circular or rectangular. Then, the preform is heated up to 1000°C, and the mold is also preheated before the preform is placed inside. At the same time, the matrix alloy is melted and heated up to 800°C in a crucible when a certain protective gas is continually injected. After pouring the heated matrix alloy onto the preform, the mold is closed with the upper die and a high pressure is applied. The pressure is held for 1 to 2 mins and fall back to zero [2]. Figure 2.1 shows schematically squeeze casting process.

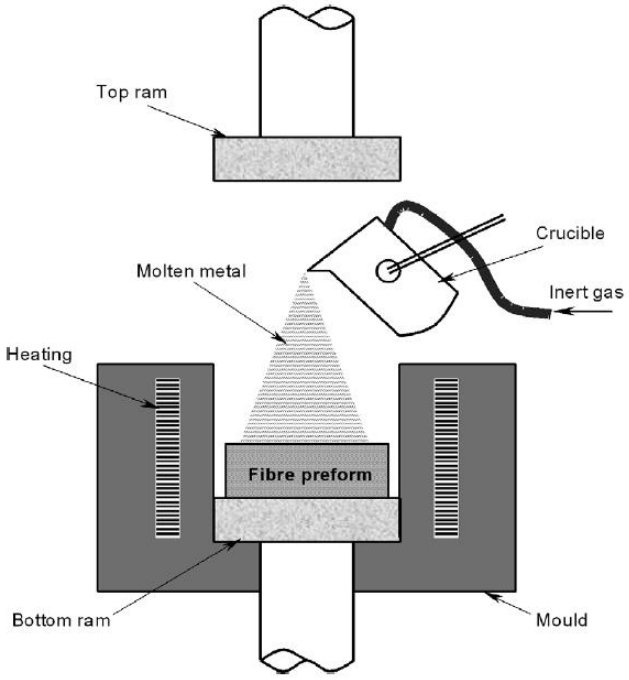

Fig. 2.1. Schematic illustration of the squeeze casting process [2].

There are another two MMCs fabrication methods which are mentioned in the reviewed literatures. Powder Metallurgy is one of the two routes which is often used to

fabricate fibre and particle reinforced magnesium matrix alloy. Since the powder form of the alloy is required and the preparation conditions are complex, it is barely used for volume production. In the study by Pardo [3], the alloy powder and various volume of particles are milled in a high-speed impeller during the fabrication process. Then the milled powder is cold compacted by an isostatic pressure for a few minutes. Finally, the MMCs is extruded at 325°C and extrusion ratio of 18:1 [3]. Another method is stir casting, described by Muhammad et al [4], in which graphene Nano-platelets (GNPs) were introduced in Mg-Al-Zn alloys. At the first, Mg ingot was melted at 740°C when CO_2-SF_6 is used as a protective atmosphere. Then, Al and granular Zn were added into Mg melt. In the next step, GNPs powder was added into molten alloy and the mixture was stirred for 1 min. After the mixture was reheated and kept to 740°C for 10 minutes, the composites mixture was poured into a steel mold and cool down normally. At last, the composites were extruded at 350°C with an extrusion ration of 5.2:1 [4].

There is a few of other production methods for MMCs, which were described in the literature. However, the above three methods, i.e, squeeze casting, powder metallurgy and stir casting, are most commonly used ways to fabricate various of reinforced metal matrix composites.

2.3. Corrosion Mechanism

Before analysing the electrochemical behavior of magnesium based MMCs, the corrosion mechanism should be clearly introduced. According to Bakkar's study [2], Magnesium reacts with water and forms its hydroxide and hydrogen like following reactions:

Anodic reaction:

$$Mg \Rightarrow Mg^{2+} + 2e^{-} \text{ and/or}$$

$$Mg_{(s)} + 2(OH)^{-} \Rightarrow Mg(OH)_{2(s)} + 2e^{-}$$

Cathodic reaction:

$$2H^{+} + 2e^{-} \Rightarrow H_{2(g)} \text{ and/or}$$

$$2H_2O + 2e^{-} \Rightarrow H_{2(g)} + 2(OH)^{-}$$

The overall reaction is: $Mg_{(s)} + 2H_2O \Rightarrow Mg(OH)_{2(s)} + H_{2(g)}$.

In the Bakkar's work [2], the alumina was introduced into magnesium matrix alloy. Thus, the model explains the corrosion mechanism of the MMC, which is shown in Figure 2.2. When the Magnesium based MMC is disclosed in a corrosive environment, an anodic behavior appears in Mg matrix high aluminum volume zone (HA). Then the corrosion initially happens near to the HA zone and the pitting corrosion is formed and localised. In addition, the pitting becomes deeper with time. The Mg^{2+} ions come from anodic reaction and diffuse outwards from the metal surface, and the chloride ions move inward inside the pits to maintain electro-neutrality. Furthermore, the pits increase to be bigger and wider, and the protective film on Mg matrix is destroyed at the last. At the same time, the HA zone near the alumina fibre no longer exists due to the interruption of the continuity of the protective layer at the fibre and matrix interface [2].

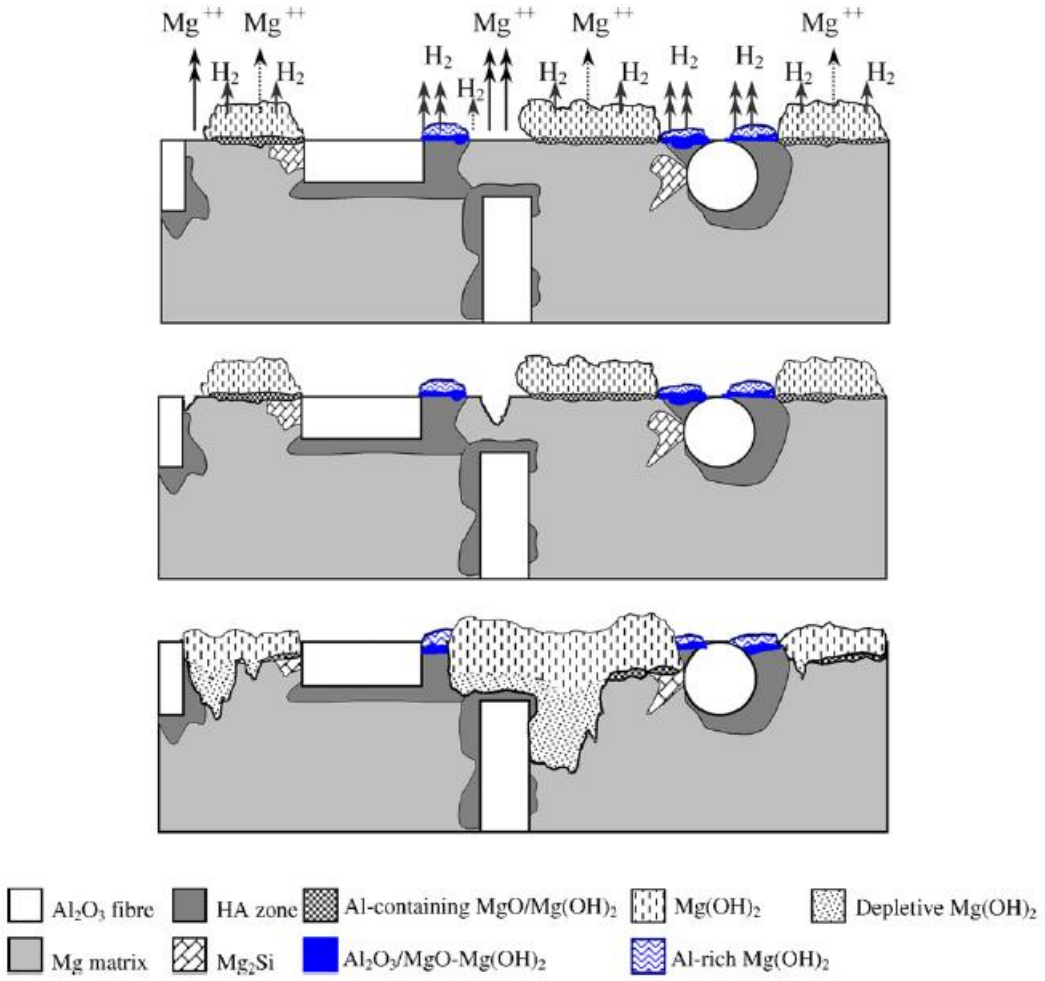

Fig. 2.2. Schematic representative model showing the corrosion mechanism of Al_2O_3/Mg MMC [2].

2.4. Analysis of the Experimental Investigations

According to different types of reinforcement are used in magnesium alloys, the fabrication methods are differed. However, the same corrosion test which is the potential-dynamic polarization is carried out for investigating the corrosion behavior of MMCs without any surface treatments and MMCs with different types of coating on surface. Meanwhile, 3.5 weight percent sodium chloride solution at room temperature is usually used to test the MMCs corrosion rate. Since different kinds of MMCs perform varies corrosion behavior, the surface morphology before and after corrosion test should be compared and analyzed by using scanning electron microscopy (SEM). The different corrosion behavior and morphology results will be reviewed in this section.

2.4.1 Electrochemical experimentation of fibre reinforced magnesium alloys

2.4.1.1 Potential dynamic polarization test of alumina fibre reinforced magnesium alloys

Alumina fibre was used to reinforce the magnesium matrix in the study of Bakkar and Neaubert et al [2]. Squeeze casting is the method for fabricating the MMCs. In addition, the corrosion behavior of alumina-magnesium (20 vol% fibre) metal matrix composites in sodium chloride solution was investigated and compared the test result with matrix magnesium alloy AS41. Table 2.1 shows the chemical composition of both magnesium matrix alloy (AS41) and alumina (Saffil) fibres.

Table 2.1. Typical chemical composition (wt. %) of both magnesium matrix alloy (AS41) and alumina (Saffil) fibres [2]

AS41	Al	Si	Mn	Zn	Fe	Ni	Cu	Pb	Sn	Zr	Mg
	4.998	0.93	0.357	0.0555	0.0014	0.0006	<0.0002	<0.002	0.0053	<0.010	Bal.

Saffil	Al_2O_3	SiO_2	Others
	95.00	4.16	0.84

The potential-dynamic polarization test was carried out in three different kinds of solutions which are Cl-free alkaline solution, Cl-containing alkaline solution and neutral sodium chloride solution with different weight percent of NaCl. Meanwhile, the corrosion behavior on horizontal and normal planes of specimens are also plotted. Figure 2.4 shows the polarization diagrams for alloy and composite specimens in PH 12 sodium hydroxide solutions. Table 2.1 is presenting the electrochemical parameters from the polarization curve in Figure 2.3.

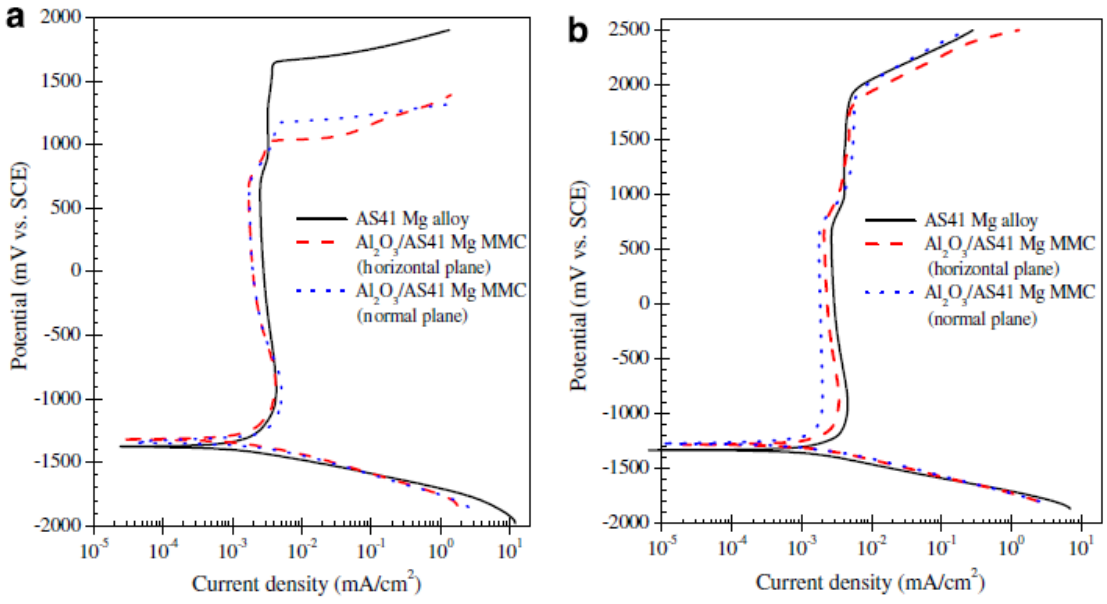

Fig. 2.3. Potential dynamic polarization diagrams for alloy and composite specimens in pH 12 sodium hydroxide solution: (a) with 100 ppm NaCl, (b) chloride-free [2].

Table 2.2. Electrochemical parameters obtained from polarization curves for Al_2O_3/AS41 Mg composite and the matrix alloy in pH 12 sodium hydroxide solution [2]

Parameter	100 NaCl solution, pH = 12			Cl-free solution, pH = 12		
	Alloy	Composite parallel	Composite normal	Alloy	Composite parallel	Composite normal
CP (mV_{SCE})	-1419 ± 56	-1327 ± 23	-1334 ± 25	-1432 ± 30	-1327 ± 10	-1316 ± 14
E_{corr} (mV_{SCE})	-1349 ± 26	-1324 ± 5	-1316 ± 30	-1313 ± 22	-1281 ± 11	-1273 ± 17
I_{corr} ($\mu A/cm^2$)	0.957 ± 0.011	1.286 ± 0.06	1.376 ± 0.212	1.075 ± 0.009	0.966 ± 0.04	0.903 ± 0.034
E_p (mV_{SCE})	**1587 ± 58**	**1080 ± 85**	**1177 ± 14**	**2085 ± 15**	**1953 ± 19**	**2037 ± 10**
I_{pass} ($\mu A/cm^2$)	2.4 ± 0.08	1.87 ± 0.15	1.37 ± 0.35	2.55 ± 0.12	2.06 ± 0.32	1.75 ± 0.22

Figure 2.4 and 2.5 show the SEM micrographs of corroded surface of the composites after submerging the samples in the above two solutions for 3 hours at 1050 mV. In the solution containing 100 ppm NaCl (Figure 2.3), the pitting corrosion is not only taking place near the fibres, but it also appears in the matrix area. Moreover, the deep pitting firstly appears in the matrix area which are pointed by white arrows, and the shallow pits which are pointed by black and dashed arrows are localized independent on the fibres sites. However, the surface of specimen was not affected by potential static polarization at 1050mV for 3 hours after potential dynamic polarization [2].

At last, 0.03, 0.3, 1.0 and 3.0 weight percent of sodium chloride solution were used to do the polarization test for the same specimens. Figure 2.6 shows the polarization curve of same specimens in different solutions. In the Figure 2.6 (a), the quasi-passive behavior where the sharp increase of the current occurred is pointed out. In addition, the quasi-passive point is shifted significantly when increase the weight percent of NaCl which is shown in Figure 2.6 (b). The polarization behavior for all the materials were almost same when the solution contains 1.0 and 3.0 weight percent of NaCl. Table 2.3 present all the parameters which are from the polarization cures in Figure 2.6.

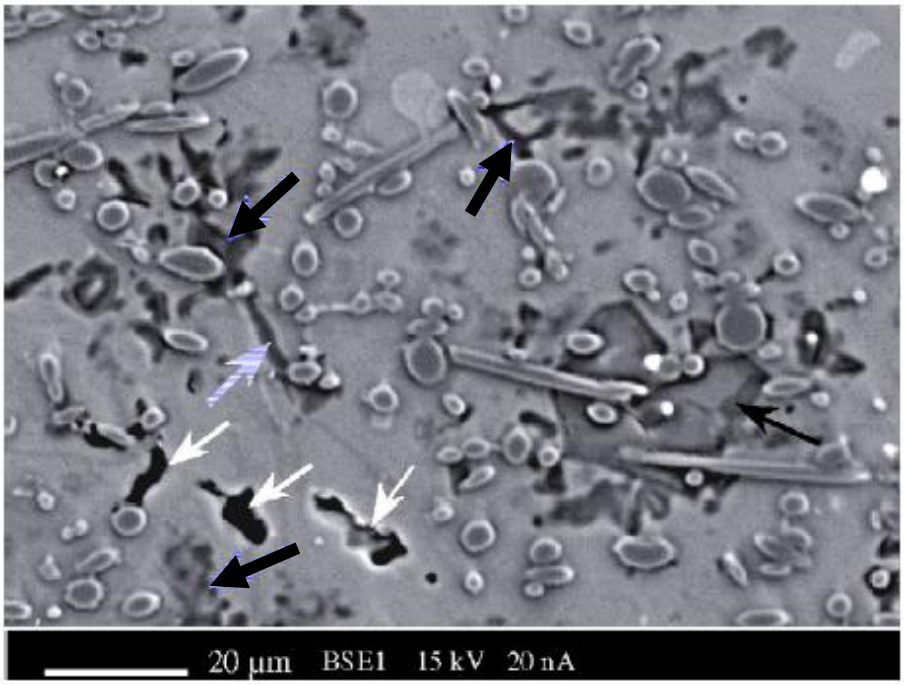

Fig. 2.4. SEM micrograph of corroded surface after 3 h polarization at 1050 mV in pH 12 sodium hydroxide solution containing 100 ppm NaCl, showing the pitting sites represented by arrows [2].

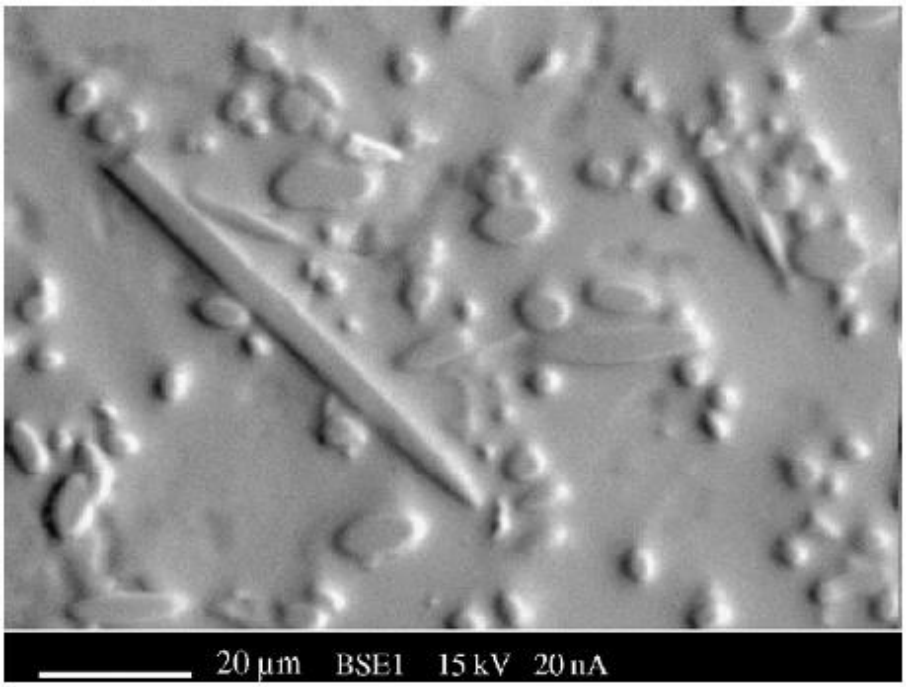

Fig. 2.5. SEM micrograph of composite surface polarized for 3 h at 1050 mV in chloride-free pH 12 sodium hydroxide solution [2].

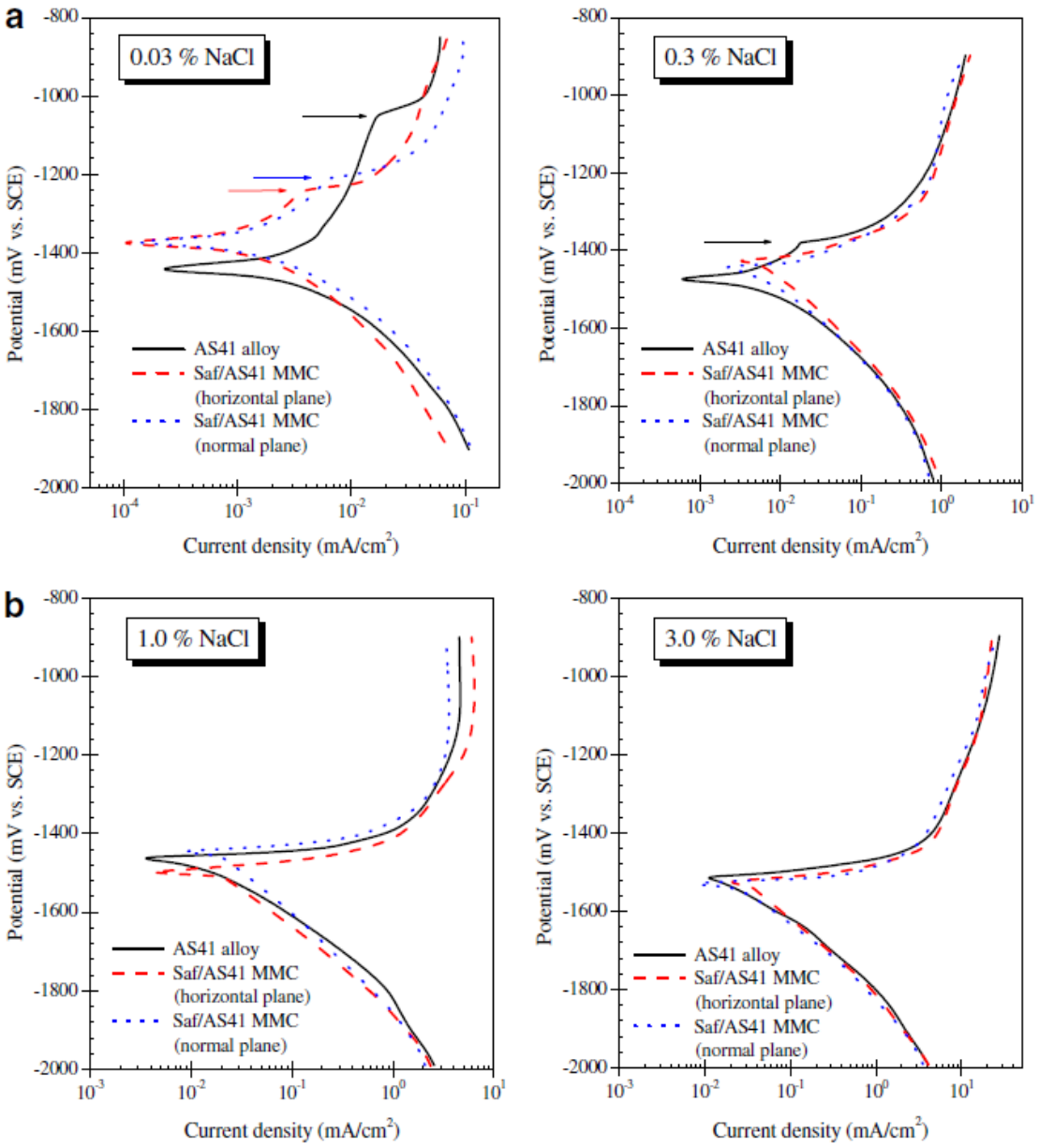

Fig. 2.6. Potential dynamic polarization diagrams for alloy and composite specimens in neutral 0.03, 0.3, 1.0 and 3.0wt% NaCl solutions [2].

Table 2.3. Electrochemical parameters obtained from polarization curves for Al_2O_3/AS41 Mg composite and its pure matrix alloy in neutral NaCl solutions [2].

Parameter	0.03% NaCl			0.3% NaCl		
	Alloy	Composite parallel	Composite normal	Alloy	Composite parallel	Composite normal
OCP (mV_{SCE})	-1495 ± 7	-1447 ± 23	-1483 ± 27	-1534 ± 13	-1472 ± 9	-1489 ± 7
E_{corr} (mV_{SCE})	-1423 ± 33	-1402 ± 21	-1406 ± 24	-1466 ± 10	-1437 ± 10	-1453 ± 14
I_{corr} ($\mu A/cm^2$)	1.537 ± 0.522	1.069 ± 0.119	1.216 ± 0.185	4.313 ± 0.281	4.884 ± 0.169	4.688 ± 0.776
E_{break} (mV_{SCE})	**-1094 ± 53**	**-1261 ± 61**	**-1224 ± 11**	**-1373 ± 9**		
I_{break} ($\mu A/cm^2$)	13.13 ± 7.05	4.47 ± 2.26	7.38 ± 0.92	16.07 ± 3.19		

Parameter	1% NaCl			3% NaCl		
	Alloy	Composite parallel	Composite normal	Alloy	Composite parallel	Composite normal
OCP (mV_{SCE})	-1524 ± 6	-1511 ± 11	-1513 ± 10	-1552 ± 7	-1540 ± 4	-1536 ± 12
E_{corr} (mV_{SCE})	-1465 ± 16	-1481 ± 11	-1478 ± 8	-1509 ± 4	-1519 ± 6	-1528 ± 9
I_{corr} ($\mu A/cm^2$)	**8.16 ± 1.14**	**12.523 ± 4.118**	**12.817 ± 3.377**	**16.313 ± 1.801**	**26.327 ± 6.343**	**22.963 ± 5.605**
E_{break} (mV_{SCE})						
I_{break} ($\mu A/cm^2$)						

2.4.1.2 Potential dynamic polarization test of carbon fibre reinforced magnesium alloys

The corrosion behavior of carbon fibre reinforced MMC was studied by Bakkar and Neubert [5]. Meanwhile, the galvanic corrosion between the magnesium matrix alloy and carbon fibres was investigated as well. Both neutral and alkaline aqueous solutions of which containing different concentrations of NaCl were used to test their corrosion behaviors. In their study, AS41 and AS41 (0.5% Ca) were employed to be the base material of the composites which contained about 25 Vol% carbon fibres and fabricated by squeeze casting. Figures 2.7 and 2.8 show the polarization curve for the matrix alloys and composites submerged in 100 ppm NaCl solution. Figure 2.7 the Ca-containing alloy shows greater corrosion resistance of the Ca-containing AS41 alloy than the AS41 alloy. However, the corrosion potentials of two composites specimens are shifted in the noble direction by more than 1000 mV after adding carbon fibres, which can be seen in the Figure 2.28. Different concentrations of NaCl solutions were used for corrosion test as well. In Figure 2.9, the polarization curves for the monolithic alloys and composites in different NaCl solution are shown. In the 300 ppm NaCl solution, both Mg alloys show a pseudo-passive behavior where the current density increased sharply when the anodic polarisation potential was about “-1200 mV”. Nonetheless, there was no pseudo-passive behavior on the MMCs polarization curve obtained in the NaCl solutions. Moreover, the current density of composites specimens was larger than the current density of monolithic alloys, which also increased with the increased NaCl concentration.

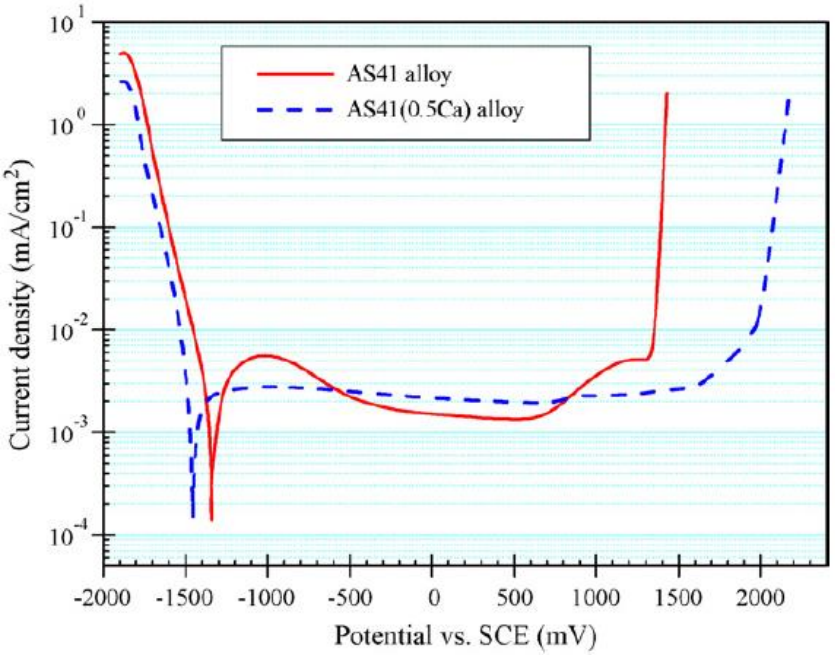

Fig. 2.7. Potential dynamic polarisation diagrams for monolithic AS41 and AS41 (0.5%Ca) Mg alloys in 100ppm NaCl solution; pH 12 [5].

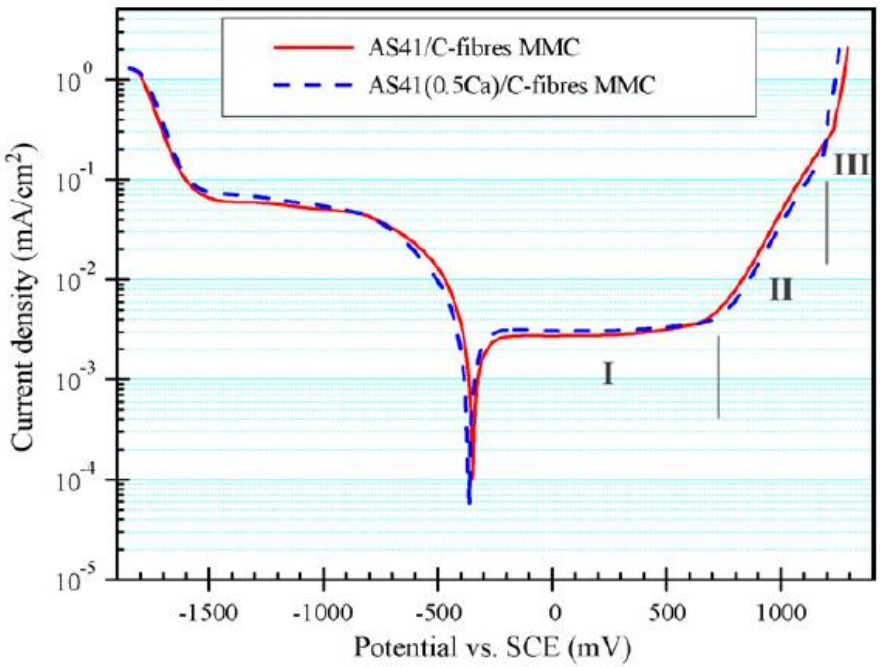

Fig. 2.8. Potential dynamic polarisation diagrams for both C/AS41 and C/AS41(0.5% Ca) Mg MMCs in 100ppm NaCl solution; pH 12 [5].

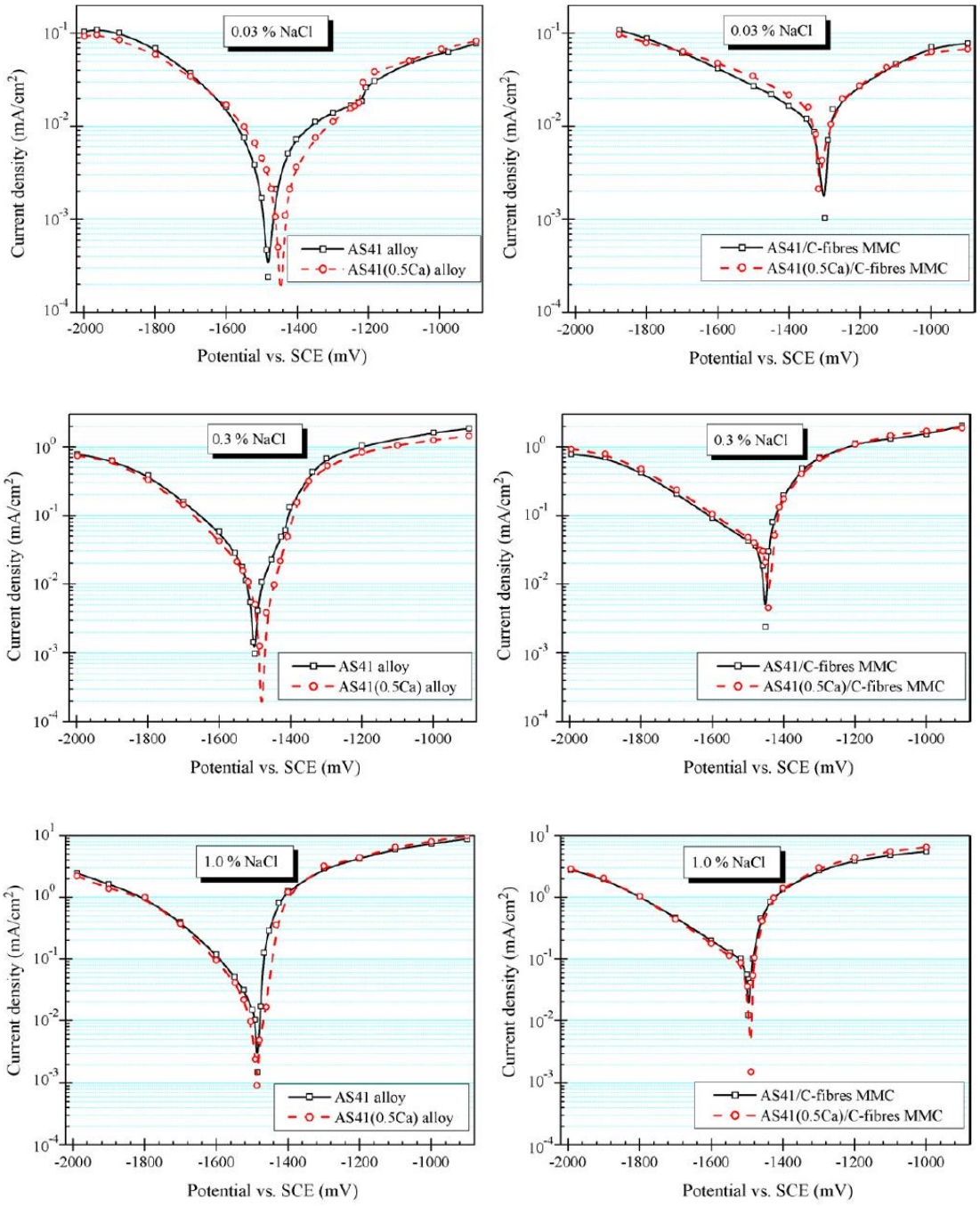

Fig. 2.9. Potentiodynamic polarisation diagrams of the matrix alloy and composite specimens in neutral 0.03, 0.3 and 1.0 wt.% NaCl solutions [5].

2.4.2 Electrochemical experimentation of micro-sized particle reinforced magnesium alloys

Micro-sized particle like silicon carbide is usually used to reinforce the magnesium matrix alloys. In the research of Tiwari et al [6], Mg-6SiC and Mg-16SiC (in volume percent) were tested to study their corrosion behaviors after submerging them into 1M NaCl solution. They compared the results with pure magnesium. By observing the results of potential-dynamic polarization test, they found that the corrosion resistance decreased with the addition of silicon carbide. Meanwhile, in the study by Pardo et al[7], not only the 3.5 wt% NaCl solution was used for corrosion test, but also the neutral salt fog (ASTM B 117) and high relative humidity (98% RH, 50°C) environments were employed to analyze corrosion behavior of silicon-carbide particle-reinforced AZ92 magnesium alloy which was produced by the powder metallurgy process. The same conclusion was also found out, the corrosion rate increased with the addition of silicon carbide particles. Figure 2.10 shows the SEM micrographs of Mg and Mg-6SiC surfaced obtained after immersion in 1M NaCl for 5 minutes. The area marked “a” is covered by MgO, the location marked “b” contain chloride, and the area with marked “c” has chloride/oxychloride/oxide, the hydroxide presents in “d” region. The surface morphologies of Mg, Mg-6SiC and Mg-16SiC submerged in 1M NaCl for 1 hour were revealed in Figure 2.11. The area “a” in Figure 2.11 (a, b, c) contains oxides of Mg and chloride ions, but the area “b” contains less chloride ions than area “a”.

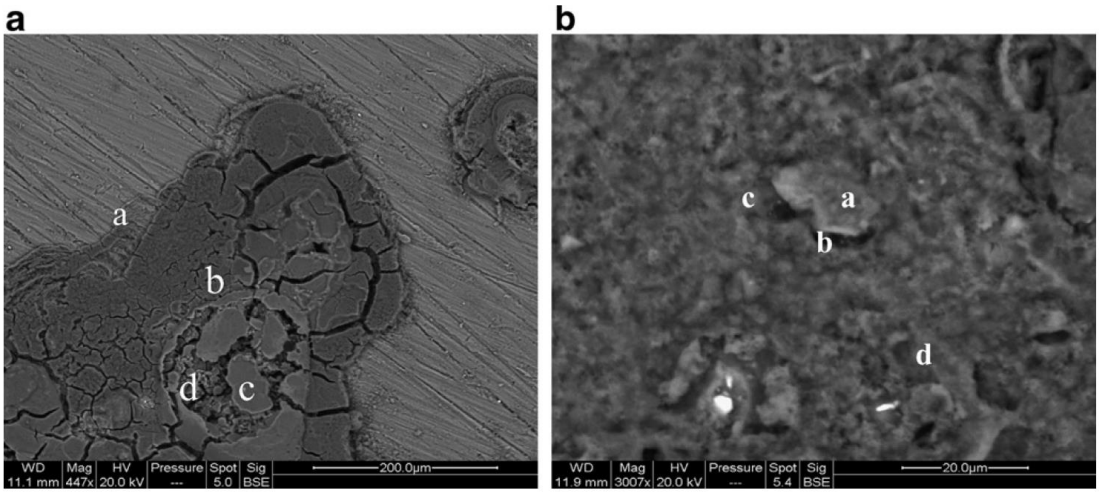

Fig. 2.10. Typical SEM micrographs of (a) Mg and (b) Mg-6SiC surfaces obtained after immersion in 1M NaCl for 5 min [6].

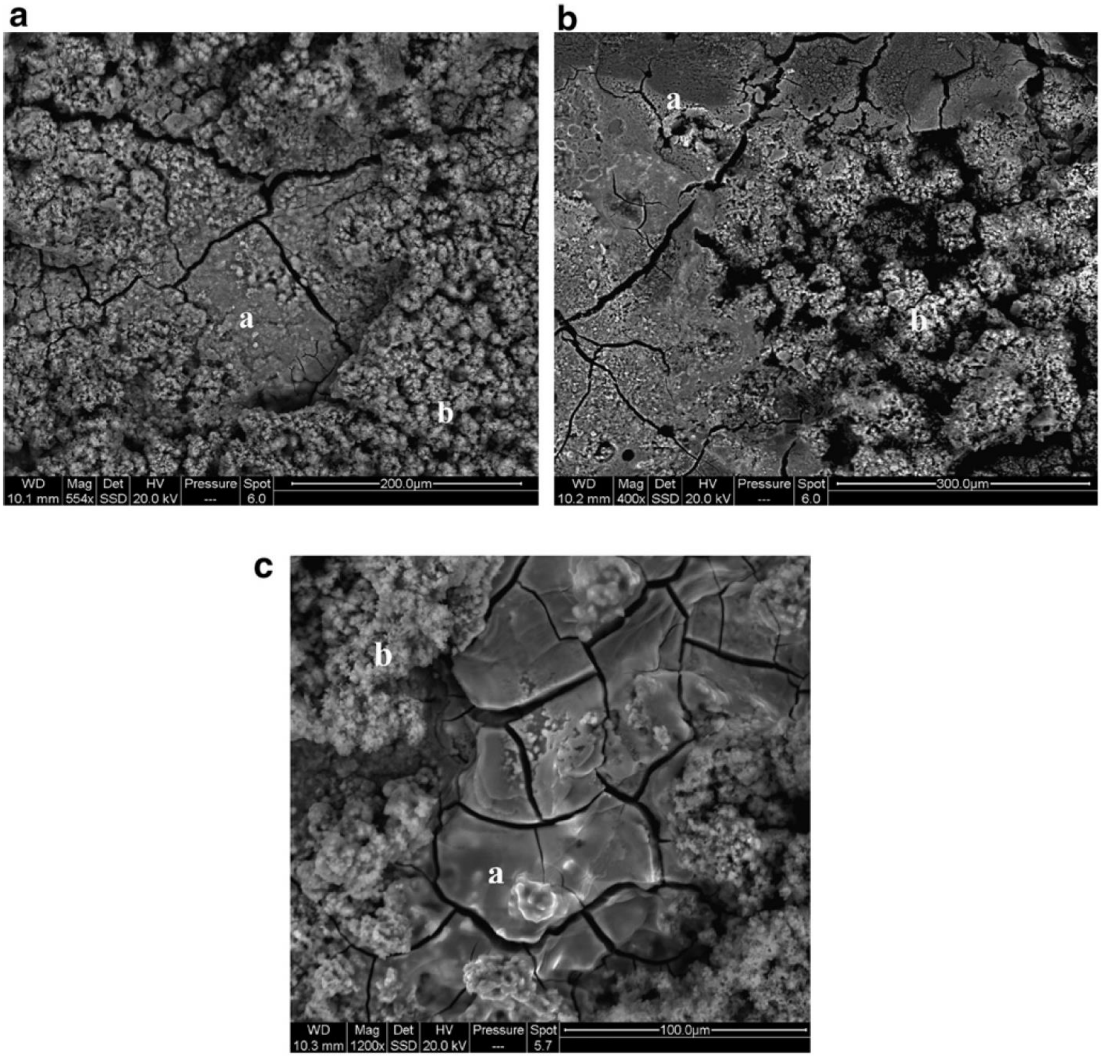

Fig. 2.11. Typical SEM micrograph of (a) Mg, (b) Mg–6SiC and (c) Mg–16SiC surfaces obtained after immersion in 1M NaCl for 1 h [6].

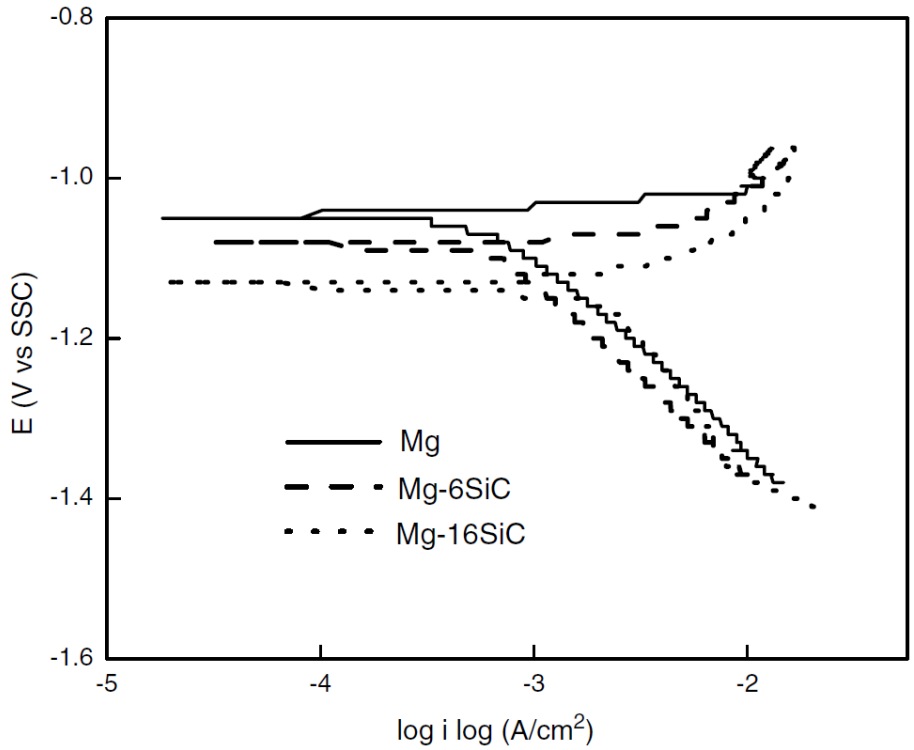

Fig. 2.12. Tafel plots for the magnesium, Mg-6SiC and Mg-16SiC in 1M NaCl [6].

Table 2.4. Corrosion rate determination by Tafel extrapolation and linear polarization (LP) experiments [6].

Parameters	Mg	Mg–6SiC	Mg–16SiC
ZCP (V vs SSC)	−1.116	−1.138	−1.145
β_c (mV/decade)	245	256	248
β_a (mV/decade)	13	17	16
i_{corr} (μA/cm^2) (Tafel)	590	794	1905
R_p (Ω cm^2)	9.11	8.53	3.43
i_{corr} (μA/cm^2) (LP)	588	811	1902
Corrosion rate (mm/year) (Tafel)	13.5	18.1	45.5

As show in Figure 2.12, all the polarization curves for Mg, Mg-6SiC and Mg-16SiC composites are similar. The slope of cathodic Tafel was about 250 mV/decade, and the anodic Tafel slope was around 10 to 20 mV/decade. All the parameters from the polarization curves in Figure 2.12 are shown in Table 2.4. The corrosion resistance of pure

Mg was the greatest among these three specimens, and the corrosion resistance reduced with the addition of silicon carbide particle, which is also shown in Figure 2.13.

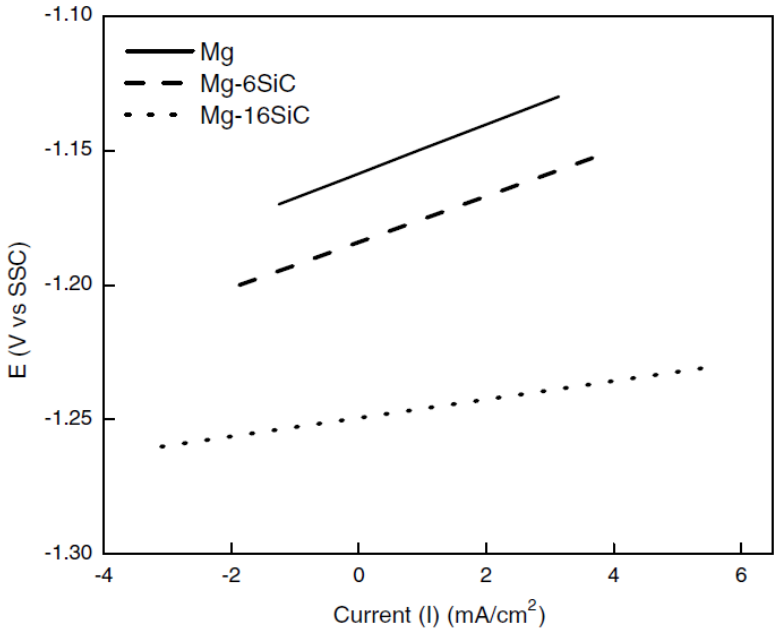

Fig. 2.13. Linear polarization plots for magnesium, Mg-6SiC and Mg-16SiC in 1M NaCl [6].

It was also found [3] that the corrosion rate increased with the addition of silicon carbide particle. Figure 2.14 presents the polarization curves for magnesium alloy AZ92, AZ92-5SiC and AZ92-10SiC after immersion in 3.5 wt% NaCl for 1 hour.

Table 2.5. Corrosion potential, polarization resistance and corrosion rate of tested materials after immersion in 3.5 wt.% NaCl for 1 h [3].

Material	E_{corr} (V/SSE)	Rp (Ω cm^2)	CR (mg cm^{-2} h^{-1})
AZ92	−1.457	142	4.2×10^{-2}
AZ92/SiC/5p	−1.472	161	4.4×10^{-2}
AZ92/SiC/10p	−1.480	50	5.6×10^{-2}

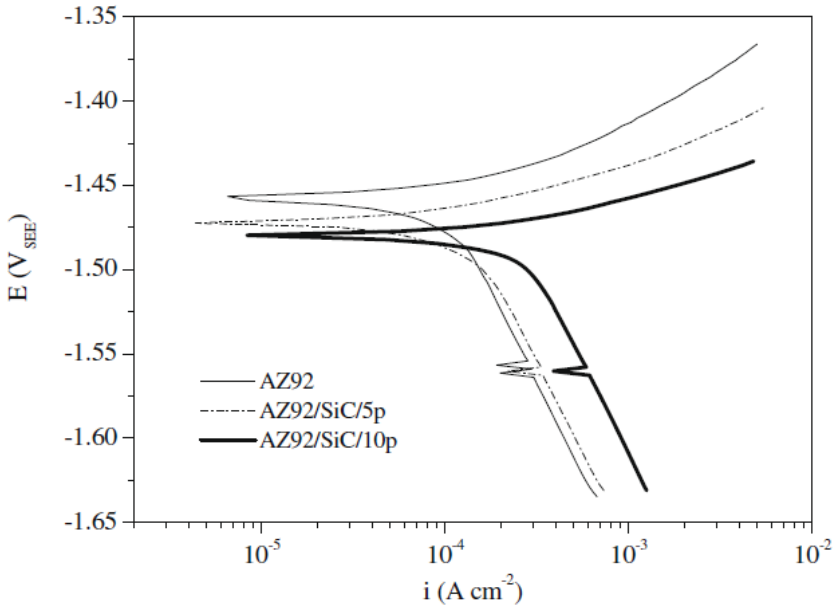

Fig. 2.14. Polarization curves of tested materials after immersion in 3.5 wt.% NaCl for 1 h at room temperature [3].

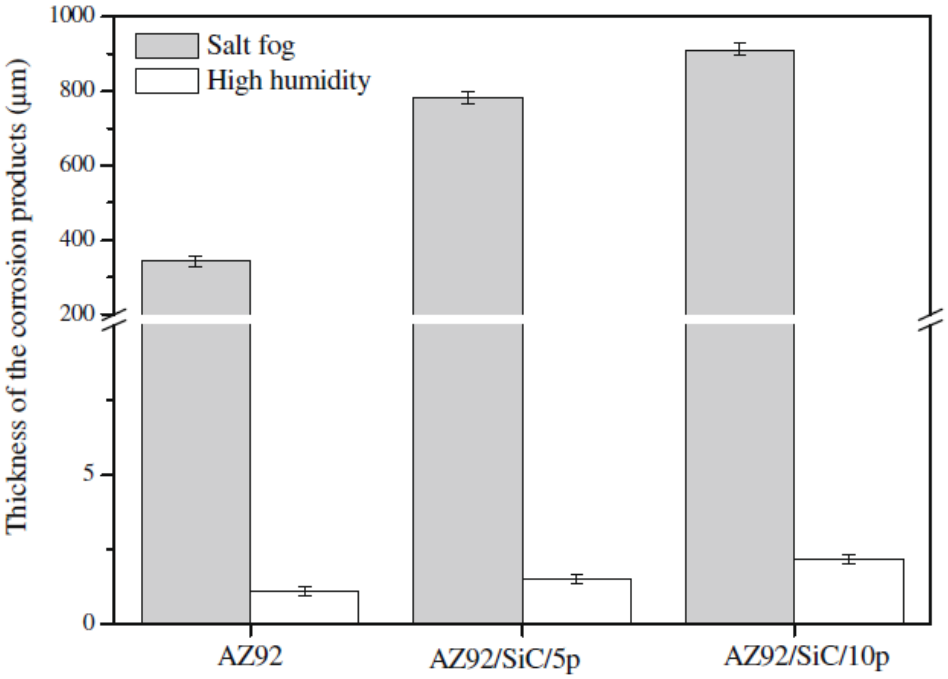

Fig. 2.15. Thickness of the corrosion layer for the tested materials exposed to salt fog (21 days) and high humidity (28 days) environments [3].

Furthermore, the corrosion behaviors of these three specimens after exposure to salt fog and high humidity environment (98% RH at 50 °C) were investigated. From Figure

2.15, it can be seen that the thickness of the corrosion layer increased 2 to 3 times with the addition of silicon carbide particle compared with the unreinforced magnesium alloy after exposing the specimens in salt fog. However, the thickness of corrosion layer was much thinner when the specimens were exposed in high humidity environments.

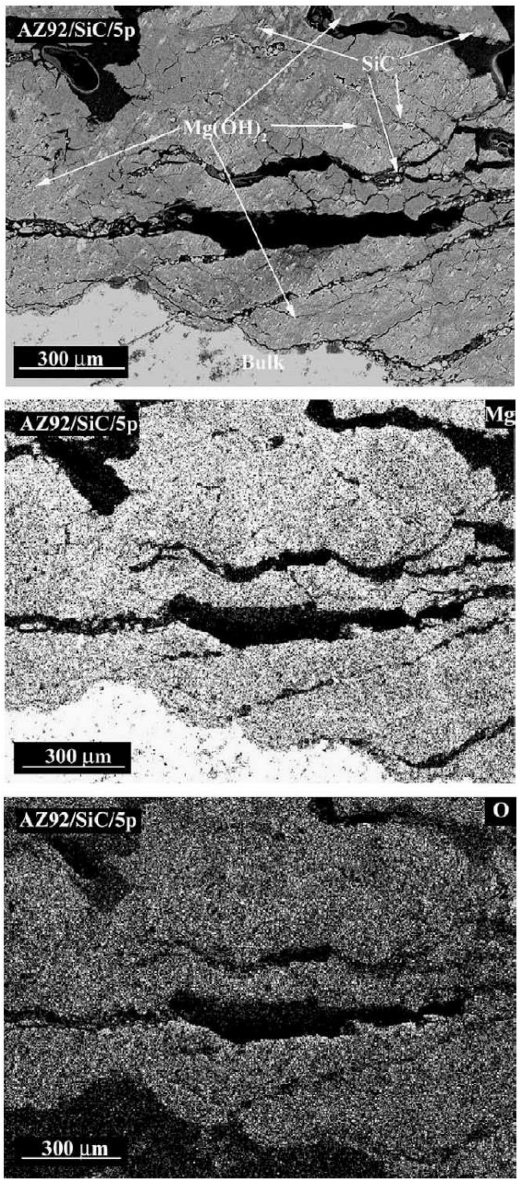

Fig. 2.16 SEM cross-section micrograph and X-ray elemental maps of Mg and O of AZ92/SiC/5p composite after exposure to salt fog atmosphere for 21 days [3].

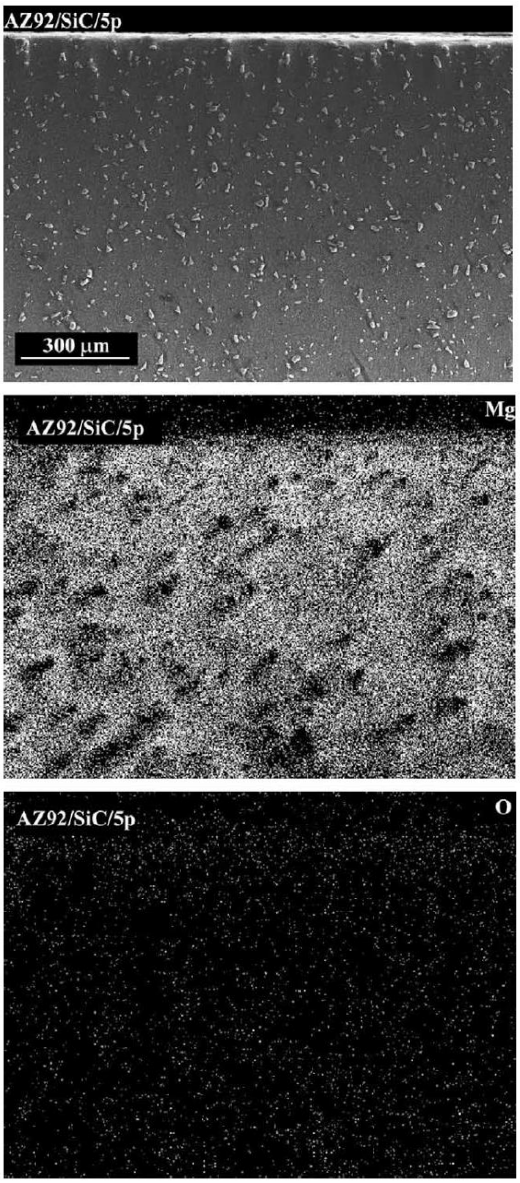

Fig. 2.17 SEM cross-section micrograph and X-ray elemental maps of Mg and O of AZ92/SiC/5p composite after 28 days of exposure to high humidity environment (98% RH at 50°C) [3].

As illustrated in Figures 2.16 and 2.17, the AZ92/SiC/5p composite had corrosion attack after exposure to salt fog for 21 days worse than expose it into high humidity environment for 28 days.

2.4.3 Electrochemical experimentation of Nano-sized particle Reinforced Magnesium Alloys

Nano-sized particle are always being used in metal matrix composites, since it can improve the mechanical properties without substantially reducing ductility, compare to the micro-sized particle reinforced MMCs. Thus, nano-sized particle MMCs sometimes could be associated with the addition of micron sized particle reinforcement for better mechanical properties and making them to be a good candidates of light weight structures applications [7].

Potential dynamic polarization tests were also carried out on the nano sized particle reinforced magnesium alloys. From the literature, there are two contradicting conclusions for their effect on corrosion behavior of the composites with the addition of nano sized particle reinforcement. Rashad et al [4] investigated the corrosion behavior of magnesium-graphene composites in sodium chloride solution [4], They found that the corrosion resistance reduced with the addition of graphene nano-platelets (GNPs), because the reinforcement resulted in the high dislocation densities at the interface of composites which created crevice attacks and to higher corrosion rates of the composites than the unreinforced magnesium matrix alloys. The polarization curves for the AZ31 composites and AZ31 alloys are shown in Figure 2.18 (a), and Figure 2.18 (b) shows the polarization curves for the AZ61 alloys and AZ61 composites. The label A in Figure 2.18 (a) and (b) represents the clear passivation, and the label B stands for the current density which increased with potential. The label C points out the occurrence of pitting corrosion. Table 2.6 lists the potential and currents for each specimen.

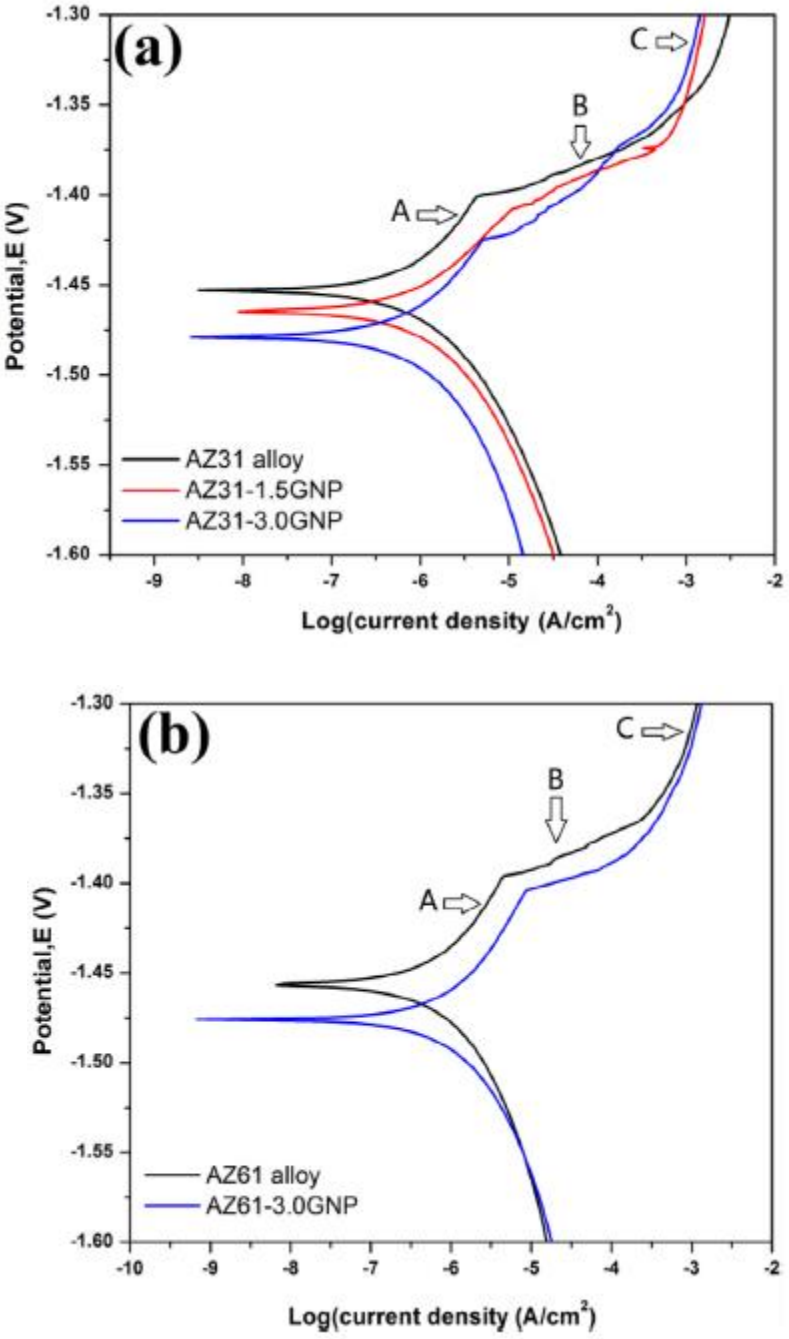

Fig. 2.18. Potential verses current density curves of as-extruded (a) AZ31 alloy and its composites; (b) AZ61 alloy and its composite samples [4].

Table 2.6. Corrosion potentials and currents of synthesized materials in 3.5 wt % NaCl solutions [4].

Samples	Potential (V)	Current (μA)	Pitting potential (V_p)
AZ31 alloy	−1.453	15.47	−1.39
AZ31-1.5wt.%GNP	−1.465	18.13	−1.41
AZ31-3.0wt.%GNP	−1.479	19.31	−1.42
AZ61 alloy	−1.457	11.54	−1.39
AZ61-3.0wt.%GNP	−1.476	14.21	−1.40

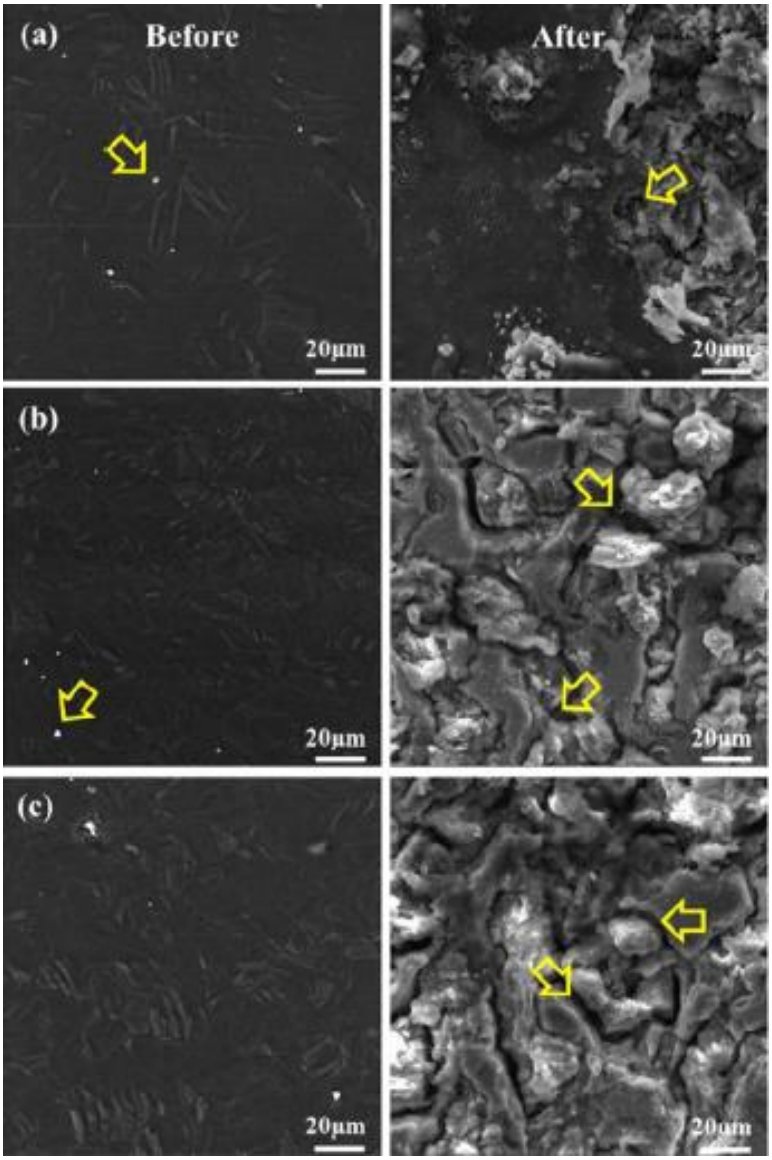

Fig. 2.19. SEM micrographs of extruded AZ31 alloy and its composites before and after corrosion tests: (a) AZ31 alloy, (b) AZ31-1.5GNP, and (c) AZ31-3.0GNP composites [4].

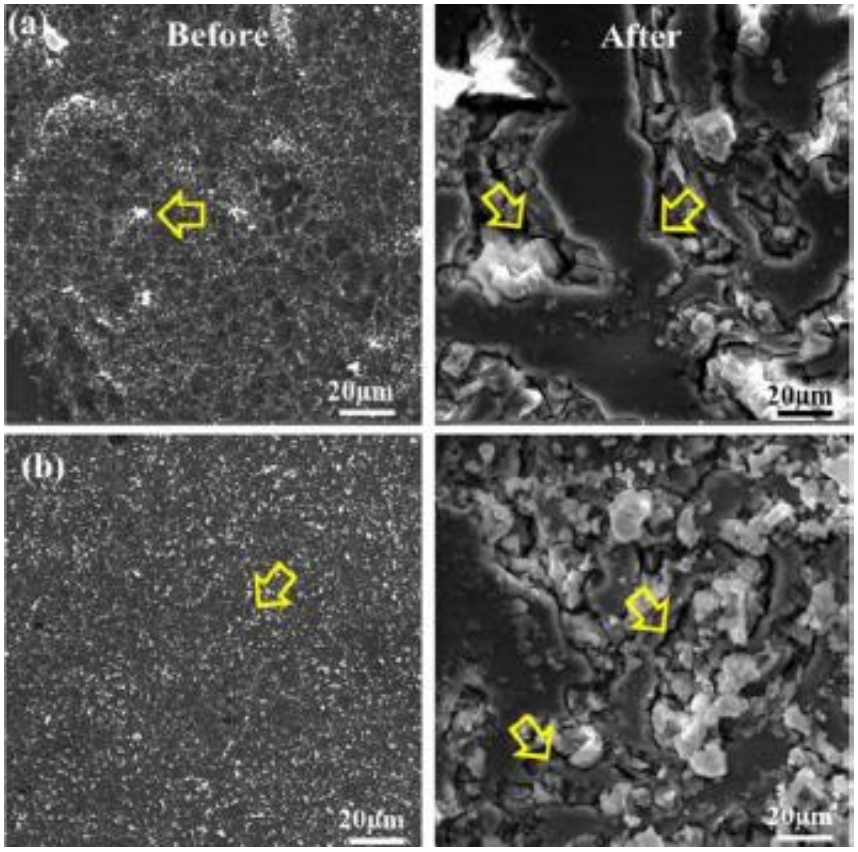

Fig. 2.20. SEM micrographs of extruded AZ61 alloy and its composites before and after corrosion tests: (a) AZ61 alloy, and (b) AZ61-3.0GNP composite [4].

The microstructure of the alloys and composites before and after corrosion test are shown in Figures 2.19 and 2.20. Before the corrosion test, the surface of the AZ31 alloy was very neat and grain boundaries could be clearly seen. However, the pitting sites appeared along the grain boundaries after the corrosion test. In addition, the pitting sites increased with the addition of GNPs, and the filiform corrosion type spread away from the pitting sites. The AZ61 alloys and composites exhibited the corrosion rate trend similar to that of the AZ31 alloys and composites. Furthermore, the AZ61 alloy had higher corrosion resistance than that of the AZ31 alloy.

Kukreja, et al [8] gave a completely opposite conclusion about the addition of nano-sized alumina reinforcement which would enhance the corrosion resistance of Mg alloy AZ31B in sodium chloride solution. They pointed out that the size of β phase $Mg_{17}Al_{12}$ and its distribution could influence the corrosion behavior. After adding the alumina nano-sized particle in the AZ31B alloy, the size of β-phase $Mg_{17}Al_{12}$ was reduced and the distribution became more evenly than before adding the reinforcement. In addition, the β phase in an AZ alloy could be either a corrosion barrier or a galvanic cathode accelerating corrosion, depending on the amount and distribution of this phase [8]. Thus, the β phase could be a galvanic cathode and increase the corrosion rate if the volume fraction was small, but it also could act as an anodic barrier to inhibit the overall corrosion of the alloy accordingly to Bland, et al [10]. Figure 2.21 presents the polarization curve for the monolithic AZ31B alloy and AZ31B composite, and Table 2.7 gives the results from polarization plots in Figure 2.21.

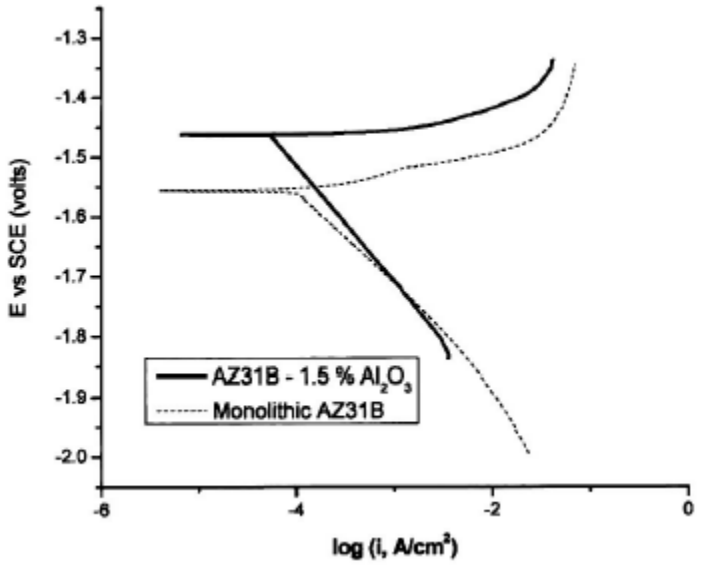

Fig. 2.21. Typical Tafel plots for monolithic AZ31B and AZ31B-1.5% Al_2O_3 in 3.5 wt% NaCl [8].

Table 2.7. Results from polarization plots using Tafel extrapolation method for case of AZ31B and AZ31B-1.5 Al_2O_3 in NaCl solution [8].

Material	ZCP, V (SCE)	β_a, mV/ decade	β_c, mV/ decade	i_{corr}, μA cm^{-2}	Corrosion rate, mm/ year
Monolithic	−1·523	16	176	81	14
AZ31B	−1·485	28	229	211	37
	−1·538	35	209	180	31
AZ31B –	−1·463	5	194	55	9
1·5%Al_2O_3	−1·467	9	191	45	10
	−1·458	11	189	40	7

2.4.4 Electrochemical experimentation of Magnesium based hybrid composites

Magnesium based hybrid composites include not only the particle reinforcement, but the fibre as be the secondary reinforcement. For such applications, the particle only reinforced Mg alloys are not suitable as the addition of particle reduces creep properties, but the fibre-only reinforced Mg composites are more expensive and exhibit anisotropic properties. Therefore, the hybrid composites which contain both fibre and particle reinforcement would be a good choice [10] from the viewpoint of materials design. Creep resistance would be a significant factor for the hybrid composites. In Mondal, et al [10] studied the corrosion behavior of the creep resistant AE42 magnesium alloy hybrid composites. The corrosion rate of different reinforcements combination was investigated by potential dynamic polarization test. 5 wt.% NaCl and pH 11 was the corrosion test environment. After the corrosion test, the unreinforced AE42 alloy performed the best corrosion resistance and the addition of Saffil alumina fibres and/or SiC particle increased its corrosion rate. Meanwhile, the Saffil fibres only reinforced composites had slightly better corrosion resistance than the hybrid composites. However, there were no systematic studies for the corrosion resistance the SiC particles. Table 2.8 lists the detail reinforcement

combinations for each specimen, and Figure 2.22 shows the polarization curves for each specimen.

Table 2.8. Abbreviated nomenclatures used for the composites [10]

Materials used	Abbreviated nomenclature
AE42 + 20 vol.% Saffil short fibres	20% Saffil
AE42 + 15 vol.% Saffil short fibres + 5 vol.% SiC particles	1505 HC
AE42 + 10 vol.% Saffil short fibres + 10 vol.% SiC particles	1010 HC
AE42 + 10 vol.% Saffil short fibres + 15 vol.% SiC particles	1015 HC

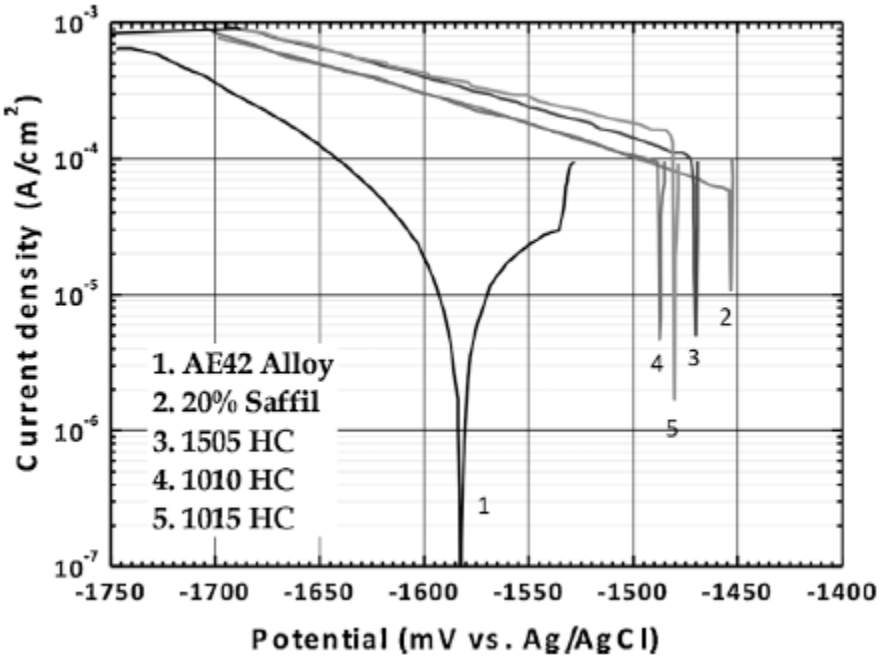

Fig. 2.22. Potential dynamic polarization curves corresponding to the AE42 alloy and its composites [10].

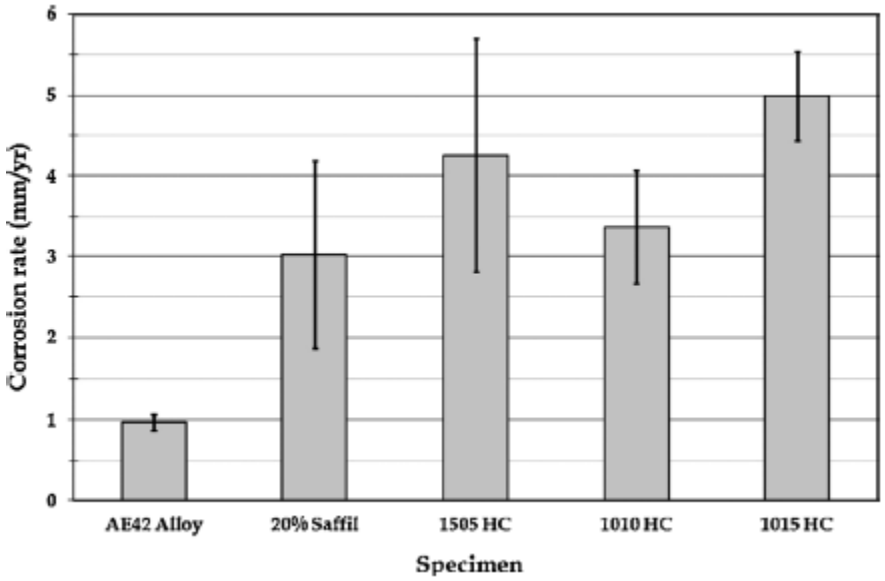

Fig. 2.23. Comparison of the corrosion rate of the AE42 alloy and its composites [10].

From Figure 2.22, it is obviously to see that all the composites could not form a stable quasi-passive film on the surface, and dislocation started right after passing the corrosion potential. Then, there was no protection at all [10]. From Figure 2.23, it can be clearly seen that the addition of reinforcement significantly increased the corrosion rate. The Saffil fibre only reinforced composites had a little bit better corrosion resistance compared with hybrid composites. Figure 2.24 presents the SEM micrograph of the surface before removing the corrosion products of AE42 alloy, 20% Saffil composite and 1010 HC. The surface film on unreinforced AE42 alloy was thin, uniform and dense, but the surface film on composite was thick but irregular and cracked at anywhere. Figure 2.25 shows the SEM micrograph of the surface after removing the corrosion production. The intermetallic Al_4RE phase could be visible at the grain boundaries in Figure 2.25 (a), and a corrosion barrier was formed. In Figure 2.25 (b) and (c), the corrosion attack appeared

uniformly and there was no localized corrosion or galvanic appeared which could increase the corrosion rate. In addition, the precipitates and reinforcement appeared clearly.

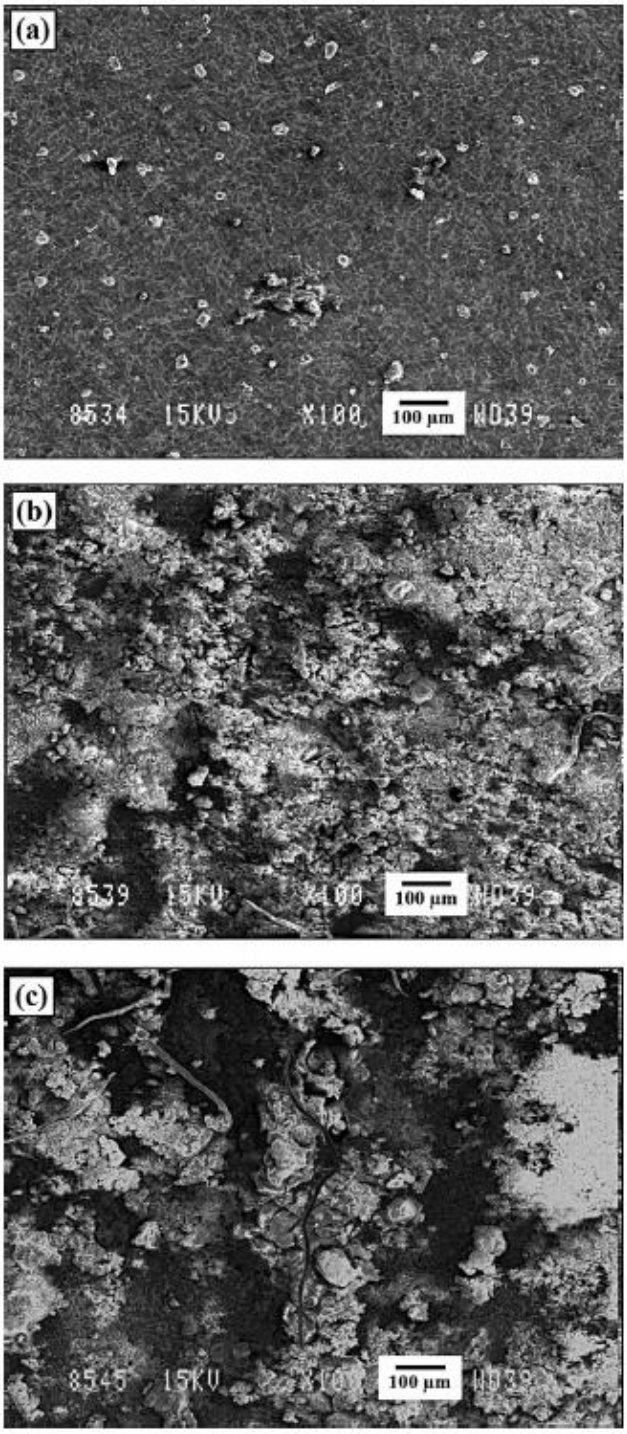

Fig. 2.24. SEM micrographs of the surfaces before removal of the corrosion products corresponding to the (a) AE42 alloy; (b) 20% Saffil composite and (c) 1010 HC [10].

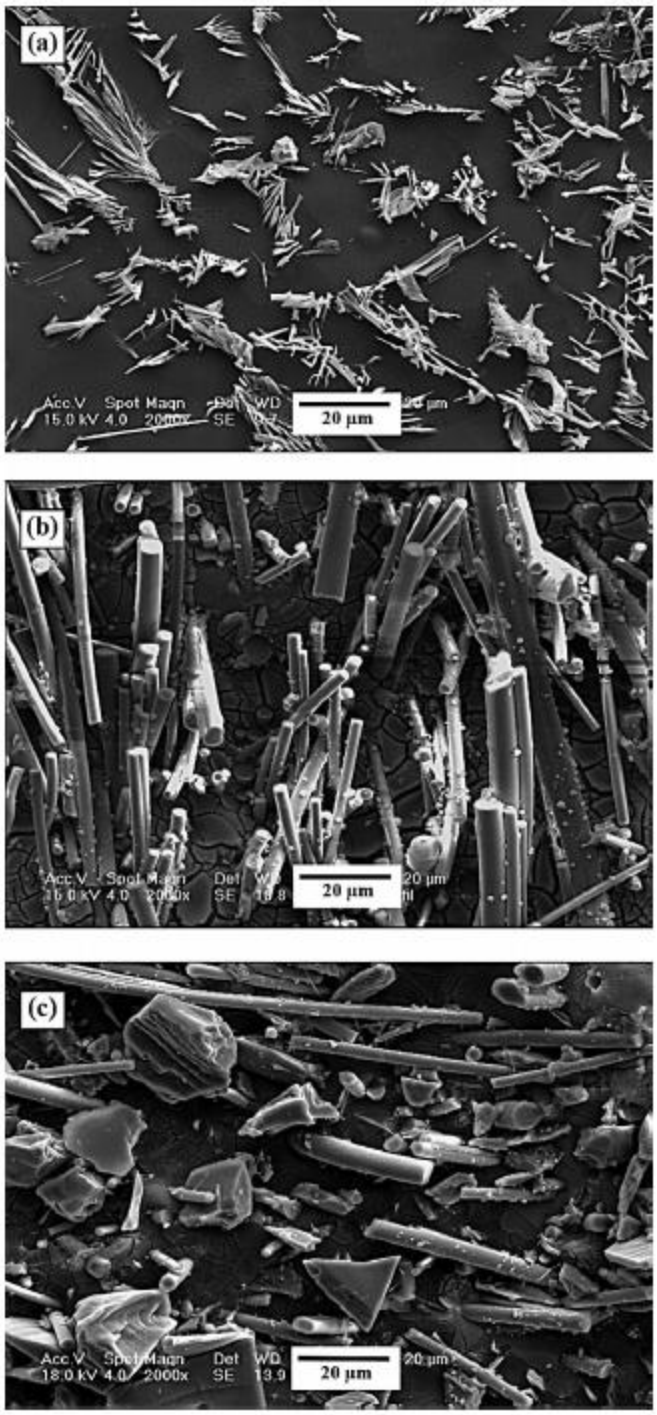

Fig. 2.25. SEM micrographs of the surfaces after removal of the corrosion products corresponding to the (a) AE42 alloy; (b) 20% Saffil composite and (c) 1010 HC (representative picture for the hybrid composites) [10].

2.4.5 Electrochemical experimentation of Magnesium based metal matrix composites with PEO coating

The mechanical properties of Magnesium based MMCs have been widely investigated in the literatures, as the magnesium-based MMCs are lightweight have high mechanical properties than unreinforced magnesium alloys. Furthermore, the creep resistance of MMCs without any surface treatment has been studied, but the research in creep resistance is still in the early stage. However, the similar conclusions generated from all the published research papers so far are that the corrosion resistance is deteriorated by the addition of reinforcements. Thus, the magnesium based MMCs is limited for use when some crucial condition is applied such as aggressive environments, since they are unable to form a stable protective passive layer [11].

Up to date, there are only a very few researchers who tried to add a coating on the magnesium based MMCs to enhance their corrosion behavior. The plasma electrolytic oxidation (PEO) is the coating method which is used to treat the MMCs surface. By carrying out the electrochemical experiment, the resistance of the MMCs with PEO coating is better than the MMCs without any coatings. However, the addition of reinforcement still performs a negative influence for the corrosion resistance. In the work of Arrabal et al [12], the corrosion behavior of AZ92/SiC/0-5-10p composites with PEO coating was investigated. It was pointed out that the coating growth rate was slightly reduced by adding the reinforcement, and the particles within the coating could result in oxidation during the coating process and form a thin reaction product. In addition, the PEO coating protection failed in the form of pitting corrosion area. Mingo, et al [11] had a similar conclusion, that the PEO treated MMCs (AZ91/SiCp) had better corrosion behavior than untreated MMCs. The potential dynamic polarization curves for the tested materials were generated by

immerging in 3.5 wt.% NaCl solution. Figure 2.26 shows the polarization curves and the current density as a function of SiCp vol.% for AZ91/SiC/0-10p and AZ91/SiC/0-10P-PEO. The SEM micrographs of the AZ91 alloy and AZ91/SiC/5p cross sections after 8 days of exposure in 3.5 wt.% NaCl aqueous solution are given in Figure 2.27, and the cross sections for the same specimens with the PEO coating after corrosion test are shown in Figure 2.28.

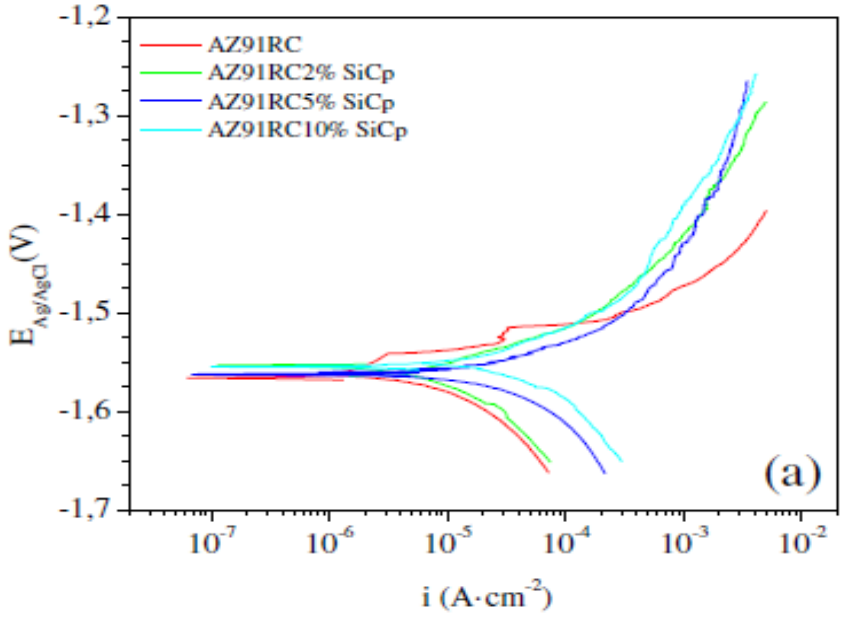

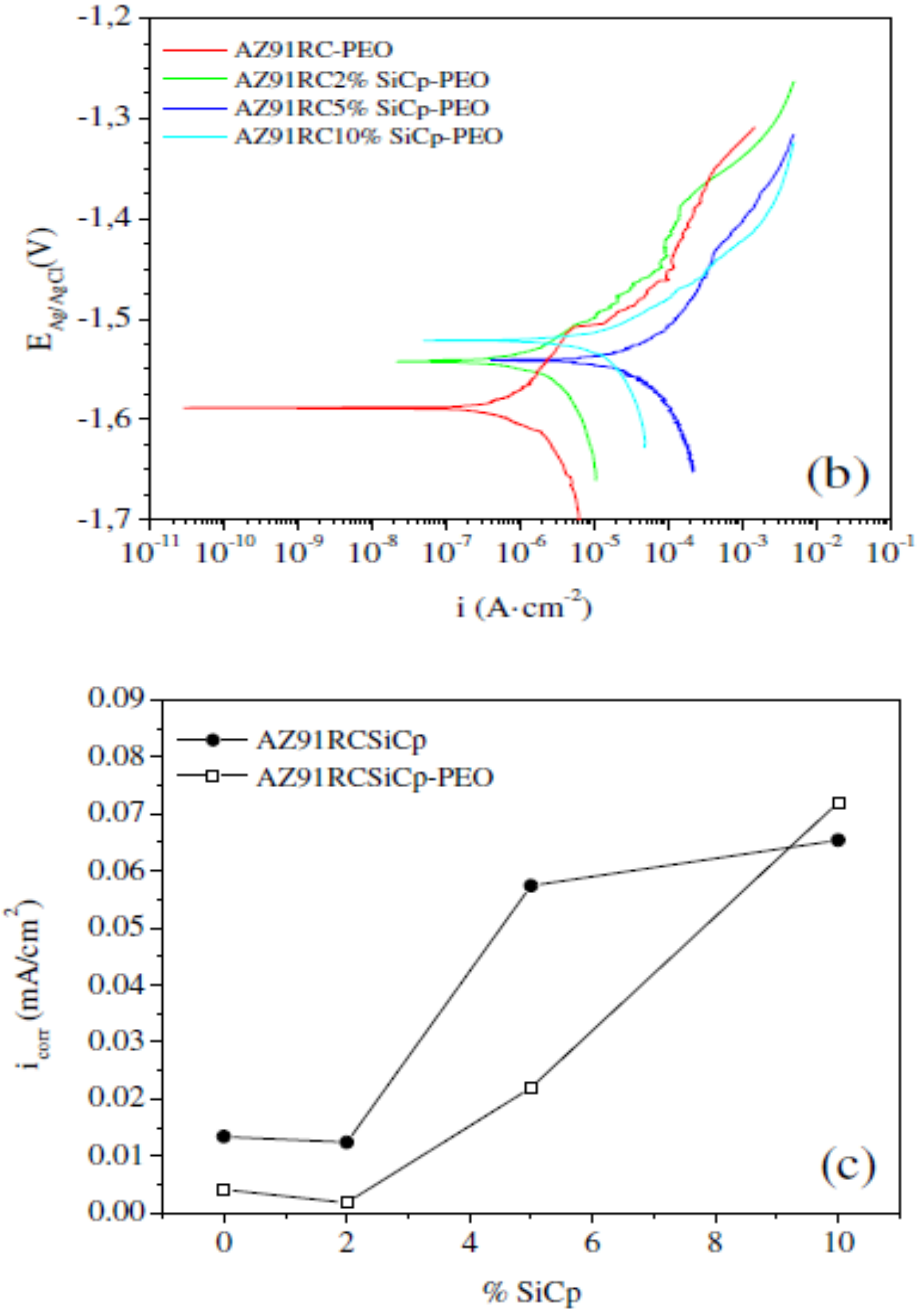

Fig. 2.26. Potential dynamic curves after 1 h of immersion in NaCl 3.5 wt.% for (a) AZ91/SiC/0-10p and (b) AZ91/SiC/0-10p-PEO. (c) Corrosion current density as a function of SiCp vol% for AZ91/SiC/0-10p and AZ91/SiC/0-10p-PEO [11].

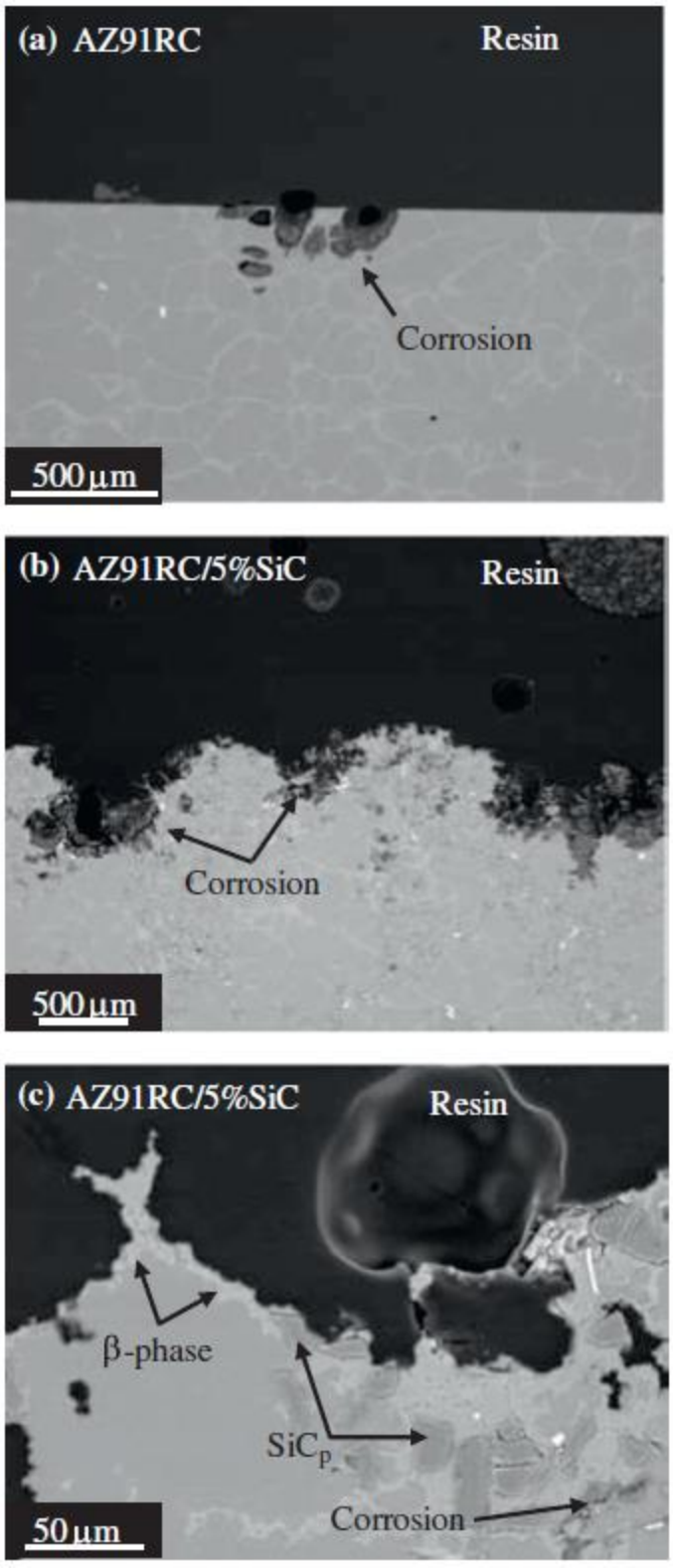

Fig. 2. 27. Scanning electron micrographs of the cross sections after 8 days of exposure in NaCl 3.5 wt.% aqueous solution (a) AZ91 and (b, c) AZ91/SiC/5p [11].

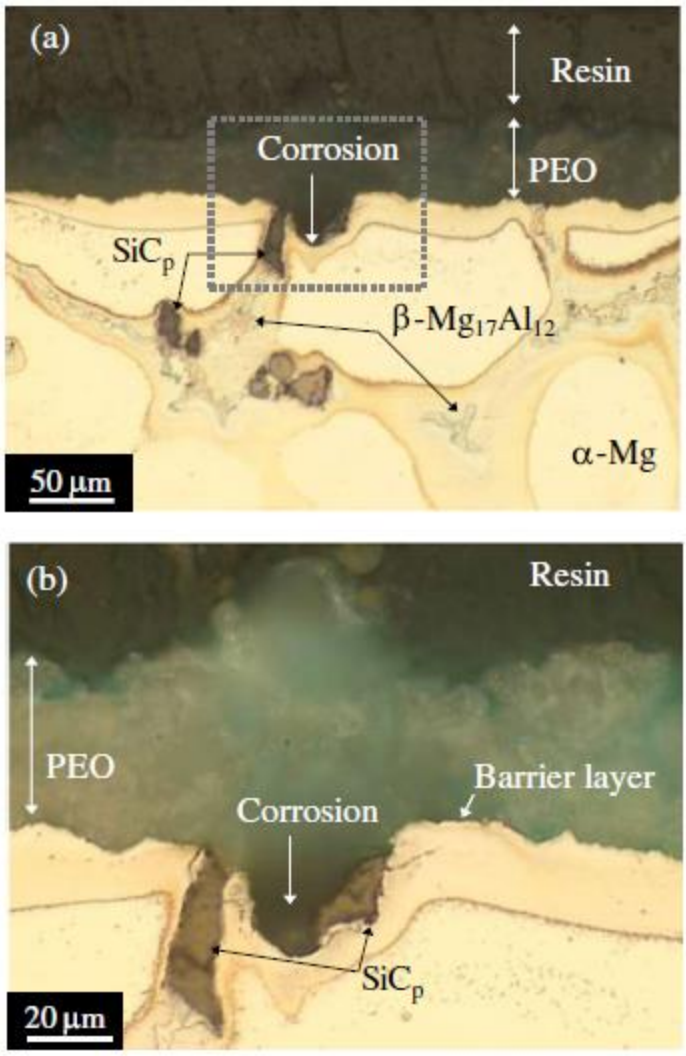

Fig. 2.28. Optical micrographs of the cross sections after 8 days of exposure in NaCl 3.5 wt.% aqueous solution AZ91/SiC/5p-PEO [11].

As shown in Figure 2.27 (a), the β phase remain unattacked and the α phase was corroded. However, in the Figure 2.27 (b) and (c) indicated that the continuity of β-phase was interrupted by SiC particles, which affected the corrosion barrier, and led to higher corrosion rates compared with that of the unreinforced alloy. From Figure 2.28, it could easily find out that the corrosion happened at the interface of coating and substrate. In addition, the corrosion appeared in the rich SiC particle region. Thus, the volume fraction of the reinforcement was a significant factor of the MMCs corrosion behavior [11].

2.5. Micro Galvanic Corrosion of Magnesium-based Metal Matrix Composites

In the above sections, the galvanic corrosion at the interface between particle or fibre and matrix alloy was discussed. It was found out that the galvanic corrosion had no significant effect on overall corrosion behavior. Lopez et al [13] showed a high purity magnesium based MMC with 1 vol.% micron sized silicon carbide particle reinforcement could be produced by magnetron sputtering magnesium on to a substrate surface impregnated with particles [13]. Due to the special preparation procedure, the magnesium has a relatively high corrosion resistance. Then, the specimens were immerged in 3.5 wt.% NaCl solution for carrying out the potential dynamic polarization test. The results indicated that there was no significant micro galvanic corrosion appears, which suggested that the silicon carbide had a good compatibility as a candidate to be reinforced in magnesium alloys-based composites. In Figure 2.29, the SEM of MMC surface before exposure to saline solution is shown. Due to the low fraction of the reinforcement in the MMC, the magnesium film was uniform across the microscopic surface, which led to fine-grained layers. Figure 2.30 shows the interface between a silicon carbide particle and the magnesium film, which revealed the silicon carbide particle located tightly with the magnesium matrix.

Fig. 2.29. Scanning electron micrograph showing the surface of the MMC before exposure to saline solution: the surface was originally in contact with lacquer during preparation of the MMC [13].

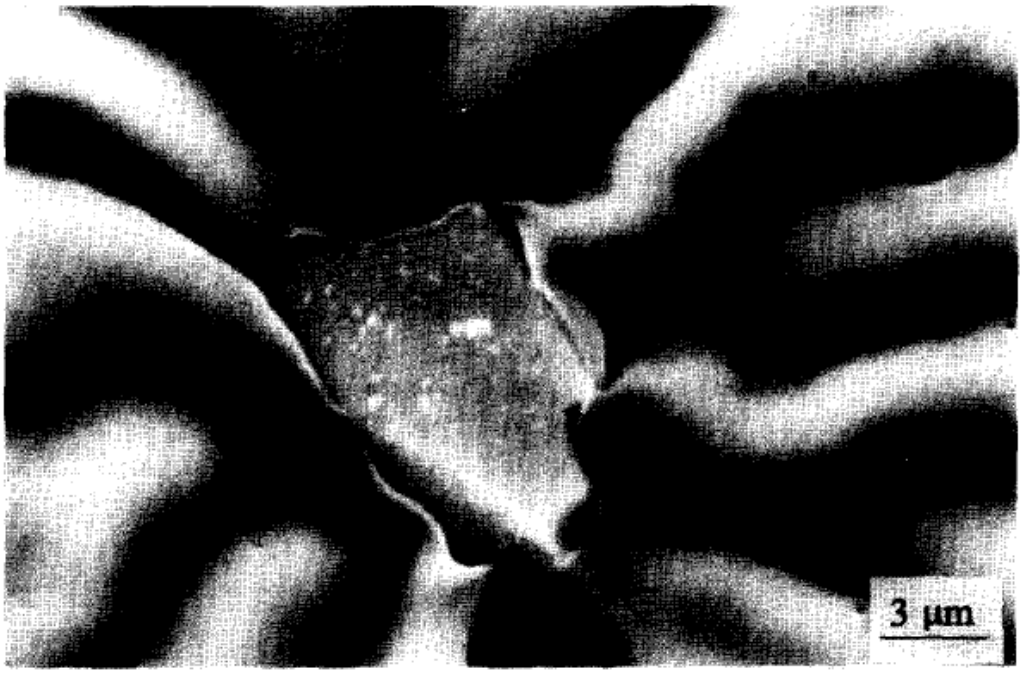

Fig. 2.30. Scanning electron micrograph revealing the interface between a silicon carbide particle and the magnesium film [13].

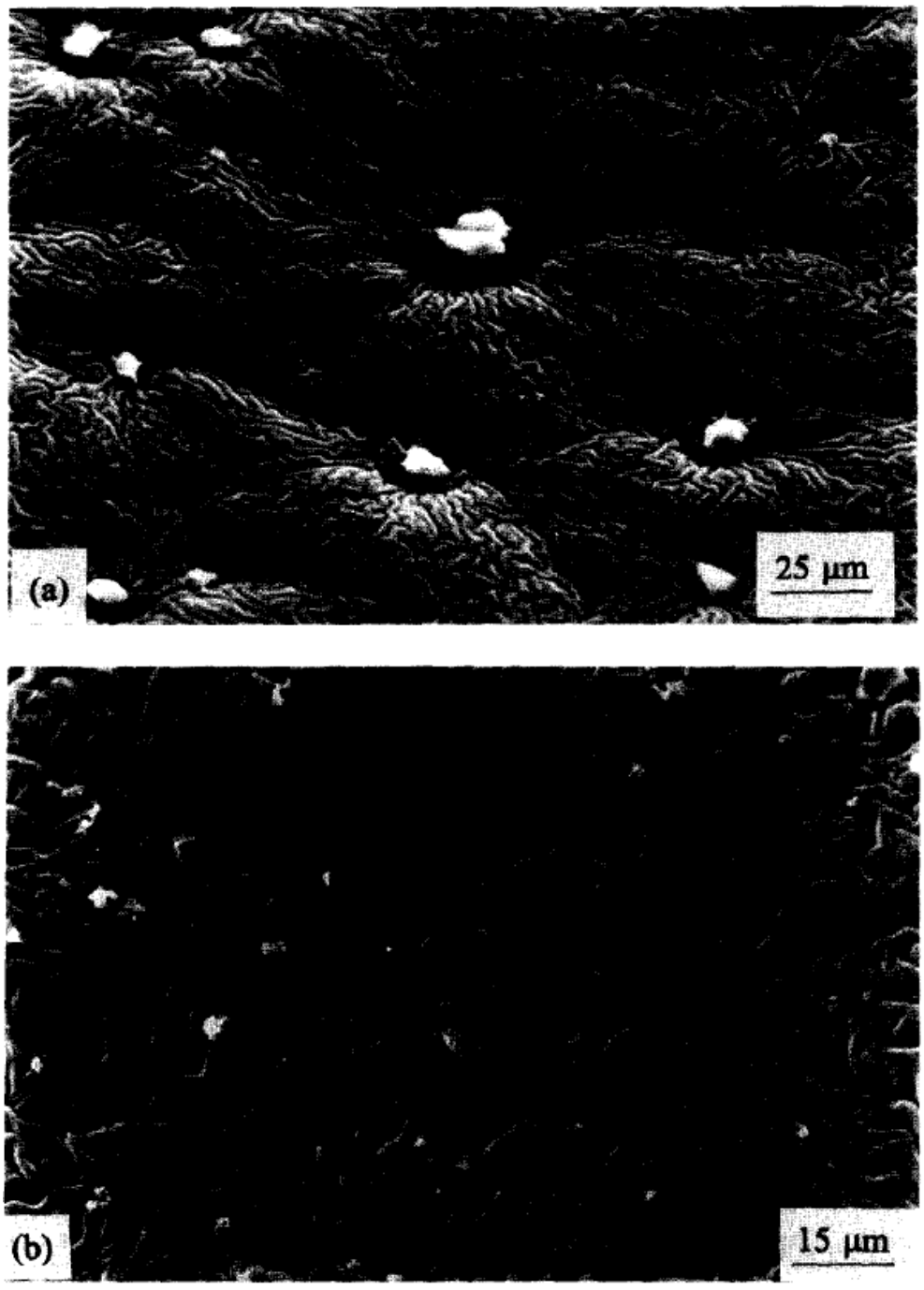

Fig. 2.31. Scanning electron micrographs of the surface of the MMC following exposure to 3.5 wt. % NaCl solution, of pH 6.5, for: (a) 1 h; and (b) 36 h [13].

Based on the SEM observation (Figure 2.31(a)), the corrosion attacks on the surface of the MMC after 1-hour immersion in NaCl solution was negligible. After 36 hours immersion, the surface appeared tarnished and relatively unchanged [13]. The results showed there was no evidence found for micro galvanic corrosion between the silicon carbide particles and the magnesium matrix which enhanced the overall corrosion behavior of the MMC.

2.6. Summary and conclusions

The corrosion behavior of magnesium based MMCs with and without PEO coating has been reviewed. A conclusion from the past research was that the corrosion rate is increased with the addition of micron-sized reinforcement. But, one article presents the results showing the corrosion behavior of magnesium alloy AZ31B could be enhanced by the addition of nano sized alumina particle, since the reinforced particles reduced the volume fraction of β phase ($Mg_{17}Al_{12}$) in the magnesium matrix. By applying the Plasma electrolytic oxidation (PEO) coating on the composite surface, the corrosion resistance of Mg-based MMCs with the low volume fraction of the reinforcement increase dramatically. However, the large addition of reinforcements might influence the coating growth during the PEO process and consequently affect the overall corrosion behavior of the MMCs. In terms of corrosion mechanisms, the micro galvanic corrosion between particles and magnesium matrix has almost no contribution to enhance the overall corrosion behavior of MMCs. Further studies on corrosion mechanisms and effects of PEO coatings on the Mg-based composites reinforced by both micron and/or nano-sized reinforcements need to be carried out.

2.7. References

[1] Lloyd, D. J. (1994). Particle reinforced aluminium and magnesium matrix composites. International Materials Reviews, 39(1), 1-23.

[2] Bakkar, A., & Neubert, V. (2007). Corrosion characterisation of alumina–magnesium metal matrix composites. Corrosion science, 49(3), 1110-1130.

[3] Pardo, A., Merino, S., Merino, M. C., Barroso, I., Mohedano, M., Arrabal, R., & Viejo, F. (2009). Corrosion behaviour of silicon–carbide-particle reinforced AZ92 magnesium alloy. Corrosion Science, 51(4), 841-849.

[4] Rashad, M., Pan, F., Asif, M., & Chen, X. (2017). Corrosion behavior of magnesium-graphene composites in sodium chloride solutions. Journal of Magnesium and Alloys.

[5] Bakkar, A., & Neubert, V. (2009). Corrosion behaviour of carbon fibres/magnesium metal matrix composite and electrochemical response of its constituents. Electrochimica Acta, 54(5), 1597-1606.

[6] Tiwari, S., Balasubramaniam, R., & Gupta, M. (2007). Corrosion behavior of SiC reinforced magnesium composites. Corrosion science, 49(2), 711-725.

[7] Gupta, M., & Wong, W. L. E. (2015). Magnesium-based nanocomposites: Lightweight materials of the future. Materials Characterization, 105, 30-46.

[8] Kukreja, M., Balasubramaniam, R., Nguyen, Q. B., & Gupta, M. (2009). Enhancing corrosion resistance of Mg alloy AZ31B in NaCl solution using alumina reinforcement at nanolength scale. Corrosion Engineering, Science and Technology, 44(5), 381-383.

[9] Bland, L. G., Scully, L. C., & Scully, J. R. (2017). Assessing the Corrosion of Multi-Phase Mg-Al Alloys with High Al Content by Electrochemical Impedance, Mass Loss, Hydrogen Collection, and Inductively Coupled Plasma Optical Emission

Spectrometry Solution Analysis. Corrosion, 73(5), 526-543.

[10] Mondal, A. K., Blawert, C., & Kumar, S. (2015). Corrosion behaviour of creep-resistant AE42 magnesium alloy-based hybrid composites developed for powertrain applications. Materials and Corrosion, 66(10), 1150-1158.

[11] Mingo, B., Arrabal, R., Mohedano, M., Pardo, A., & Matykina, E. (2017). Corrosion and wear of PEO coated AZ91/SiC composites. Surface and Coatings Technology, 309, 1023-1032.

[12] Arrabal, R., Pardo, A., Merino, M. C., Mohedano, M., Casajús, P., Matykina, E., ... & Thompson, G. E. (2010). Corrosion behaviour of a magnesium matrix composite with a silicate plasma electrolytic oxidation coating. Corrosion Science, 52(11), 3738-3749.

[13] Nunez-Lopez, C. A., Habazaki, H., Skeldon, P., Thompson, G. E., Karimzadeh, H., Lyon, P., & Wilks, T. E. (1996). An investigation of microgalvanic corrosion using a model magnesium-silicon carbide metal matrix composite. Corrosion science, 38(10), 1721-1729.

CHAPTER 3

Corrosion and Microstructure of As-Cast Magnesium Alloy AM60-based Hybrid Nanocomposite

3.1. Introduction

Magnesium (Mg) based materials have become one of the most significant candidates for structural engineering applications due to their light weight, high thermal conductivity and good ductility. In automotive industry, magnesium alloys are widely used for building vehicle components such as instrumental panels, cylinder head covers, intake manifolds, transfer cases and so on. Further expansion of new magnesium-based engineering applications is still on-going owing to the stringent government regulations on auto emissions and weight reduction. Hence, magnesium-based metal matrix composites (MMCs) including fibre reinforced composites, particle reinforced composites and fibre-particle hybrid reinforced composites are emerging and being investigated for the improvement of mechanical properties of monolithic matrix alloys, including high yield strength, tensile strength, creep resistance, thermal shock resistance and wear resistance [1-6]. But, the introduction of foreign particles and/or fibre could deteriorate the corrosion resistance of magnesium alloys.

Bakkar and Neaubert [7] fabricated the microns-sized alumina fibre (20 vol%) reinforced magnesium alloy AS41 based metal matrix composite and investigated its corrosion behavior in 100 ppm sodium chloride (NaCl) solution for 3 hours by employing electrochemical tests and potential dynamic polarization diagrams. Their results showed that, compared with the matrix alloy, the corrosion resistance of the composite was reduced No evidence for the galvanic corrosion appeared at the interface between fibre and matrix

alloy was found. Bakkar and Neaubert [8] also studied the corrosion of the carbon fibre (25%) reinforced magnesium alloy (AS41) based composites. They observed that, after submerging the carbon fibre containing composite in 100 ppm NaCl solution, the presence of micron-sized carbon fibres reduced the corrosion resistance of AS41 alloy with increasing the corrosion current density. In the study by Shruti Tiwari [9], micron-sized silicon carbide (SiC) particles was introduced to reinforce the pure magnesium matrix., The corrosion behaviors of the Mg–SiC composites, containing 6 and 16 vol.% SiC particulate reinforcement (Mg-6SiC and Mg-16SiC) were investigated by submerging them into 1M NaCl solution. The results of potential-dynamic polarization tests indicated that the corrosion resistance of the pure magnesium decreased with the addition of micron-sized silicon carbide particles, because the particle interrupted the continuity of magnesium matrix. The electrochemical behaviors of magnesium alloys (AZ31 and AZ61) and their composites reinforced with graphene nanoplatelets (GNPs) in micron diameters were investigated in 3.5% NaCl solution by the polarization method [9]. The presence of graphene nanoplatelets in different matrices decreased corrosion resistance of the composites due to the occurrence of galvanic corrosion. This effect increased with increasing graphene nanoplatelets contents.

In the past few years, magnesium alloy-based hybrid composites are emerging since the combined advantages of different sizes of short fibres, and particles provide a high degree of design freedom, which enable fibres to increase strengths and particles to improve wear resistance [6]. Mondal et al [11] studied the corrosion behavior of creep resistant AE42 magnesium alloy hybrid composites containing micron-sized Al_2O_3 short fibres and SiC particles. The corrosion rates of different reinforcements combination were

evaluated by potential dynamic polarization tests in 5 wt.% NaCl solution. Their results showed that the tested composites exhibited much higher corrosion rates as compared to that of the unreinforced alloy. The addition of micron sized SiC particles increased the corrosion rates of the hybrid composites by over 30%. Zhang et al [6] pointed out that the introduction of micron-size reinforcements into the hybrid composite adversely affected the plasticity of Mg matrix alloys due to particle or fibre cracking and void formation at reinforcement-matrix interface leading to accelerated failure. Recently, the study by Zhou et al [12] demonstrated that the replacement of the micron-sized particles with the nanoparticles in the Mg-based hybrid composite effectively recovered the ductility of the composite by almost 120%. The presence of the low dislocation density in the matrix of the Magnesium-based hybrid nanocomposite (MHNC) should be responsible for the ductility restoration. However, there is no information about the corrosion behavior of the MHNC in the open literature.

In the present work, the microstructures of the monolithic matrix alloy AM60, its micron fibre-only composite and the MHNC were analyzed by the optical (OM) and scanning electron microscopies (SEM) and X-ray energy dispersive spectroscopy (EDS). The corrosion behavior of the monolithic matrix alloy AM60, its micron fibre-only composite and the MHNC were assessed by potentiodynamic polarization tests. The changes of the surface morphologies of the tested matrix alloy and composites were analyzed by electron scanning microscopy, and corrosion products were identified by the (EDS) analyses.

3.2. Experimental Procedure

3.2.1. Composites Preparation

Magnesium alloy AM60 with a chemical composition (wt.%) of 6.0Al-0.22Zn-0.4Mn-0.1Si-0.01Cu-0.004Fe-0.002Ni-Mg was chosen as matrix alloy. Nano-sized Al_2O_3 ceramic particles with an average particulate size of 100 nm (US Research Nanomaterials, Inc., USA), and Al_2O_3 short fibres (Morgan Advanced Materials, United Kingdom) with an average diameter of 4 µm and length of 50 µm were employed as raw materials for the preparation of hybrid reinforcements since they are relatively inexpensive and possess adequate properties.

The preparation steps for fabrication of the hybrid preforms involve: mixing the ceramic short fibres and particles, introducing the binding compounds, forming the preform shape under pressure, drying, and sintering. In the hybrid preform, the fibres serve as the skeleton for a cellular structure. The content level of the fibre was pre-determined based on the desired amount of porosity in the cellular solid. The particulate reinforcements were dispersed in the pores present in the cellular solid. The content, size and type of the ceramic reinforcements were adjusted to yield the required quantity, and shape of preform. In addition, for the purpose of a comparative study of the hybrid preform characteristics; a pure fibre preform was also fabricated using the same process without adding particulate reinforcements.

During composite fabrication, a hybrid preform was first preheated to 700 ^{0}C. Then, molten matrix alloy AM60 at 750 ^{0}C infiltrated into the preheated preform under an applied pressure of 90 MPa. The pressure was maintained at the desired level for 30 seconds. After squeeze casting, a cylindrical disk of single or dual-phase reinforced composite with 3

vol.% Al_2O_3 nano-sized particles and 7 vol.% Al_2O_3 fibres, was obtained. In the hybrid composite, the short fibres constituted the primary reinforcement phase, and the particles served as the secondary reinforcement phase. For the purpose of comparisons, three different types of 7 vol.% micron fibre/AM60, and (7 vol.% Fibre+3 vol.% nano-particle)/AM60 composites were prepared, which were named the fibre-only composite (7FC), and the MHNC-7F3NP, respectively. More details on the process for fabricating the composites are given in references 6 and 12.

3.2.2. Electrochemical Experimentation

Electrochemical studies were carried out by using EC-LAB SP-150 electrochemical apparatus with corrosion analysis EC-lab software. A three-electrode cell was set up through assigning the samples as working electrode, Ag/AgCl/sat'd KCl electrode as a reference electrode and a Pt metal electrode as counter-electrode. At the beginning of experiments, samples were held in a salt solution allowing the open circuit potential to settle to a constant value. Potentiodynamic polarization scans were conducted at a rate of 10mv/s from -0.5v versus open circuit potential in a more noble direction up to 0.5v versus the reference electrode. Machined samples were ground with silicon carbide papers with various grades from 280 to 2500 grit, and then cleaned in acetone, rinsed with deionized water and dried prior to potentiodynamic polarization. The values of corrosion potential (E_{corr}) and current density (i_{corr}) was determined at the intersection between the anodic and cathodic Tafel slopes, which were extrapolated by the linear parts of the polarization curves.

3.2.3. Microstructure Analysis

Specimens were sectioned, mounted, and polished from the center of cast cylindrical specimens with a diameter of 100 mm and a height of 20 mm and prepared following the standard metallographic procedures. Due to indistinct grain boundaries in the as-cast microstructure of AM60 alloy and FC and MHNC composites, which were disguised by the β intermetallics ($Mg_{17}Al_{12}$), it was necessary to subject the as-cast specimens to an anti-germination solution heat treatment (T4), which dissolved the β intermetallics and revealed the grain boundaries. The detailed features of the microstructure were characterized at high magnifications using a FEI Quanta 200 FEG (Tokyo, Japan) scanning electron microscope (SEM) with a maximum resolution of 100 nm in a backscattered (BSE) mode / l μm in X-ray diffraction mapping mode, and maximum useful magnification of 30,000. Energy dispersive X-ray analyses were used to define the elements distribution. To maximize the composition reading of the energy dispersive spectroscopy (EDS) data, an etchant was applied to the polished specimens for microscopic examination. The corroded surfaces and subsurface of the unreinforced alloy AM60, and the 7FC and MHNC-7F3NP composites were analyzed by the SEM in secondary electron (SE) mode to ascertain their corrosion mechanisms.

3.3. Results and Discussion

3.3.1. Microstructure Analysis

The OM analyses revealed the grain structures in the etched microstructure of the unreinforced as-cast AM60, the 7FC and MHNC-7F3NP composites before corrosion testing, as shown in Figure 3.1. The grain sizes between the unreinforced alloy and the composites were quite different. Table 3.1 gives the measured grain sizes for the

unreinforced matrix and the composites. The introduction of the micron-sized fibres and nano-sized particles refined grain structure in the composites. As can be seen from Figure 3.1 and the data in Table 3.1, compared to the matrix alloy, the grain size of the 7FC and MHNC-7F3NP composites decreased significantly, while the variation of grain sizes seemed less significant after the addition of the fibres and particles. The grain size decreased from 65 µm for the matrix alloy AM60 to 37 µm for the 7FC composite by 43%. The introduction of the nano particles (3 vol.%) resulted in a minor reduction in the grain size from 37 to 26 µm. Also, Figure 3.1 (b) and (c) reveals a homogeneous distribution of the reinforcements throughout the matrices in the 7FC and MHNC-7F3NP composites at the macroscopic scale.

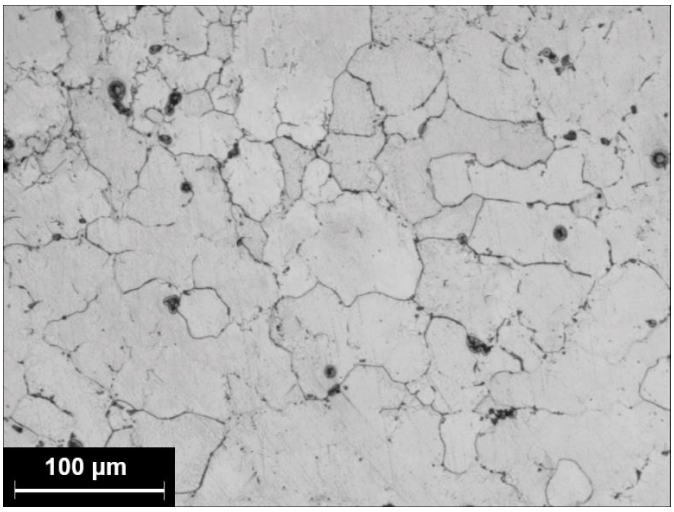

(a)

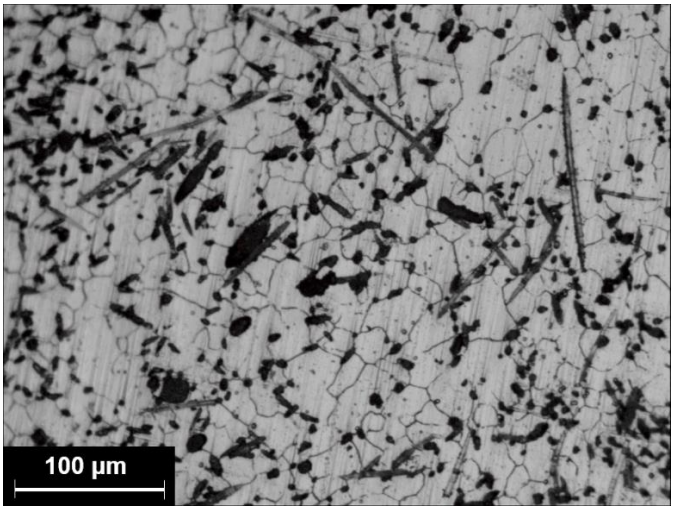

(b)

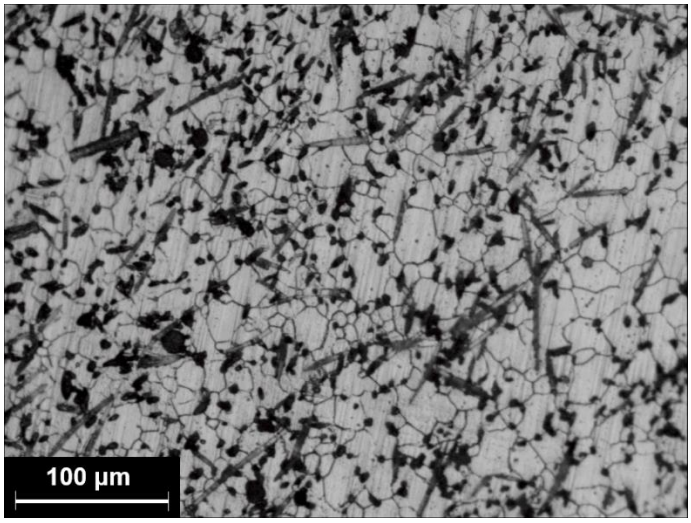

(c)

Fig. 3.1. Optical micrographs showing grain structures of etched (a) unreinforced matrix alloy AM60, (b) 7FC, and (c) MHNC-7F3NP.

Table 3.1 Measured grain sizes of the unreinforced matrix alloy, and the 7FC and MHNC-7F3NP composites

Material	**AM60**	**7FC**	**MHNC-7F3NP**
Grain Size (µm)	65	37	26

Figure 3.2 presents the backscattered SEM images showing the etched microstructure of the unreinforced as-cast AM60 in details at a high magnification. The results of the EDS analysis as shown in Figure 3.3 and the element analysis in atomic

percentages listed in Table 3.2 indicated that the microstructure of the etched AM60 consisted of primary α-Mg grains (dark contrast), eutectic β-$Mg_{17}Al_{12}$ phases (bright contrast), and Al-Mn intermetallics (white spots). The size of the primary α-Mg grains was around 65 μm as also revealed by the OM analysis. The eutectic β-$Mg_{17}Al_{12}$ phases, and Al-Mn intermetallics were present in the form of isolated fine particles surrounding the boundaries of the primary α-Mg grains.

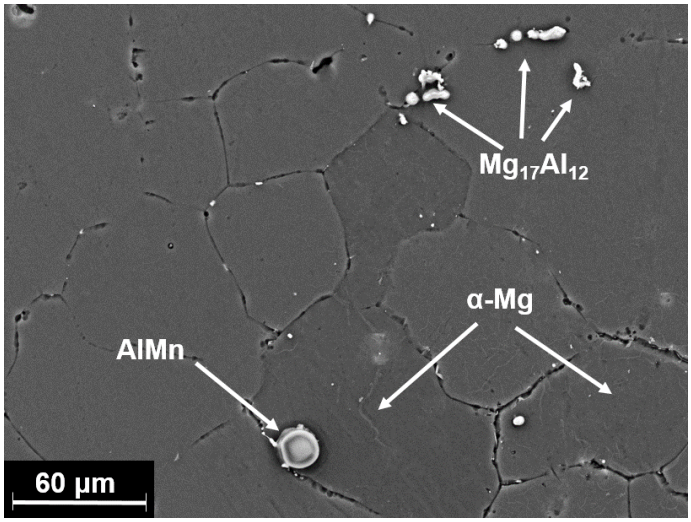

Fig. 3.2. SEM micrographs in BSE mode showing constituent phases in microstructure of etched unreinforced matrix alloy AM60.

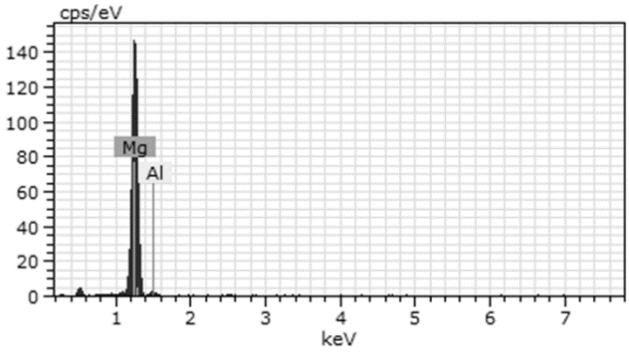

(a)

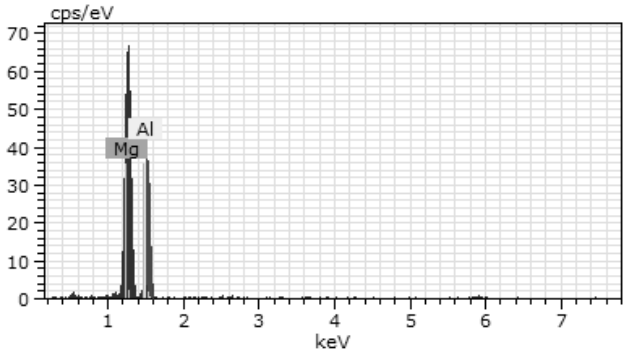

(b)

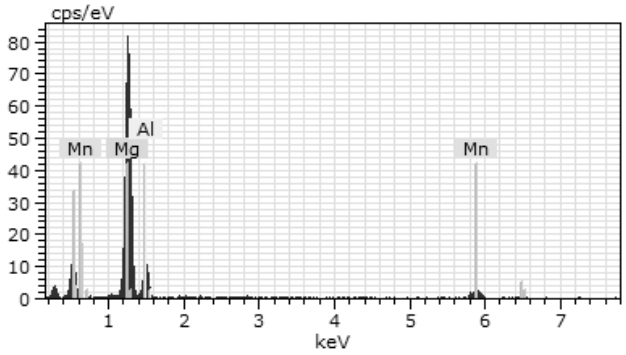

(c)

Fig. 3.3. EDS spectra (a), (b) and (c) for the areas containing α-Mg grains (dark contrast), and β-$Mg_{17}Al_{12}$ phases (bright contrast), and Al-Mn intermetallic (white spots) as shown in Figure 2, respectively.

Table 3.2. Elements in analyzed phases shown in Figure 3.2

Phase	Element	Atomic (at. %)
α-Mg	Mg	97.25
	Al	2.75
$Mg_{17}Al_{12}$	Mg	52.57
	Al	47.43
AlMn	Mg	73.12
	Al	18.53
	Mn	8.35

Figures 3.4 and 3.5 gives SEM micrographs in BSE mode and EDS spectra showing constituent phases the microstructure of the 7FC and MHNC-7F3NP composites at high magnifications, respectively. Table 3.3 and 3.4 list the results of the element analysis for the constituent phases detected in the 7FC and MHNC-7F3NP composites. There were the

same types of the constituent phases, i.e., primary α-Mg grains (dark contrast), eutectic β-$Mg_{17}Al_{12}$ phases (bright contrast), and Al-Mn intermetallics (white spots), in the matrix microstructure of the 7FC composite. Compared to those of the unreinforced AM60, the SEM results verified the reduction in grain sizes with the introduction of the reinforcements. Also, the refinement of both the eutectic β-$Mg_{17}Al_{12}$ phase and Al-Mn intermetallic appeared in the microstructure of both the 7FC and MHNC-7F3NP composites. The attachment of the detected eutectic β-$Mg_{17}Al_{12}$ phase and Al-Mn intermetallic to the surface of the fibres implied that they might be nucleate on the reinforcement. This was because Al_2O_3 fibres and particles preheated to 700 ^{0}C provided a heat source and slowed down the cooling of the melt around them, where the last solidification took place during the pressurized infiltration of the molten AM60 into the alumina fibre and particle preform. The high Al phases, i.e., eutectic β-$Mg_{17}Al_{12}$ phase and Al-Mn intermetallic, tended to segregate close to the surface of the Al_2O_3 fibres and particles. Similar phenomena were also observed by Zhang et al [1] and Bakkar and Neubert [7] for Mg-Al alloys.

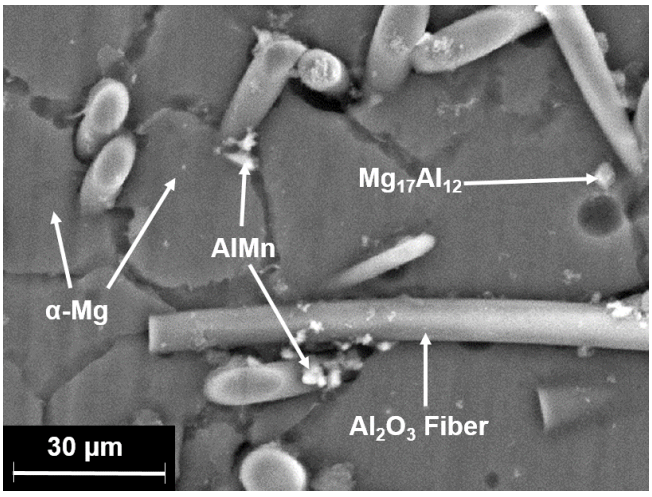

(a)

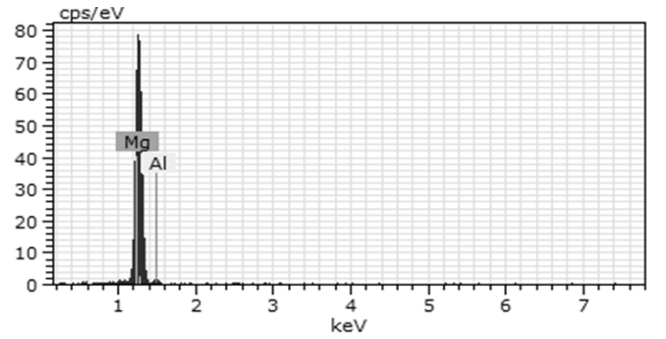

(b)

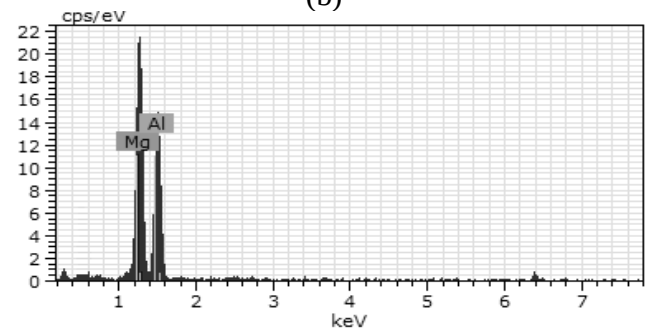

(c)

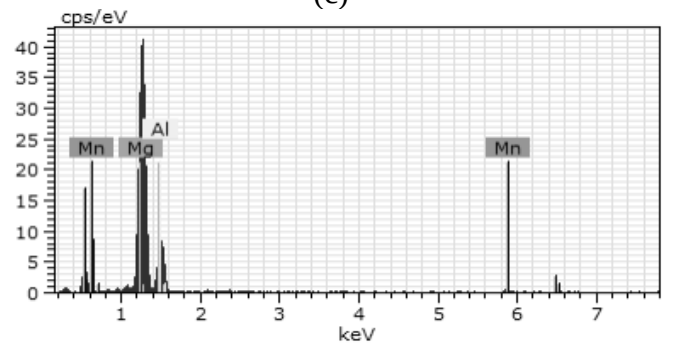

(d)

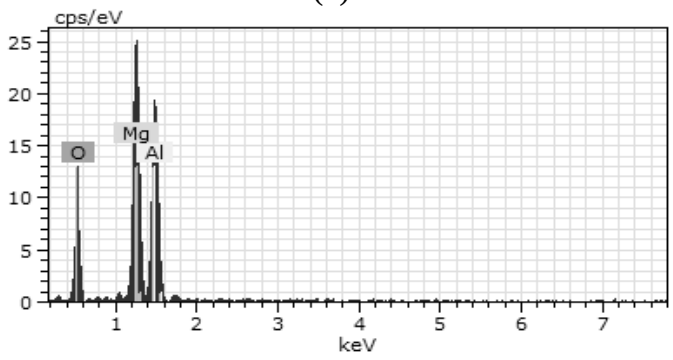

(e)

Fig. 3.4. (a) SEM micrographs in BSE mode showing constituent phases in microstructure of the 7FC composite; EDS spectra (b), (c) and (d) for the areas containing α-Mg grains (dark contrast), and β-$Mg_{17}Al_{12}$ phases (bright contrast), and Al-Mn intermetallic (white spots) as shown in (a), respectively; EDS spectrum (e) for the Al_2O_3 fibre.

Table 3.3. Elements in analyzed phases shown in Figure 3.4

Phase	Element	Atomic (at. %)
α-Mg	Mg	96.38
	Al	3.62
$Mg_{17}Al_{12}$	Mg	51.79
	Al	48.21
AlMn	Mg	74.84
	Al	16.22
	Mn	8.94
Al_2O_3 Fibre	Mg	21.33
	Al	29.44
	O	49.23

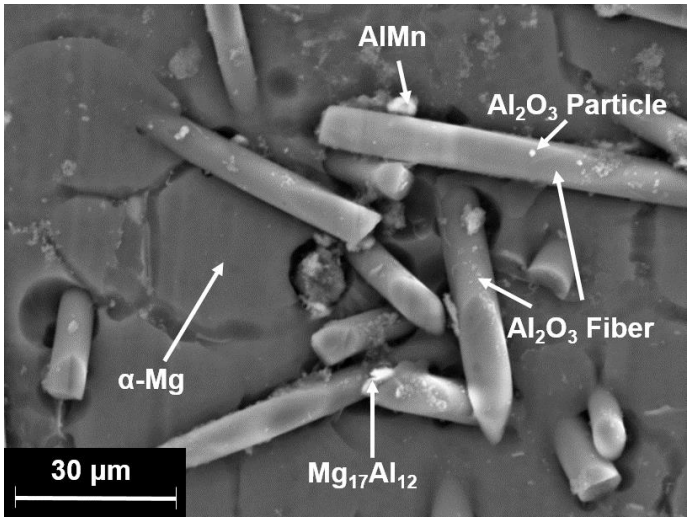

(a)

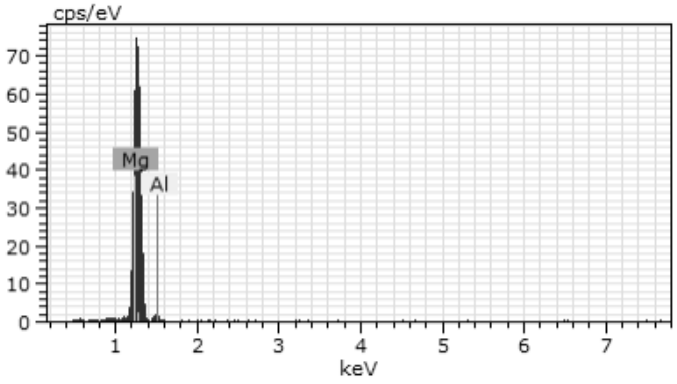

(b)

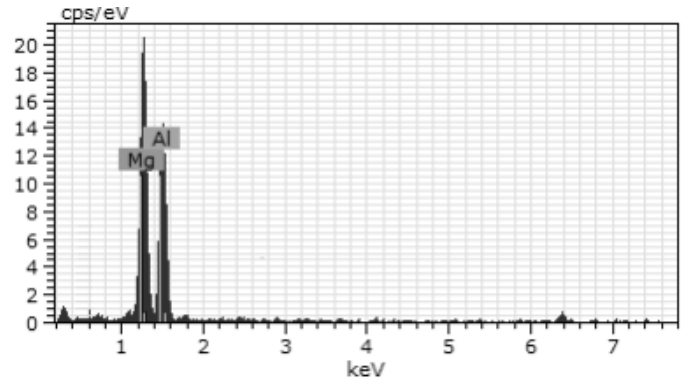

(c)

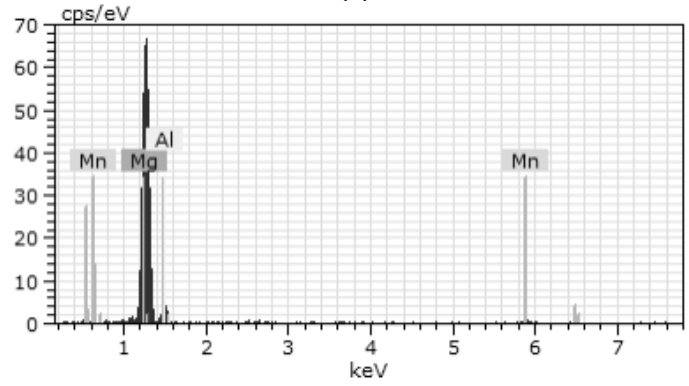

(d)

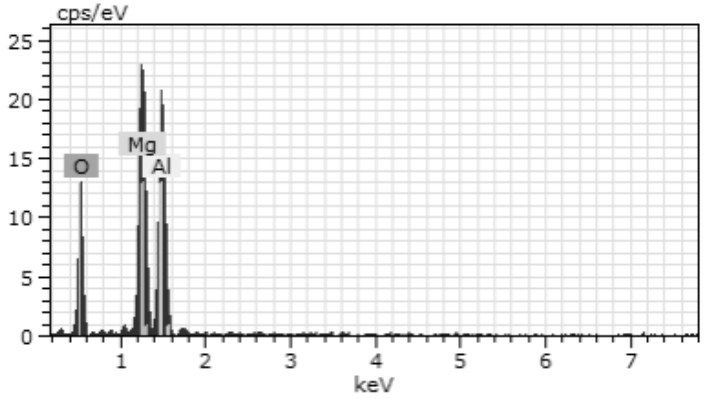

(e)

Fig. 3.5. (a) SEM micrographs in BSE mode showing constituent phases in microstructure of the MHNC-7F3NP composite; EDS spectra (b), (c) and (d) for the areas containing α-Mg grains (dark contrast), and β-$Mg_{17}Al_{12}$ phases (bright contrast), and Al-Mn intermetallic (white spots) as shown in (a), respectively; EDS spectrum (e) for the Al_2O_3 fibre.

Table 3.4. Elements in analyzed phases shown in Figure 3.5

Phase	Element	Atomic (at. %)
α-Mg	Mg	97.77
	Al	2.23
$Mg_{17}Al_{12}$	Mg	54.34
	Al	45.66
AlMn	Mg	72.13
	Al	19.58
	Mn	8.29
Al_2O_3 Fibre	Mg	20.48
	Al	30.15
	O	49.37

3.3.2. Electrochemical Tests

Figure 3.6 shows the polarization curves of the as-cast unreinforced alloy AM60, and 7FC and MHNC composites. Potentiodynamic polarization curves, measured in 3.5 wt.% NaCl solution, were similar for the three tested materials. A summary of the results of potentiodynamic corrosion tests was given in Table 3.5. The corrosion potentials were in the range from – 1.417 to – 1.441 V(SCE), typical of magnesium alloys. The curves indicated film breakdown at potentials immediately above the corrosion potential with characteristically low apparent Tafel slopes of about 52.9 – 29.1 mV decade. At high current densities, the curves were affected by a potential drop due to the solution resistance, and on the cathodic side by the additional resistance due to the formation of hydrogen bubbles. At the end of the tests, the electrodes were covered by a black layer of corrosion products. The color of the products was changed to white after they dried.

Figure 3.7 displays the corrosion current densities and potentials of the as-cast AM60, and the 7FC and MHNC-7F3NP composites based on the data extracted from Figure 3.6. Among the three tested materials, the unreinforced alloy AM60 (Curve 1) had

a negative corrosion potential (-1.417 V), which was the highest, while the value of its corrosion current density (4.71 μA/cm^2) was the lowest. Compared to that of the AM60, the polarization curve of the 7FC composite (Curve 2) was shifted to the right and downward. The value of the corrosion potential of the 7FC composite was more negative than that of the AM60 alloy, although the 7FC composite had a corrosion current density higher than that of the AM60 alloy. The polarization curve of the MHNC-7F3NP composite (Curve 3) exhibited a shift to the left and downward in comparison with that of the FC. The MHNC-7F3NP composite possessed a slightly lower corrosion potential and higher density than that of the 7FC.

The corrosion potentials, corrosion current density, and anodic/cathodic Tafel slopes (anodic: β_a and cathodic: β_c) were derived from the test data. Based on the approximate linear polarization at the corrosion potential (E_{corr}), polarization resistance (R_p) values were determined by the relationship [13]:

$$R_p = \frac{\beta_a * \beta_c}{2.3 * i_{corr} * (\beta_a + \beta_c)} \quad (1)$$

where i_{corr} is the corrosion current density. The data in Table 3.5 denoted that the corrosion resistance of the AM60 alloy (4.07 kΩ·cm^2) was decreased by the introduction of micron-sized fibres and nano-sized particles. The 7FC composite possessed a high corrosion current density, which was 20% higher than that of the matrix AM60 alloy. The corrosion resistance of the 7FC composite (2.08 kΩ·cm^2) was only a half of that of the matrix alloy. The addition of the micron-sized fibres as reinforcement significantly reduced the corrosion resistance of the matrix alloy AM60 by almost 50%. The corrosion resistance of the MHNC-7F3NP was 1.88 kΩ·cm^2. The presence of the nano-sized particles resulted in a reduction of the corrosion resistance of the 7FC composite from 2.08 to 1.88 kΩ·cm^2 by

0.20 kΩ·cm^2. This observation indicated that the introduction of the nano-sized particles up to 3 vol.% had almost no effect on the corrosion resistance of the FC composite.

In the Tafel extrapolation method for measuring corrosion rates of Mg-based materials, the corrosion current density, i_{corr} (μA/cm^2) is estimated by Tafel extrapolation of the cathodic branch of the polarisation curve, and the obtained i_{corr} can be linearly related to the average corrosion rate, P_i (mm/year) by the following equation [11, 14, 15]

$$P_i = 0.02285 \times i_{corr} \qquad (2)$$

The calculated P_i values are listed in Table 3.5. Corrosion rates determined based on Tafel extrapolations demonstrate quantitatively the corrosion nature of various materials, although they are somewhat different from those obtained from weight loss or hydrogen evolution measurement [15]. Figure 3.8 shows the corrosion rates of the as-cast unreinforced alloy AM60, and 7FC and MHNC composites, which were 0.108, 0.130 and 0.136 mm/year, respectively. The introduction of the micron Al_2O_3 fibres increased the corrosion rate of the matrix alloy by 20%. But, the corrosion rate of the composite rose by only 4% with the further addition of the nano Al_2O_3 particles.

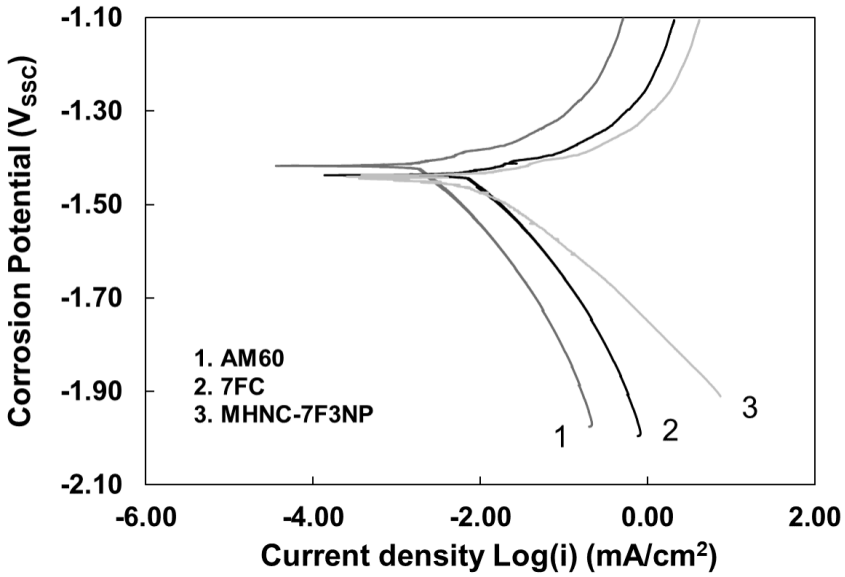

Fig. 3.6. Polarization curves of the as-cast AM60, 7FC and MHNC-7F3NP composites.

Table 3. 5. Electrochemical parameters of the unreinforced alloy AM60, and the 7FC and MHNC-7F3NP composites

Materials	β_a (mV/dec)	β_c (mV/dec)	i_{corr} ($\mu A/cm^2$)	R_p ($k\Omega \cdot cm^2$)	E_{corr} (V)	P_i (mm/year)
AM60	52.9	262.5	4.71	4.07	-1.417	0.108
7FC	31.8	188.7	5.68	2.08	-1.437	0.130
MHNC-7F3NP	29.1	128	5.95	1.88	-1.441	0.136

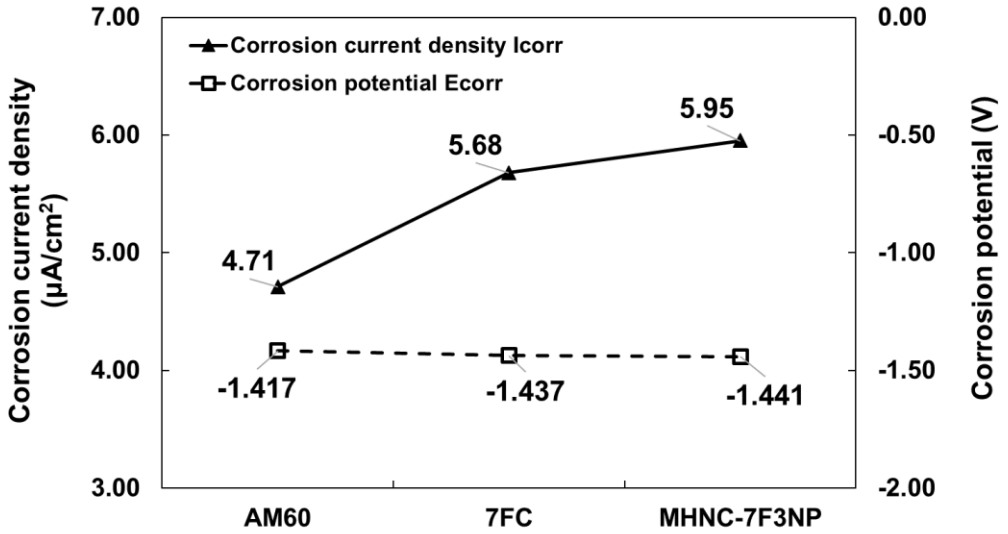

Fig. 3.7. Corrosion current densities and potentials of the as-cast AM60, and the 7FC and MHNC-7F3NP composites.

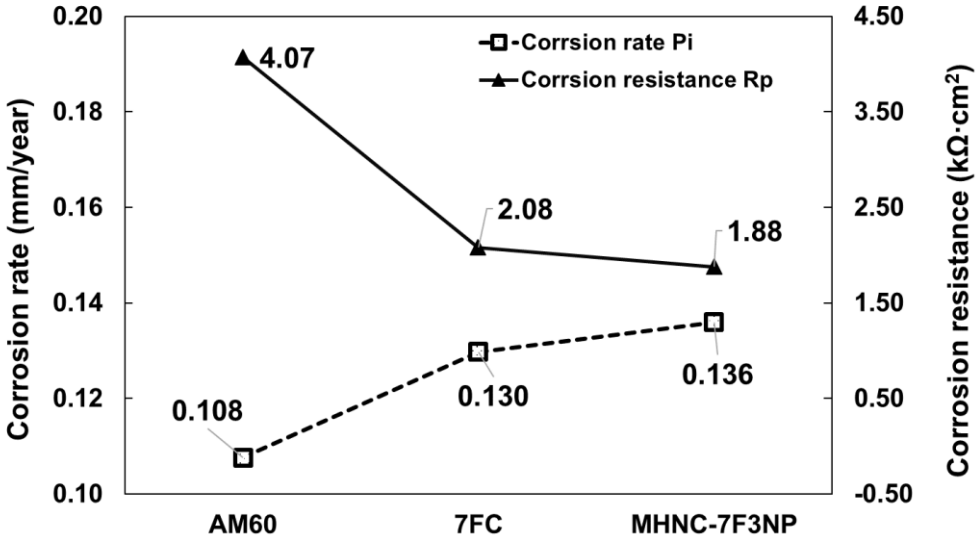

Fig. 3.8. Corrosion resistances and rates of the as-cast AM60, and the 7FC and MHNC-7F3NP composites.

3.3.3. Corroded Surfaces and Corrosion Mechanisms

The surface morphologies of the corroded unreinforced alloy AM60, and 7FC and MHNC-7F3NP composites are shown in Figure 3.9, after they were immersed in 3.5 wt.% NaCl aqueous solution for one hour. The SEM micrograph given in Figure 3.9(a) showed a layer of the discontinuous film with corroded products. Figure 3.10 presents the EDS spectra showing the presence of oxygen and chlorine in the corroded surface of the unreinforced alloy AM60, and 7FC and MHNC-7F3NP composites, which suggested there were $Mg(OH)_2$ and $MgCl_2$ in the corroded products. The corrosion behavior of AM60 alloy was significantly influenced by the alloy elements, such as aluminum and manganese. The formation of the surface morphology on the corroded unreinforced alloy AM60 resulted from a combined effect of galvanic corrosion, and pitting corrosion. The presence of different phases in the microstructure of the unreinforced alloy AM60 should be responsible for these types of corrosion mechanisms. The eutectic β-$Mg_{17}Al_{12}$ and Al-Mn

intermetallic phases in the Mg-Al alloy could serve as cathodic sites, and the primary α-Mg matrix would be anodic.

Anodic reaction:

$Mg \Rightarrow Mg^{2+} + 2e^-$ and/or

$Mg_{(s)} + 2(OH)^- \Rightarrow Mg(OH)_{2(s)} + 2e^-$

Cathodic reaction:

$2H^+ + 2e^- \Rightarrow H_{2(g)}$ and/or

$2H_2O + 2e^- \Rightarrow H_{2(g)} + 2(OH)^-$

The overall reaction is:

$Mg_{(s)} + 2H_2O \Rightarrow Mg(OH)_{2(s)} + H_{2(g)}$

As pointed out by Bakkar and Neubert [7, 8] for magnesium alloy AS41, owing to the high pH region around cathodic area, the passivation surface which contained $MgO/Mg(OH)_2$ was formed. The generation of hydrogen kept increasing the pH value and the protective film grew thicker consequently. At the anodic region, the protective film was hardly to be formed due the pH was too low and Mg^{2+} was produced at a high rate from the alloy surface and the pit developed. As a result of maintaining electroneutrality, chloride ions were attracted into the pit. As the corrosion proceeded, the pit grew bigger and deeper and led to the formation of the discontinuous film. Song et. al. [17] found that, in magnesium alloy AZ91, the β-$Mg_{17}Al_{12}$ phase mainly served as a galvanic cathode and accelerated the corrosion process of the primary α-Mg matrix if the volume fraction of β-$Mg_{17}Al_{12}$ phase was small, although the β-$Mg_{17}Al_{12}$ phase was very stable in NaCl solutions and was inert to corrosion. Besides the β-$Mg_{17}Al_{12}$ phase, the most potent

cathodes in an Mg-Al alloy are the iron-rich precipitate phases. Heavy metal contamination promoted general pitting attack.

Figures 3.9(b) and (c) present a SEM micrograph showing the surface morphology of the 7FC and MHNC-7F3NP composites after corrosion testing, which exhibited thick but irregular and loose films. The large and deep corrosion attack can be clearly observed on two composites samples which could be attribute to the crevice attacks of reinforcements. Meanwhile, the cross-section at the corrosion attack of all three samples is shown in Figure 3.11. It can be clearly seen from Figure 3.11 that, for the two composites, the corrosion extended to a depth in the range of 10-35 μm, while the depth of the corroded subsurface for the unreinforced AM60 alloy varied around 10-20 μm. The deepest corrosion attack occurred in the MHNC-7F3NP composite, while the subsurface corrosion of the as-cast AM60 was relatively minor in comparison with those of the composites. At the subsurface of the AM60 alloy, the presence of the noble phases of eutectic β-$Mg_{17}Al_{12}$ and Al-Mn intermetallic limited the advancement of corrosion. However, the excessive interfaces in the composites offsetting the corrosion resistance of the noble phases facilitated the penetration of the NaCl aqueous solution, which led to the occurrence of corrosion further deep into the matrix of the composites.

It is known that galvanic corrosion is the primary prospect when active magnesium is coupled with a relatively noble material [7]. But, no galvanic interaction between the alloy matrix and reinforcing fibres and particles could take place since the Al_2O_3 fibres and particles are an insulator. Hypothetically, it implies that the addition of Al_2O_3 fibre to the AM60 alloy should increase the corrosion resistance of the composite.

The previous corrosion study on pure magnesium was carried out in the same 3.5% NaCl solution [17]. It has found that the grain refinement decreased the corrosion resistance of magnesium, which was attributed to the higher density of grain boundaries and other defects from the grain refinement. However, in the case of fibre reinforced composite, the high density of grain boundaries might not be the main mechanism of decreasing in corrosion resistance. The changes in the grain boundary precipitation might appear to be another reason for the reduction in corrosion resistance for the composites. The existence of noble precipitates such as $Mg_{17}Al_{12}$ phases and Al-Mn intermetallics at the grain boundaries make the grain boundaries more corrosion resistant than the matrix and increase the overall corrosion resistance of the material [11]. In the 7FC and MHNC-7F3NP composites, the lack of such relatively more noble precipitates at the grain boundaries could result in a low corrosion resistance.

The introduction of the fibres and particles in the 7FC and MHNC-7F3NP composites generated new interfaces between the matrix alloy and reinforcements. As both the fibres and particles existed, a large number of new interfaces generated in the composite. As a result, the presence of the new interfaces broke the continuity of the matrix and formed preferential spots for corrosion attack. The poor corrosion resistance of the composites should be attributed to the irregular and less adherent film. No evidence of any localized corrosion or galvanic enhanced corrosion around either the fibres or particles was found. The entire matrix alloy in the composites was uniformly corroded as the remaining fibres and particles stood out of the surface. This type of corrosion was observed in SiC_p/ZC71 composites by Nunez-lopez et al [18]. For their practical applications in

corrosive environment, the developed composites need to be treated for surface protection, of which investigation proceed.

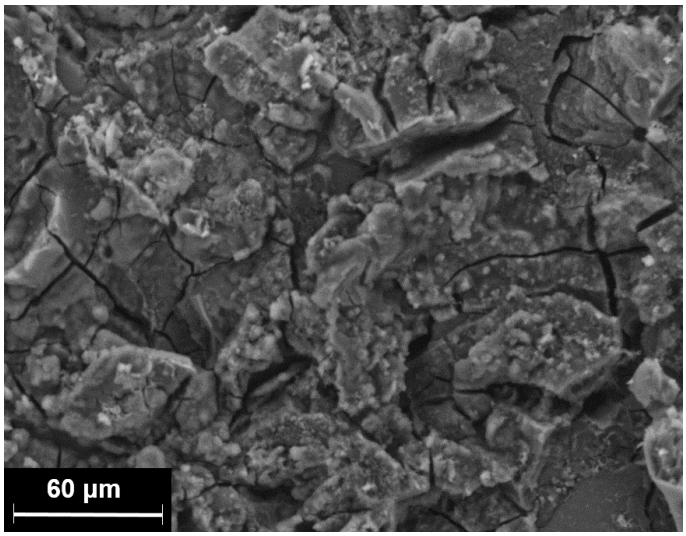

(a)

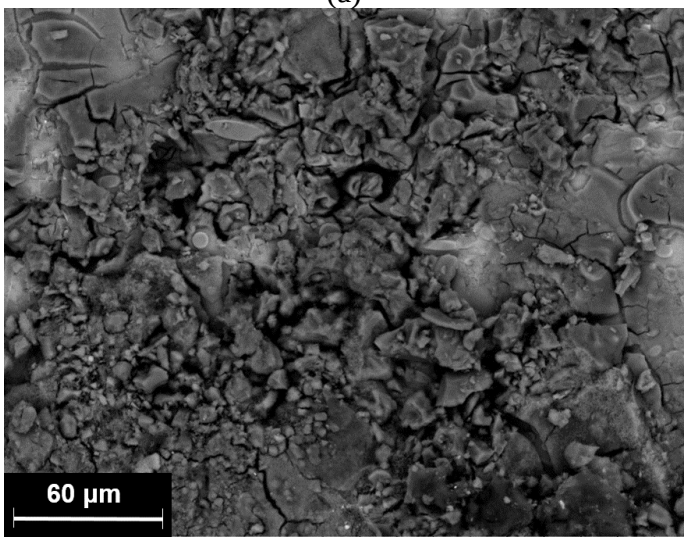

(b)

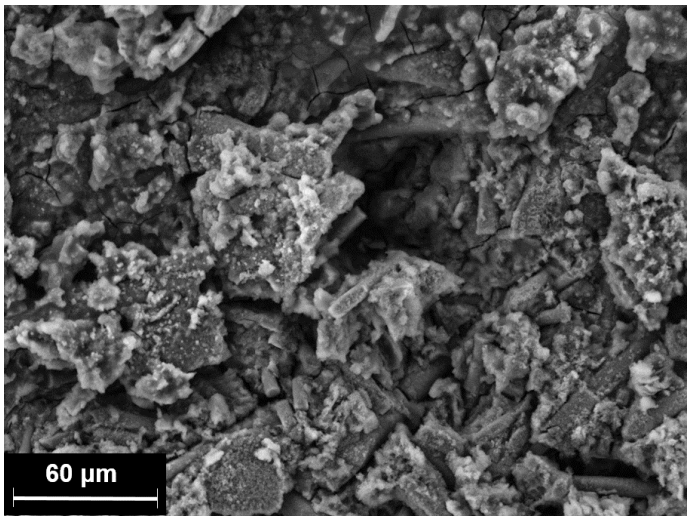

(c)

Fig. 3.9. SEM micrographs in SE mode showing corroded surfaces of (a) the unreinforced alloy AM60, and the (b) 7FC and (c) MHNC-7F3NP composites.

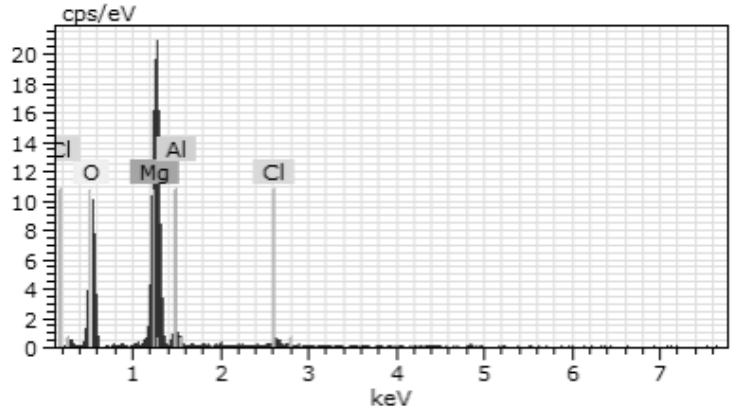

(a)

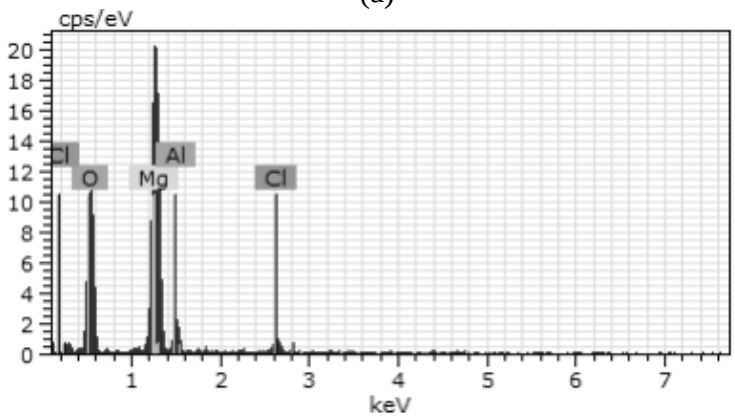

(b)

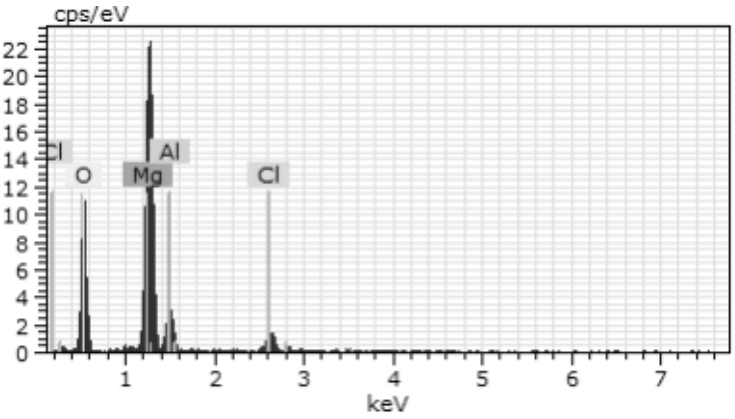

(c)

Fig. 3.10. EDS spectra identifying oxygen and chlorine for the (a) unreinforced alloy AM60, and (b) 7FC and (c) MHNC-7F3NP composites respectively, which corresponds the SEM graphs in Figure 3.9.

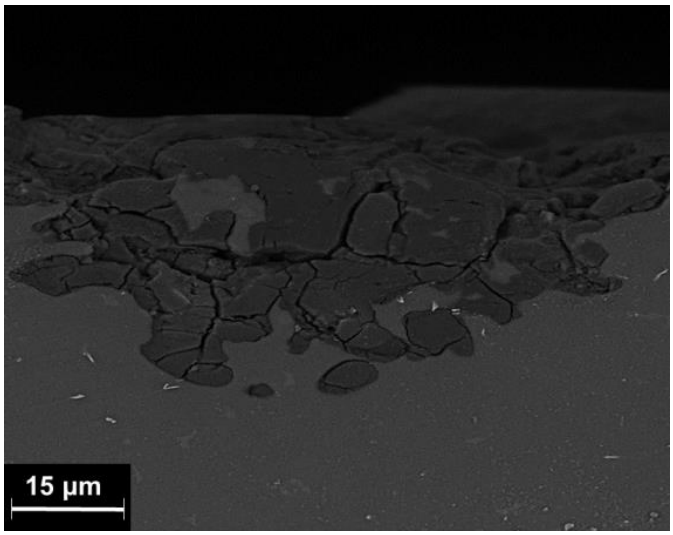

(a)

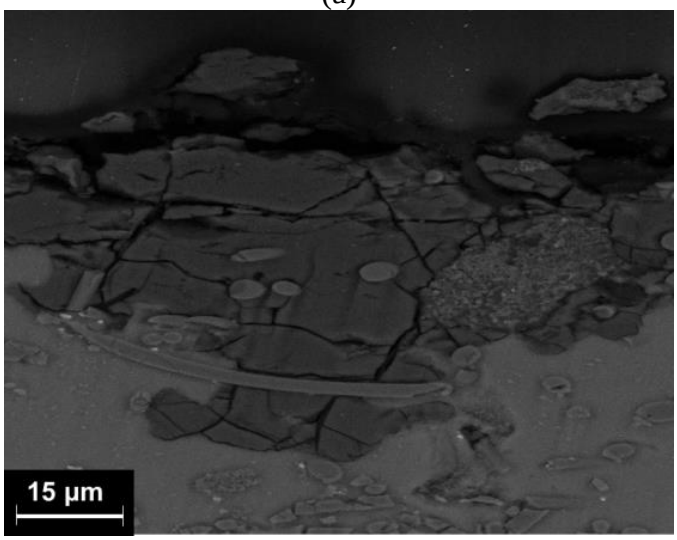

(b)

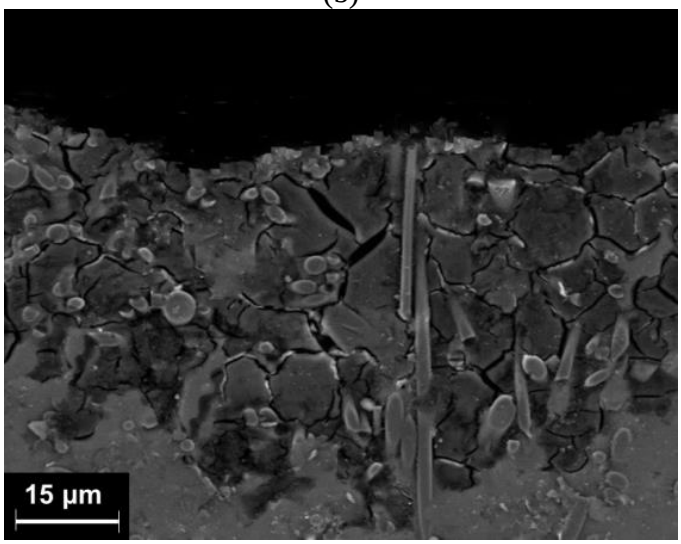

(c)

Fig. 3.11. SEM micrographs in SE mode showing corroded sub surfaces in the cross-section of (a) the unreinforced alloy AM60, and the (b) 7FC and (c) MHNC-7F3NP composites.

3.4. Conclusions

The corrosion behaviors and microstructure of the as-cast AM60 and its hybrid nanocomposites containing 7 vol.% of micron-sized Al_2O_3 fibres and 3 vol.% of nano-sized Al_2O_3 particles have been investigated, and the following conclusions arising out of the present study.

1. The microstructure of the matrix alloy AM60 consisted of primary α-Mg grains, eutectic β-$Mg_{17}Al_{12}$ phases, and Al-Mn intermetallics. The eutectic β-$Mg_{17}Al_{12}$ phases, and Al-Mn intermetallics were present in the form of isolated fine particles surrounding the boundaries of the primary α-Mg grains. But, in the 7FC and MHNC-7F3NP composites, the eutectic β-$Mg_{17}Al_{12}$ phases, and Al-Mn intermetallics attached to the surface of the fibres and particles.

2. The introduction of the micron-sized fibres and nano-sized particles refined grain structure in the composites. The grain size decreased from 65 μm for the matrix alloy AM60 to 37 μm for the 7FC composite by 43%. The introduction of the nano particles (3 vol.%) resulted in a minor reduction in the grain size from 37 to 26 μm.
3. The unreinforced as-cast AM60 performed the best corrosion resistance, and the micron-sized Al_2O_3 fibres and nano-sized Al_2O_3 particles reinforcement deteriorates its corrosion resistance. The addition of the micron-sized fibres at 7 vol.% as reinforcement significantly reduced the corrosion resistance of the matrix alloy AM60 from 4.07 to 2.08 $k\Omega \cdot cm^2$ by almost 50%. The presence of the nano-sized particles resulted in a reduction of the corrosion resistance of the 7FC composite from 2.08 to 1.88 $k\Omega \cdot cm^2$ by 0.20 $k\Omega \cdot cm^2$. This observation indicated that the introduction of the nano-sized particles up to 3 vol.% had almost no effect on the corrosion resistance of the FC composite.
4. The formation of the surface morphology on the corroded unreinforced alloy AM60 resulted from a combined effect of galvanic corrosion, and pitting corrosion. The presence of different phases in the microstructure of the unreinforced alloy AM60 should be responsible for these types of corrosion mechanisms. The eutectic β-$Mg_{17}Al_{12}$ and Al-Mn intermetallic phases in the Mg-Al alloy could serve as cathodic sites, and the primary α-Mg matrix would be anodic.
5. No galvanic interaction between the alloy matrix and reinforcing fibres and particles could take place since the Al_2O_3 fibres and particles are an insulator. In the composites, the lack of such relatively more noble precipitates such as β-$Mg_{17}Al_{12}$ phases and Al-Mn intermetallics at the grain boundaries could result in a low corrosion

resistance, although the high density of grain boundaries might not be the main mechanism of decreasing in corrosion resistance.

6. The introduction of the fibres and particles in the 7FC and MHNC-7F3NP composites generated new interfaces between the matrix alloy and reinforcements, which broke the continuity of the matrix and formed preferential spots for corrosion attack. The poor corrosion resistance of the composites should be attributed to the irregular and less adherent film on their surface.

3.5. Acknowledgements

The authors would like to thank the Natural Sciences and Engineering Research Council of Canada, and University of Windsor for supporting this work.

3.6. Disclosure statement

No potential conflict of interest was reported by the authors.

3.7. Funding

This work was supported by the Natural Sciences and Engineering Research Council of Canada and University of Windsor.

3.8. References

[1] Zhang, Q., Hu, H. & Lo, J. (2011). Solidification of discontinuous Al_2O_3 fibre reinforced magnesium (AM60) matrix composite. Defect and Diffusion Forum. 312-315: 277-282.

[2] Banerji, A., Hu, H. & Alpas, A. T. (2012). Ultra-mild wear of Al_2O_3 fibre and particle reinforced magnesium matrix composites. Adv. Mat. Res. 445: 503-508.

[3] Banerji, A., Hu, H. & Alpas, A. T. (2013). Sliding wear mechanisms of magnesium composites AM60 reinforced with Al_2O_3 fibres under ultra-mild wear conditions. Wear. 301: 626-635.

[4] Zhang, X., Fang, L., Zhang, Q., Hu, H. & Nie, X. (2014). Fabrication and tensile properties of Al_2O_3 particle and fibre hybrid magnesium-based composites. J. Chin. Ceramic Soc. 1(2): 122-128.

[5] Zhang, X., Fang, L., Xiong, B. & Hu, H. (2015). Microstructure and tensile properties of Mg(AM60)/Al_2O_3 metal matrix composites with varying volume fractions of fibre reinforcement. J. Mater. Eng. Perform. 24(12): 4601-4611.

[6] Zhang, X., Zhang, Q. & Hu, H. (2014). Tensile behavior and microstructure of magnesium AM60-based hybrid composite containing Al_2O_3 fibres and particles. Mat. Sci. Eng A. 607: 269-276.

[7] Bakkar, A., & Neubert, V. (2007). Corrosion characterisation of alumina–magnesium metal matrix composites. Corrosion science, 49(3), 1110-1130.

[8] Bakkar, A., & Neubert, V. (2009). Corrosion behaviour of carbon fibres/magnesium metal matrix composite and electrochemical response of its constituents. Electrochimica Acta, 54(5), 1597-1606.

[9] Tiwari, S., Balasubramaniam, R., & Gupta, M. (2007). Corrosion behavior of SiC reinforced magnesium composites. Corrosion science, 49(2), 711-725.

[10] Rashad, M., Pan, F., Asif, M., & Chen, X. (2017). Corrosion behavior of magnesium-graphene composites in sodium chloride solutions. Journal of Magnesium and Alloys.

[11] Mondal, A. K., Blawert, C., & Kumar, S. (2015). Corrosion behaviour of creep-resistant AE42 magnesium alloy-based hybrid composites developed for powertrain applications. Materials and Corrosion, 66(10), 1150-1158.

[12] Zhou, J., Ren, L., Geng, X., Fang, L. & Hu, H. (2017). As-cast magnesium AM60-based hybrid nanocomposite containing alumina fibres and nanoparticles: Microstructure and tensile behavior. Materials Science & Engineering A, https://doi.org/10.1016/j.msea.2017.10.070.

[13] John, W. & Sons. (2000). R.W. Revie, Uhlig's Corrosion Handbook, 2nd ed. New York.

[14] Shi, Z. & Atrens, A. (2011). An innovative specimen configuration for the study of Mg Corrosion, Corrosion Science, 53, 226-246.

[15] Shi, Z., Liu, M. & Atrens, A. (2010). Measurement of the corrosion rate of magnesium alloys using Tafel extrapolation, Corrosion Science 52, 579–588.

[16] Song, G. L. &Atrens, A. (1999). Corrosion Mechanisms of Magnesium Alloys, Adv. Eng. Mater. 1(1), 11-33.

[17] Ghali, E. (2010). Corrosion Resistance of Aluminum and Magnesium Alloy: Understanding, Perfromance, and Testing, Wiley, P537

[18] Nunez-lopez, C.A., Skeldon, P., Thomson, G.E., Lyon, P., Karimzadeh, H. & Wilks, T.E. (1995). The Corrosion Behaviour of Mg Alloy ZC71/SiCp Metal Matrix Composites, Corrosion Science, Vol.37, No.5, 689-708.

CHAPTER 4

Enhanced corrosion resistance of as-cast magnesium alloy AM60-based hybrid nanocomposite by plasma electrolytic oxidation (PEO) coating

4.1. Introduction

Metal matrix composites (MMC) have become one of the most significant candidate materials for the automotive and aerospace industry for their light weight, high strength, wear resistance and improved creep resistance at higher temperatures. Since MMCs possess enhanced mechanical properties by comparing the pure matrix alloy, the automotive engineering applications of the Mg-based MMCs have been attempted, such as cylinder heads, connecting rods, and brake calipers. Extensive research [1-7] in magnesium alloys-based composites reinforced with different size of fibers and particles introduced inside by infiltration techniques under specified pressures has been carried out. It is revealed that, the corrosion resistances of the MMCs were deteriorated by the addition of reinforcement, although the mechanical properties of were higher than those of the matrix alloy.

Plasma electrolytic oxidation (PEO) process is an emerging and environmentally friendly surface technique to deposit ceramic coating on magnesium alloy for improving the corrosion resistance [8, 9]. PEO technology has been used for depositing ceramic coatings on Mg alloys for corrosion protection [10-21]. The coatings can be as thick as a few hundreds of micrometers and their corrosion behavior strongly depends on the process parameters employed, the chemical compositions of the materials studied, and the electrolytes used. The effect of electrolyte composition on properties of EPO oxide coatings on Mg alloys has also been an interesting subject of investigation to the

automobile industry. The electrolytes consisted of potassium hydroxide and some other passive agents that can modify the characteristics of the oxide coatings. Wang et al. [10] reported different characteristics of oxidized coatings at different voltages on AZ91D in an alkali-silicate solution. Hsiao and Tsai [11] studied the effect electrolyte concentrations on the structure of PEO coatings on AZ91D. The process parameters employed play an important role in the characteristics of oxide coatings. Zhang et al. [12] found that with an increase of solution temperature, the film thickness decreased. On the other hand, the film thickness increased with an increase in treatment time and current density. The voltages rise during the PEO process is always accompanied by the increase of film thickness. Higher voltage indicates thicker film. Khaselev et al [13] investigated the characteristics of the oxide coatings on binary Mg-Al alloys in a solution containing 3 M KOH, 0.6 M KF, and 0.21 M Na_3PO_4 with 1.1 M aluminate. Yerokhin et al [14] utilized a pulsed bipolar current to make oxide ceramic layers dense and uniform with a fine-grained microstructure on a Mg-Al-Zn alloy. The pulsed bipolar current was also beneficial to elimination of the fatigue cracks by strain distortion of the metal subsurface layers induced during the oxidation process. Guo et al [15] demonstrated that ultrasonic power can play an important role in the coating formation and enhance the coating growth. Also, MMCs inherently exhibit poor corrosion resistance due to the presence of excessive interfaces for pitting or crevice corrosion attacks. Zhang et al [16, 17] demonstrated the effectiveness of PEO coatings on 5-20 vol.%(SiO_2)p/Al383 composites for wear and corrosion protection. However, the fabrication of PEO coatings on Mg-based MMCs and their effect on corrosion behaviors are barely studied.

In the present work, the PEO process was employed for fabrication of ceramic coatings on the 7 vol.% micron sized Al_2O_3 fiber-reinforced composite (PEO-7FC) and 7 vol.% Micron-sized Al_2O_3 fiber and 3 vol.% nano-sized Al_2O_3 particles both reinforced hybrid composite (PEO-MHNC-7F3NP) as well as the Mg alloy AM60 for comparison. The microstructures of the PEO coated composites and the matrix alloy AM60 were analyzed by the optical (OM) and scanning electron microscopies (SEM). Potentiodynamic polarization tests were carried out to evaluate the corrosion behavior of the PEO coated composites and the matrix alloy AM60. The surface morphologies of the PEO coatings before and after polarization testing were assessed by SEM. Various phases present in the PEO coatings and substrates as well as corrosion products were identified by the X-ray energy dispersive spectroscopy (EDS).

4.2. Experimental procedure

4.2.1. Composites Preparation

The matrix alloy of the MMCs was magnesium alloy AM60 with a chemical composition (wt.%) of 6.0Al-0.22Zn-0.4Mn-0.1Si-0.01Cu-0.004Fe-0.002Ni-Mg. Micron-sized Al_2O_3 short fibers (Morgan Advanced Materials, United Kingdom) with an average diameter of 4 µm and length of 50 µm and Nano-sized Al_2O_3 ceramic particles with an average particulate size of 100 nm (US Research Nanomaterials, Inc., USA) served as reinforcements which were employed for fabricating only fiber reinforced MMCs and fiber and particle both reinforced hybrid MMCs.

The reinforcement preforms were prepared for fabricating MMCs and hybrid MMCs. The preform of hybrid MMCs was made by several steps which include mixing the Al_2O_3 short fibers and particles, introducing the binding compounds, forming the

preform in a pressurized die, drying at room temperature, and employing heat treatment for sintering. A cellular structure was formed in the hybrid MMCs preform, and the fibers were served as the inside skeleton. The volume percent of the fiber was determined by desired amount of porosity in the cellular solid. The preform for only fiber reinforced MMCs was also fabricated for the comparison with hybrid MHNCs.

For composite fabrication, molten matrix alloy AM60 was heated up to 750℃. During the melting of the matrix alloy, a protective gas was employed for preventing oxidation and burning. Meanwhile, the preform was pre-heated to 700℃ before the molten matrix alloy AM60 was infiltrated under an applied pressure of 90 MPa, and the applied pressure was maintained for 30 seconds. For the purpose of comparison, a single-material reinforced AM60 based composite with 7 vol.% Al_2O_3 fiber (7FC) and a dual-material reinforced hybrid AM60 based composite with 7 vol.% Al_2O_3 fiber and 3 vol.% Al_2O_3 nano particles (MHNC-7F3NP) were fabricated by squeeze casting. More details on the process for fabricating the composites are given in references 3, 4 and 5.

4.2.2. Plasma electrolytic oxidation (PEO) process

PEO processing involved the substrate preparation, the electrolyte selection and the submersion of the substrate materials into the aqueous electrolyte. Prior to the PEO coating, squeeze cast AM60 (AM60), AM60-based composite with 7 vol.% Al_2O_3 fiber (7FC) and AM60-based hybrid composites with 7 vol.% Al_2O_3 fiber and 3 vol.% Al_2O_3 nano-sized particles (MHNC-7F3NP) were cut into small coupons (20×20×5 mm). Sectioned specimens were polished with silicon carbide sand papers up to 2400 Grit, rinsed and dried. The surfaces of the polished 7FC and MHNC-7F3NP for coating were electrochemically etched by the alkaline solution in which the 7FC or MHNC-7F3NP, as an anode, were

connected to the power supply. As a result, the Mg matrix surface was etched down by a few microns, and the nanoparticles and fibers in the matrix was protruded from the surface with the exposed peak height of up to tens of microns. It was expected that the Mg matrix surface grew with the formation of a thin oxide layer by plasma oxidation during PEO processing, and the resultant surface consisted of Mg oxides in the matrix areas and intact original nanoparticles and fibers. The $NaAlO_2$ with concentration of 8 g/L was served as the electrolyte, and KOH with concentration of 0.8 g/L was added to balance the pH value of the solution. A bipolar current was applied with current density of 0.05 A/cm^2 for 7 mins, and the positive current was 1 A before the negative current was provided by 0.7 A. Three PEO coated materials, i.e. squeeze cast AM60 (AM60), AM60-based composite with 7 vol.% Al_2O_3 fiber (7FC) and AM60-based hybrid composites with 7 vol.% Al_2O_3 fiber and 3 vol.% Al_2O_3 nano-sized particles (MHNC-7F3NP) are named PEO-AM60, PEO-7FC and PEO-MHNC-7F3NP, respectively.

Table 4.1. PEO process parameters of the unreinforced alloy AM60, and the 7FC and MHNC-7F3NP composites

	Electrolyte concentration $NaAlO_2$ (g/L)	**Current Mode**	**Current density (A/cm^2)**	**I^+ (A)**	**I^- (A)**	**Time (mins)**
PEO-AM60	8	Bipolar	0.05	1.0	0.7	7
PEO-7FC	8	Bipolar	0.05	1.0	0.7	7
PEO-MHNC-7F3NP	8	Bipolar	0.05	1.0	0.7	7

4.2.3. Electrochemical experimentation

To determine the corrosion resistances of the three selected materials, the electrochemical test was carried out by EC-LAB SP-150 electrochemical apparatus with corrosion analysis EC-lab software. A three-electrode cell was built by the samples served

as working electrode, Ag/AgCl/sat'd KCl electrode as a reference electrode and a Pt metal electrode as counter-electrode. The samples were held in a salt solution with 3.5 wt.% NaCl for a half hour to settle the open circuit potential to a constant value before the experiment. The corrosion test potential scans were directed from noble direction open circuit potential -0.5 V to reference electrode potential 0.5 V. All test samples were ground with silicon carbide papers from grade of 280 to 2500 grit, which were all cleaned by acetone and dried in room temperature after grinding prior to potentiodynamic polarization. Corrosion potential (E_{corr}) and current density (i_{corr}) were indicated from the intersection of anodic and cathodic Tafel slopes which were determined by the linear parts of the Tafel curves.

4.2.4. Microstructure analysis

All samples for microstructure analysis cut from the center of the tested specimens were prepared by following the standard metallographic procedures. Test samples were all polished and etched for a clean and optimized microscopic examination result. The top surface profile and cross section view of the PEO coating on test samples were characterized at high magnifications using a FEI Quanta 200 FEG (Tokyo, Japan) scanning electron microscope (SEM) with a maximum resolution of 100 nm in a secondary electron (SE) or backscatter electron (BE) mode / l µm in X-ray diffraction mapping mode, and maximum useful magnification of 30,000. The phases in the matrix alloy AM60 and around fibers and the element concentration of PEO coating were identified by X-ray energy dispersive spectroscopy (EDS), of which data was applied for maximizing the composition.

4.3. Results and discussion

4.3.1. Surface morphology of PEO coating

Figure 4.1 presents the SEM micrographs showing the surface morphologies in secondary electrons (SE) mode of samples PEO-AM60, PEO-7FC and PEO-MHNC-7F3NP. The PEO coatings on all samples had similar surface morphologies which were inhomogeneous and uncontentious layers with massive different size of micro-pores. The black contrast holes on the surface were the formation of the micro-pores which were presented as black holes in Figure 4.1 resulted from the melting of metal and oxides in micro-discharging the_quenching by electrolyte deposited the molten metal and oxides around the micro pores. Meanwhile, microcracks were found on the PEO coating surface, which were caused by the thermal stresses during the rapid solidification of molten products in the strong discharge channels [18, 19]. The main composition of PEO coating was indicated to be $MgAl_2O_4$, and phase identification of PEO coating on each sample is to be shown in following EDS analysis of cross section views.

The cross-section views of each sample are shown in Figure 4.2, which gives SEM images in secondary electrons (SE) mode after 7 minutes of PEO process. The interfaces of PEO coating and substrate exhibited a wavy-jagged appearance due to the substrate dissolution at high temperature in the early PEO process stage. The adhesion between the coating and substrate is also beneficial from the irregularity interface [19]. The α-Mg, β-$Mg_{17}Al_{12}$, and Al-Mn phase were present in the substrate of the sample. Figure 4.3 shows that the average thickness of PEO coating on AM60 was 13 μm which was thicker than the coatings on other two composites (10 μm). The reason why the composites had thinner PEO coatings was that the reinforcement in composite broke down the continuity of the

barrier layer which formed on PEO coating, and the alumina fiber and particle were insulators, which affected the discharge during the PEO process and delayed the passivation of the metal surface.

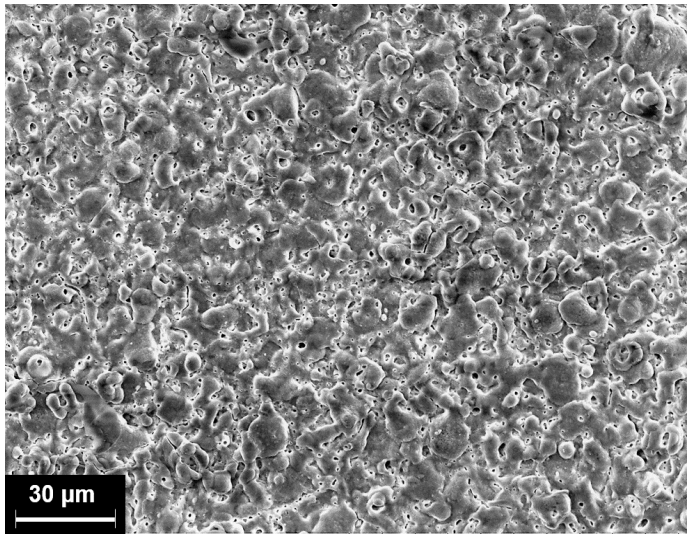

(a)

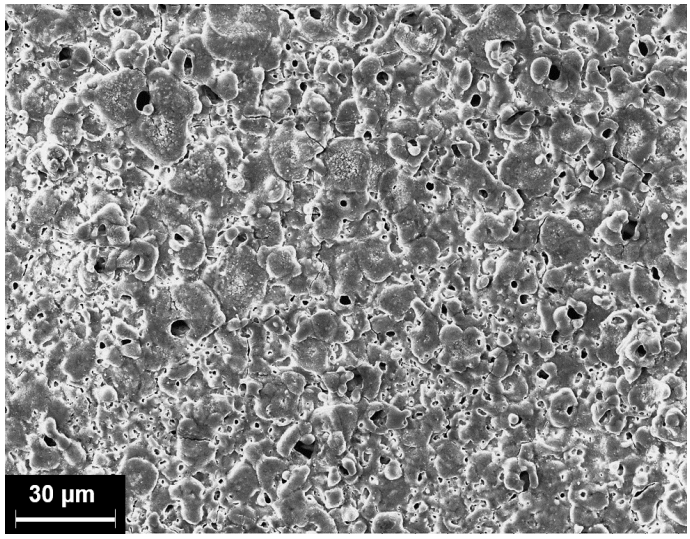

(b)

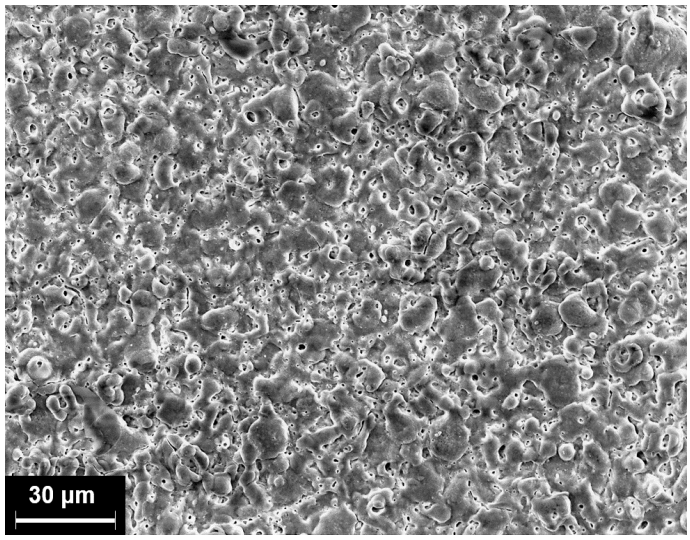

(c)

Fig. 4.1. SEM micrographs in SE mode showing PEO coating surfaces of (a) PEO-AM60, (b) PEO-7FC and (c) PEO-MHNC-7F3NP, respectively.

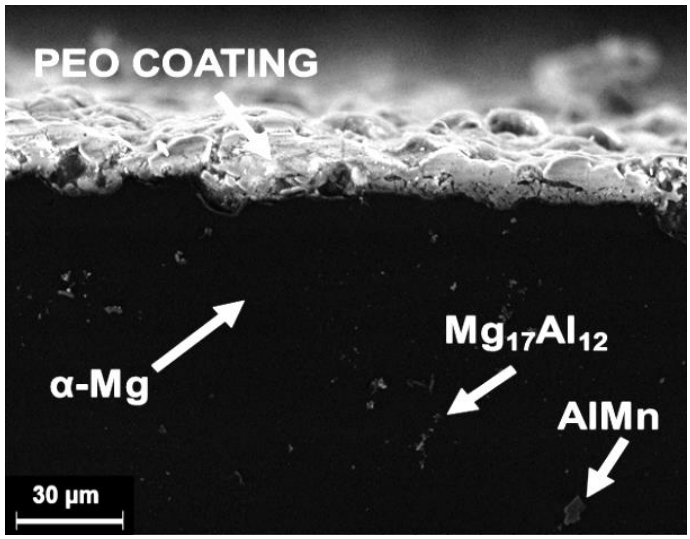

(a)

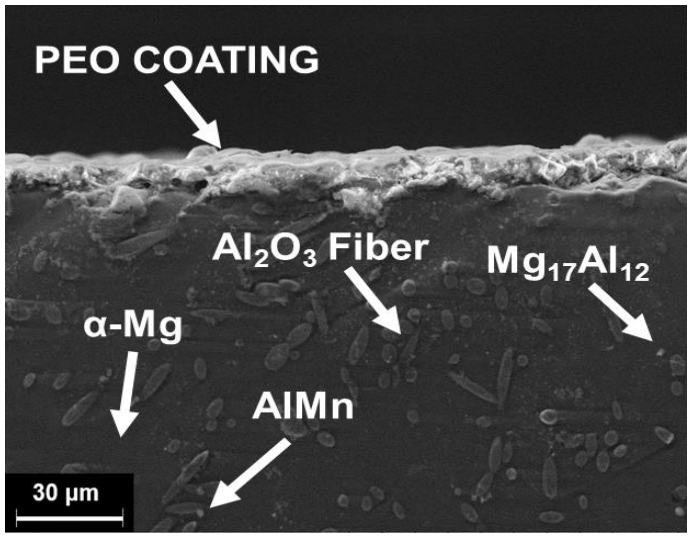

(b)

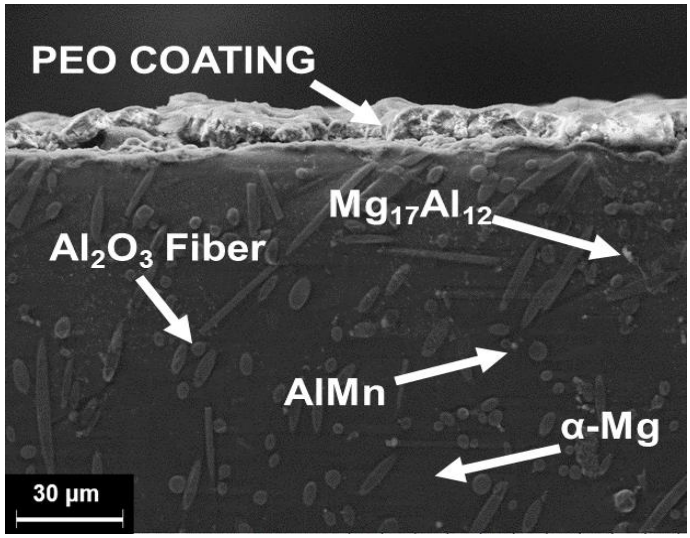

(c)

Fig. 4.2. SEM micrograph in SE mode showing the PEO coating cross-sections of PEO coatings for (a) PEO-AM60, (b) PEO-7FC and (c) PEO-MHNC-7F3NP, respectively.

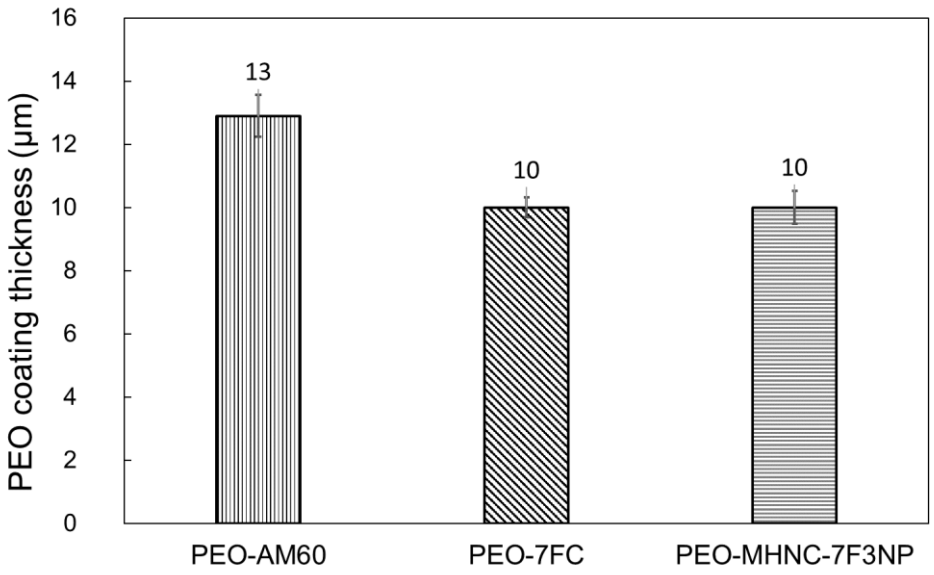

Fig. 4.3. PEO coating thicknesses of PEO-AM60, PEO-7FC and PEO-MHNC-7F3NP.

To identify phases present in the PEO coating and substrates, the cross-sections of the PEO coating along with the substrates of the PEO-AM60, PEO-7FC and PEO-MHNC-7F3NP samples were analyzed by EDS and SEM at high magnification as shown in Figures 4.4-4.6. Figure 4.4(a) presents the SEM image in SE mode showing the cross-section microstructure of PEO-AM60 in details at a high magnification. The results of the EDS analyses on phases in atomic percentages are listed in Table 4.2. The substrate beneath the PEO coating consisted of the primary α-Mg grains (dark contrast), eutectic β-$Mg_{17}Al_{12}$ phases (bright contrast strip), and Al-Mn intermetallics (white spots). Since the PEO electrolyte contained sodium aluminate, the aluminum and oxygen were found in the PEO coating besides magnesium.

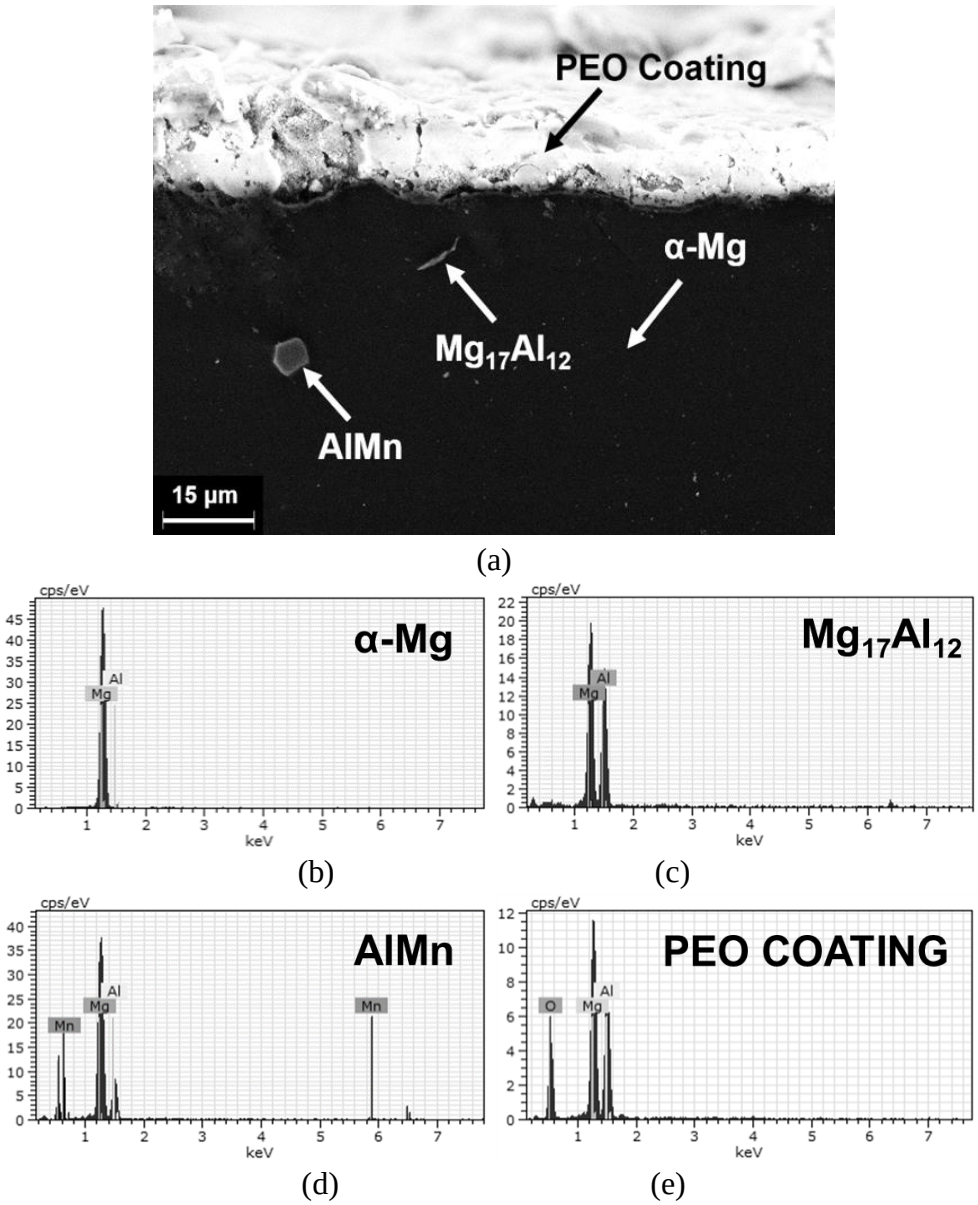

Fig. 4.4. (a) SEM micrograph in SE mode showing constituent phases in microstructure of the PEO-AM60; EDS spectra (b), (c) and (d) for the areas containing α-Mg grains (dark contrast), and β-$Mg_{17}Al_{12}$ phases (bright contrast strip), and Al-Mn intermetallic (white spots) in the substrate of AM60 and (e) for the PEO coating.

Table 4.2. Elements in analyzed phases of the substrate and PEO coating shown in Figure 4.4

Phase & Coating	Element	Atomic (at. %)
α-Mg	Mg Al	98.15 1.85
β-$Mg_{17}Al_{12}$	Mg Al	52.78 47.22
AlMn	Mg Al Mn	74.28 19.53 6.19
PEO coating	Mg Al O	27.71 23.20 49.09

Figures 4.5 and 4.6 show the SEM micrographs in SE mode and EDS spectra revealing the phases in the PEO-7FC and PEO-MHNC-7F3NP composites and their PEO coatings at high magnifications, respectively. The element analyses for the constituent phases in the PEO-7FC and PEO-MHNC-7F3NP are listed in Tables 4.3 and 4.4. The same types of phases were detected in the matrix of both composites which were the primary α-Mg grains (dark contrast), eutectic β-$Mg_{17}Al_{12}$ phases (bright contrast), and Al-Mn intermetallics (white spots). The eutectic β-$Mg_{17}Al_{12}$ phases (bright contrast) and Al-Mn intermetallics (white spots) were attached to the surface of fibers that might arose from their nucleation on reinforcement. When the Al_2O_3 fibers and particles were preheated to 700℃, they became a heat source and slowed down the solidification of the surrounding molten matrix AM60 alloy when the pressurized infiltration into the fiber and particle preform took place. The similar phenomena were also found by Zhang et al [20] for Mg-based composites.

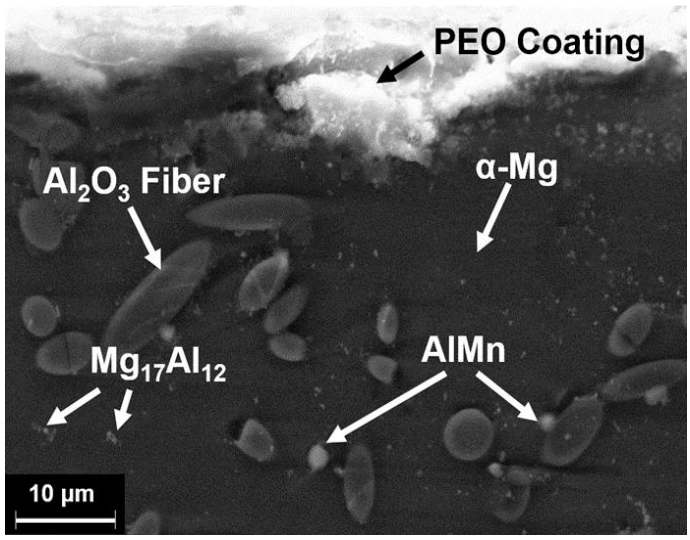

(a)

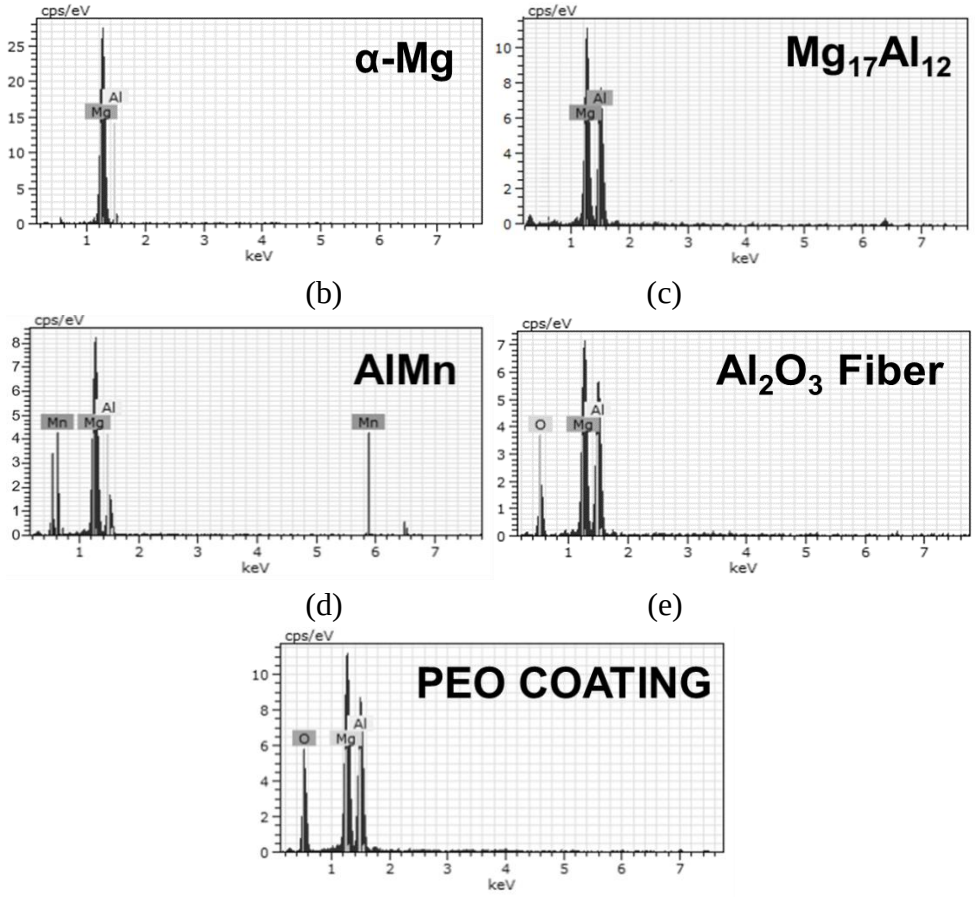

(b) (c)

(d) (e)

(f)

Fig. 4.5. (a) SEM micrograph in SE mode showing constituent phases in the microstructure of the PEO-7FC; and EDS spectra (b), (c) and (d) for the areas containing α-Mg grains (dark contrast), and β-$Mg_{17}Al_{12}$ phases (bright contrast strip), and Al-Mn intermetallic (white spots); (e) for the Al_2O_3 fiber in the composite and (f) for PEO coating.

Table 4.3. Elements in analyzed phases respectively in the substrate and PEO coating shown in Figure 4.5

Phase & Coating	Element	Atomic (at. %)
α-Mg	Mg Al	97.35 2.65
β-$Mg_{17}Al_{12}$	Mg Al	50.68 49.32
AlMn	Mg Al Mn	72.74 17.24 10.02
Al_2O_3 Fiber	Mg Al O	21.15 29.31 49.54
PEO coating	Mg Al O	25.82 24.25 49.93

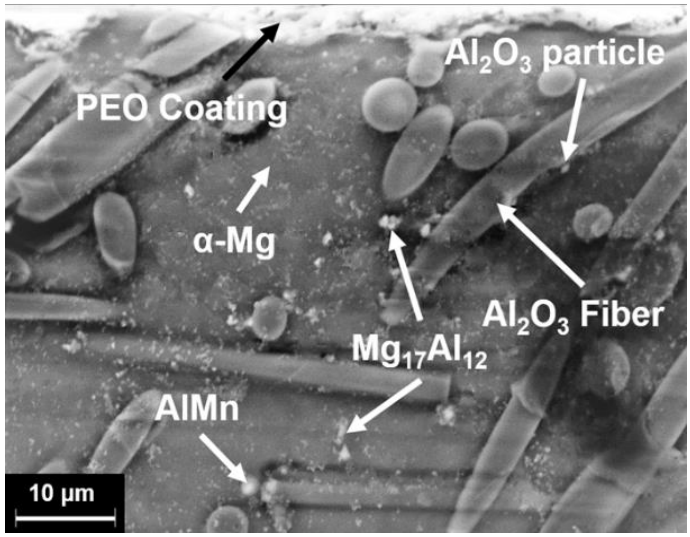

(a)

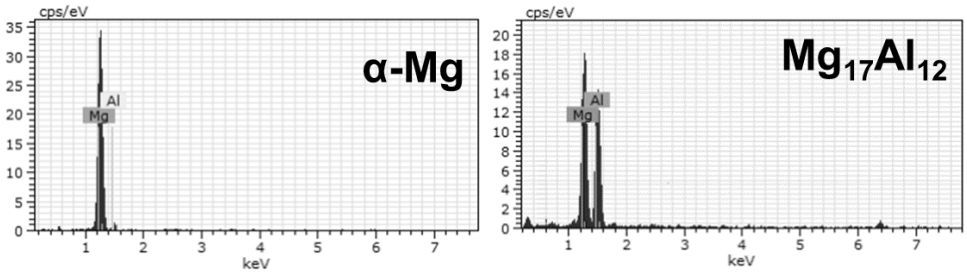

(b) (c)

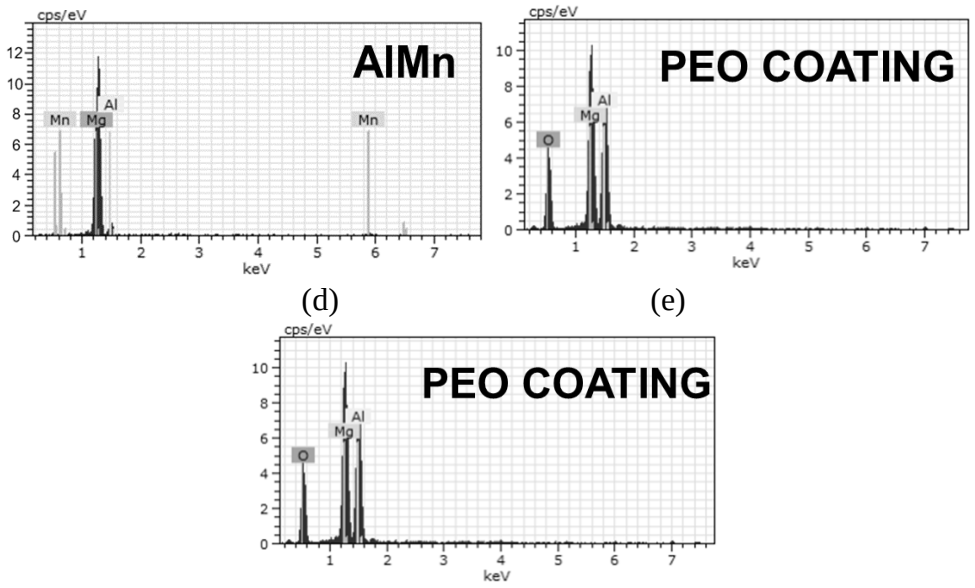

Fig. 4.6. (a) SEM micrograph in SE mode showing constituent phases in the microstructure of the PEO-MHNC-7F3NP; and EDS spectra (b), (c) and (d) for the areas containing α-Mg grains (dark contrast), and β-$Mg_{17}Al_{12}$ phases (bright contrast strip), and Al-Mn intermetallic (white spots); (e) for the Al_2O_3 fiber in the composite and (f) for PEO coating.

Table 4.4. Elements in analyzed phases respectively in the substrate and PEO coating shown in Figure 4.6

Phase & Coating	Element	Atomic (at. %)
α-Mg	Mg	98.65
	Al	1.35
β-$Mg_{17}Al_{12}$	Mg	55.21
	Al	44.79
AlMn	Mg	72.37
	Al	19.10
	Mn	8.53
Al_2O_3 Fiber	Mg	20.71
	Al	31.46
	O	47.83
PEO coating	Mg	23.62
	Al	25.38
	O	51.00

4.3.2. Electrochemical tests

Figure 4.7 shows the polarization curves of the PEO coated samples PEO-AM60, PEO-7FC, PEO-MHNC-7F3NP and the same samples without PEO coating. The 3.5 wt.% NaCl aqueous solution was applied to all samples. Table 4.5 summarizes the potentiodynamic corrosion test results. All the Tafel curves of the PEO coated samples shifted upward to the left relative to the curves for the samples without PEO coating. This observation indicated that the PEO coating increased the corrosion potential and decreased the corrosion current for all the three tested samples. The corrosion resistances of the PEO coated samples were much higher than those of the uncoated samples. However, the reinforcement in the composites still had negative influences on the corrosion resistance.

Figure 4.8 shows the corrosion current density and corrosion potential of the PEO coated samples PEO-AM60, PEO-7FC and PEO-MHNC-7F3NP based on the results extracted from the Tafel curves in Figure 4.7, which are summarized in Table 4.5. The PEO coated unreinforced AM60 possessed the highest negative corrosion potential (-1.360 V), and the lowest corrosion current density (0.125 $\mu A/cm^2$). The other two PEO coated composites PEO-7FC and PEO-MHNC-7F3NP had the lower corrosion potentials of -1.364 V and -1.376 V, as well as higher corrosion current densities of 0.150 $\mu A/cm^2$ and 0.153 $\mu A/cm^2$. From Figure 4.8, it can be seen that the difference in corrosion current density between the PEO-7FC and PEO-MHNC-7F3NP was much less than that difference between the PEO-AM60 and PEO-7FC, which was also displayed by the uncoated samples in Figure 4.9. Hence, the addition of the nano-sized particles had almost no influence on the corrosion behaviors of both the coated and uncoated samples.

From the corrosion Tafel curves, the corrosion potentials, corrosion current density, and anodic/cathodic Tafel slopes (anodic slope β_a and cathodic slope β_c) could be defined. The corrosion resistance (R_p) values would be determined by the relationship [21, 22] based on the approximate linear polarization at the corrosion potential (E_{corr}):

$$R_p = \frac{\beta_a * \beta_c}{2.3 * i_{corr} * (\beta_a + \beta_c)} \qquad (1)$$

where i_{corr} is the corrosion current density. The PEO-AM60 exhibited the highest value (342.81 $k\Omega \cdot cm^2$) of corrosion resistance among the three PEO coated samples. The introduction of the Al_2O_3 fibers in PEO-7FC decreased the corrosion resistance to 301.73 $k\Omega \cdot cm^2$, and the both Al_2O_3 fibers and nano particles reinforced composites PEO-MHNC-7F3NP had the lowest corrosion resistance of 290.44 $k\Omega \cdot cm^2$. However, the PEO coating improved the corrosion resistance of the composites by comparing with the uncoated samples. The corrosion resistance of PEO-AM60 was 85 times higher than that of the uncoated AM60 alloy, while the PEO coating increased the corrosion resistance of the 7FC and MHNC-7F3NP by 145 times and 154 times by employing PEO coating process.

The corrosion current density (i_{corr}) could be estimated by Tafel extrapolation of the cathodic branch of the polarization curve, and the corrosion rate would be determined by the following equation [23-25]:

$$P_i = 0.02285 \times i_{corr} \qquad (2)$$

The calculated corrosion rate P_i for the PEO coated samples are listed in the Table 4.5. The PEO-AM60 sample had the slowest corrosion rate of 2.86E-03 mm/year. The corrosion rate of the PEO-7FC was 3.43E-03 mm/year which was higher than that of the PEO-AM60 by 20%. The highest corrosion rate among the three PEO coated samples was 3.50E-03

mm/year for the PEO-MHNC-7F3NP. The corrosion rate of PEO coated samples was much lower than the uncoated samples. Figure 4.10 summarized the corrosion resistance and corrosion rate of the PEO coated and uncoated samples. It can be seen that the corrosion resistance of the PEO coated composites was close to the PEO coated AM60, although the corrosion resistance of the uncoated AM60 was almost 2 times of the uncoated composites. The comparison of the corrosion rates revealed that the difference in the corrosion rate between the 7FC and MHNC-7F3NP composites with and without PEO coatings was less than the difference between the AM60 and 7FC with and without PEO coatings.

Table 4.5. Electrochemical parameters of the PEO coated and uncoated AM60 alloy, and the 7FC and MHNC-7F3NP composites

Samples	β_a (mV/dec)	β_c (mV/dec)	i_{corr} ($\mu A/cm^2$)	E_{corr} (V)	R_p ($k\Omega \cdot cm^2$)	Pi (mm/year)
PEO-AM60	181.981	215.001	0.125	-1.360	342.811	2.860E-03
PEO-7FC	220.922	196.862	0.150	-1.364	301.731	3.430E-03
PEO-MHNC-7F3NP	215.580	194.351	0.153	-1.376	290.442	3.500E-03
AM60	52.903	262.503	4.711	-1.417	4.072	0.108
7FC	31.811	188.712	5.684	-1.437	2.083	0.130
MHNC-7F3P	29.101	128.011	5.953	-1.441	1.883	0.136

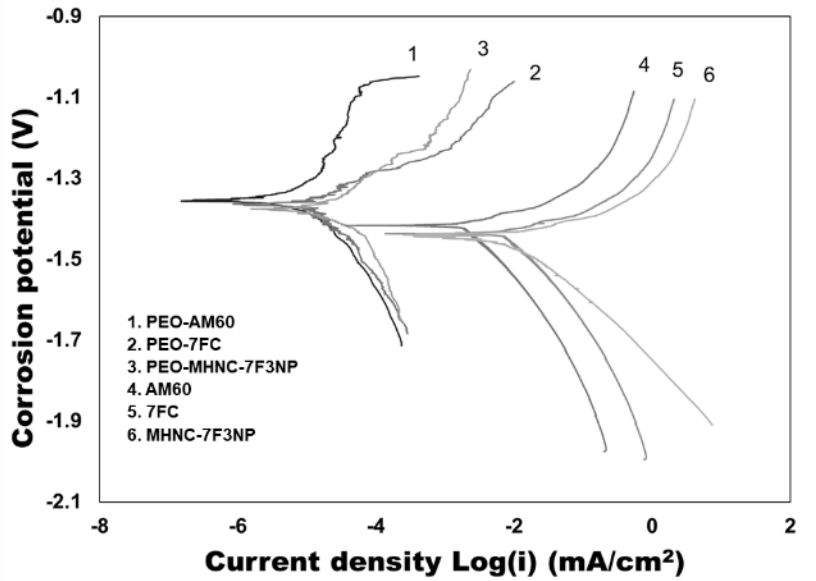

Fig. 4.7. Polarization curves of the PEO coated and uncoated AM60 alloy, 7FC and MHNC-7F3NP composites.

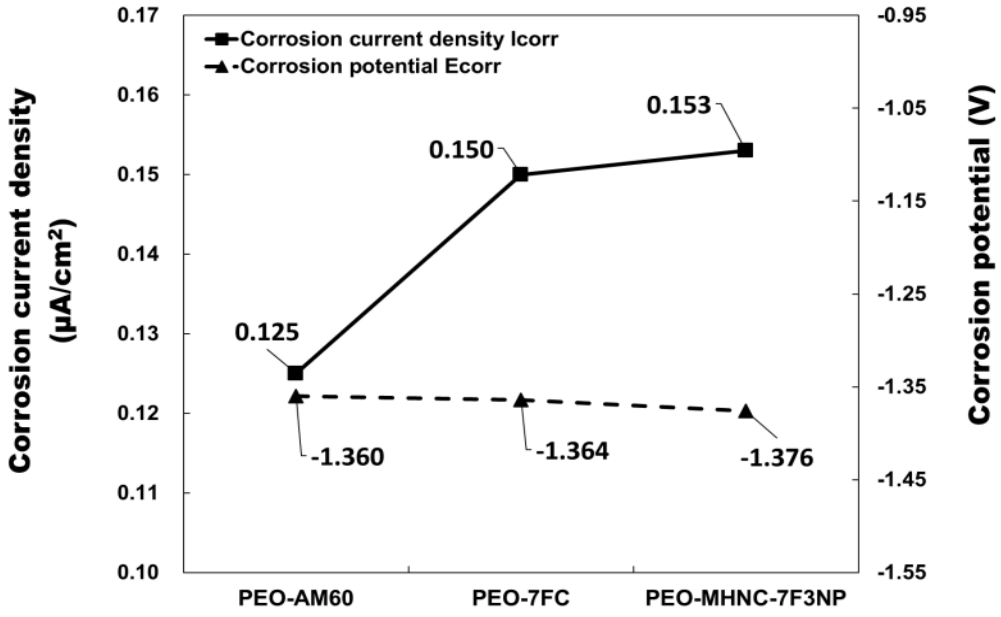

Fig. 4.8. Corrosion current densities and potentials of the PEO coated samples PEO-AM60, PEO-7FC and PEO-MHNC-7F3NP composites.

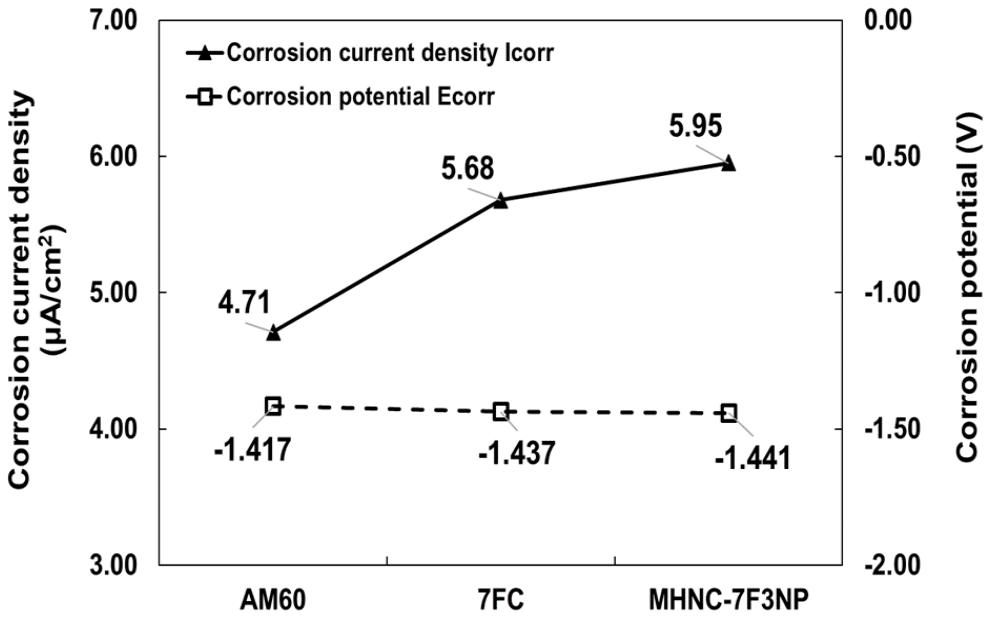

Fig. 4.9. Corrosion current densities and potentials of the uncoated samples AM60, 7FC and MHNC-7F3NP composites.

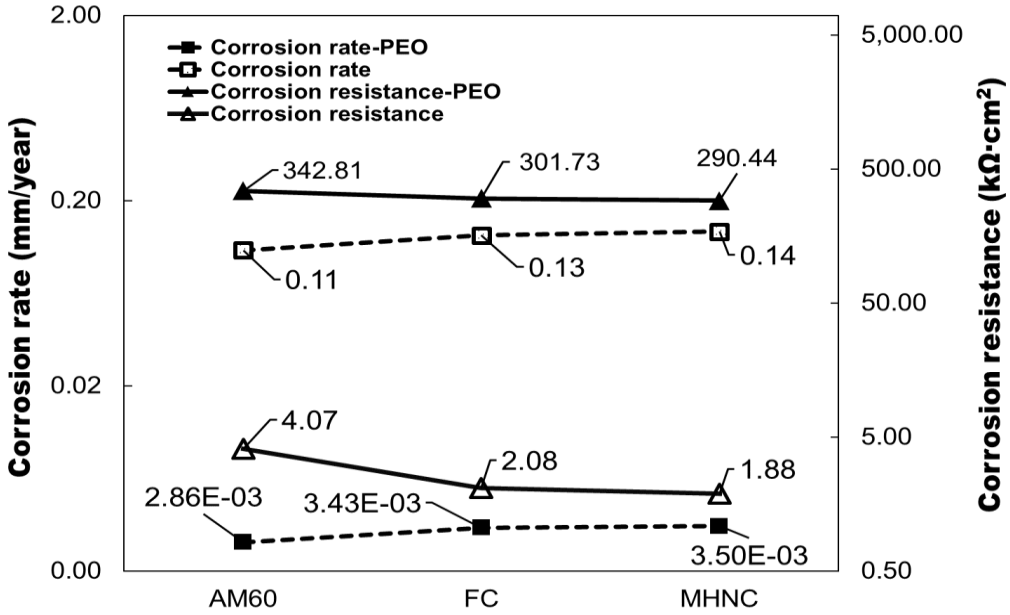

Fig. 4.10. Corrosion resistances and rates of the uncoated AM60, 7FC and MHNC-7F3NP composites and the PEO coated PEO-AM60, PEO-7FC and PEO-MHNC-7F3NP.

4.3.3. Surface appearance of corrosion

Figure 4.11 shows the comparison of SEM micrographs of the corroded surfaces of coated and uncoated samples after immersion in 3.5 wt.% NaCl solution for 1 hour. The difference of corrosion attack on the uncoated and coated samples was evident by comparing the corrosion surfaces. The pitting corrosion and galvanic corrosion happened everywhere on the surface of the uncoated AM60, 7FC and MHNC-7F3NP. Meanwhile the composites (7FC and MHNC-7F3NP) had corrosion behavior poorer than the AM60 alloy, of which the surface showed larger and deeper corrosion attack. The presence of the excessive interfaces generated by the introduction of the Al_2O_3 short fibers and particles into the matrix alloy interrupted the continuity of the matrix. However, the PEO coated samples (PEO-AM60, PEO-7FC and PEO-MHNC-7F3NP) had significantly improved corrosion behavior by comparing with the uncoated samples, since there were only a few small corroded points on the surface. The PEO-7FC and PEO-MHNC-7F3NP still showed slightly more corroded area than those of the PEO-AM60. This is because the addition of Al_2O_3 short fibers and particles had affected the coating growth during the PEO process, of which the coating thickness became thinner than that of the coating on the matrix AM60 alloy. After immersion in 3.5 wt.% NaCl solution for 1 hour, the PEO coated samples exhibited a relatively clean and complete coating on the substrate. The corrosion appeared evenly over the entire coating surface without the formation of deep pits into the substrates of all three PEO coated samples as can be seen from Figure 4.12. The presence of Al_2O_3 fibers still had a negative influence on the corrosion behavior due to the thinner PEO coating on composites. However, the addition of nano-sized Al_2O_3 particles caused almost no further deterioration of corrosion for the PEO-MHNC-7F3NP. Figure 4.13 presents the

EDS spectra of the corrosion surfaces on the three samples, showing the presence of oxygen, chloride and aluminum in the corrosion product.

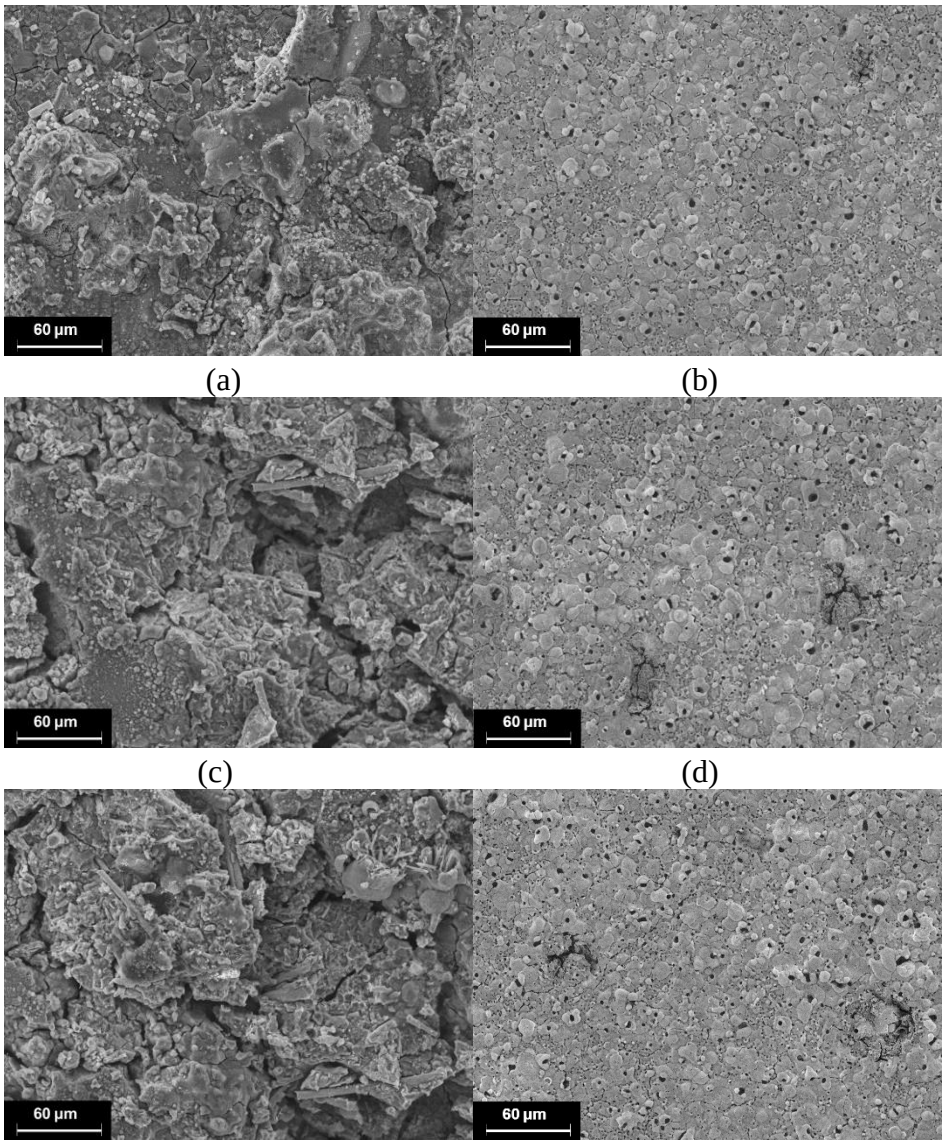

Fig. 4.11. SEM micrographs in SE mode showing corroded surfaces of (a) AM60, (b)PEO-AM60, (c) 7FC, (d) PEO-7FC, (e) MHNC-7F3NP and (f) PEO-MHNC-7F3NP composites.

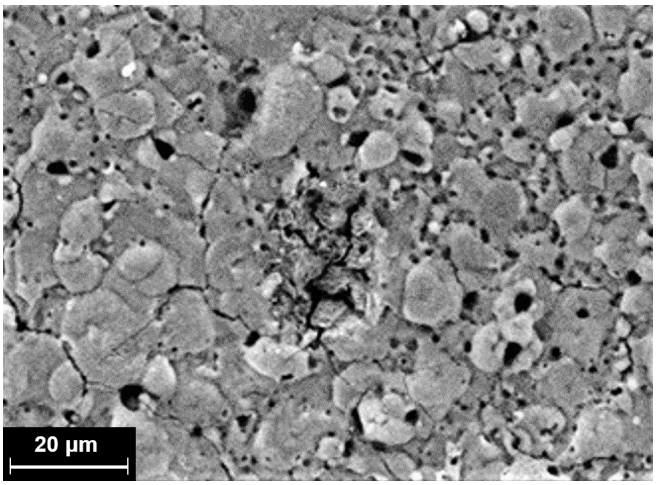

(a)

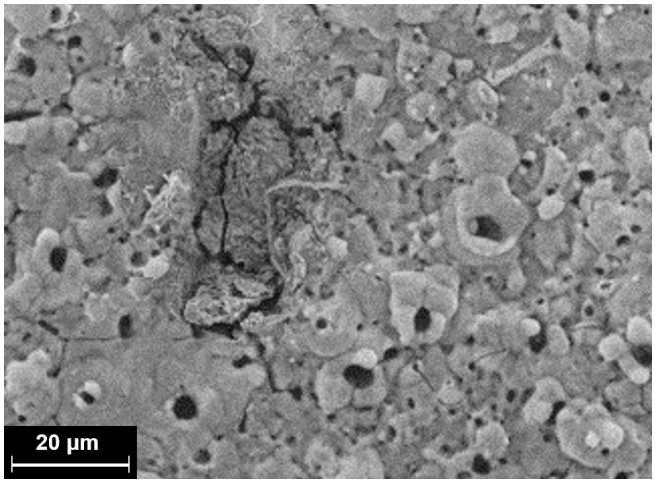

(b)

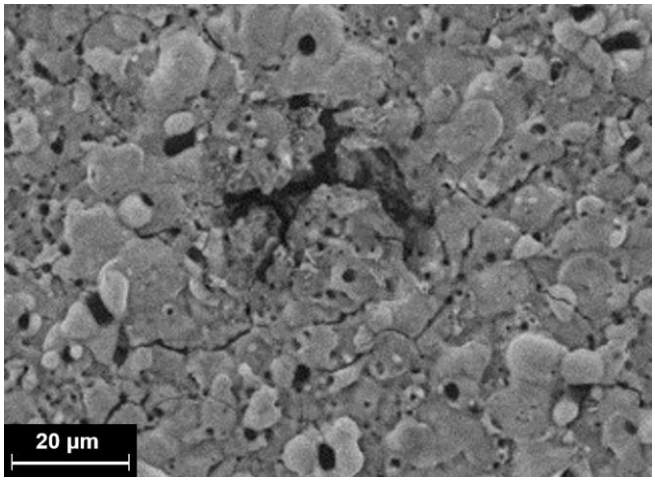

(c)

Fig. 4.12. SEM micrographs in SE mode showing corroded surfaces of (a) PEO-AM60, and the (b) PEO-7FC and (c) PEO-MHNC-7F3NP composites.

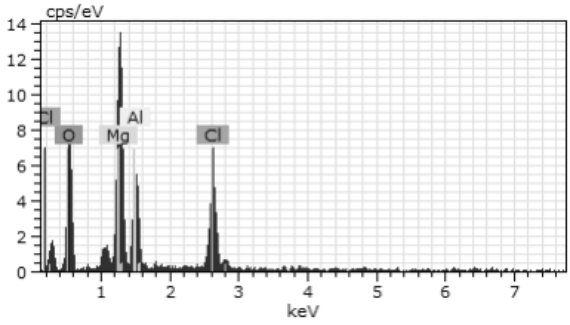

(a)

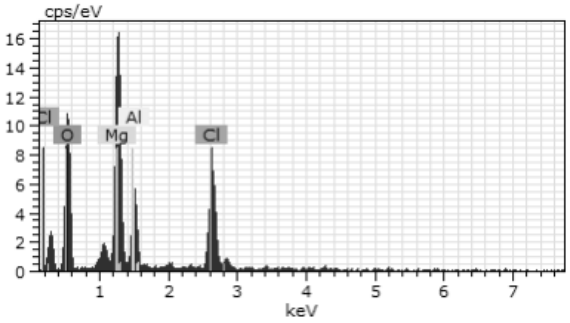

(b)

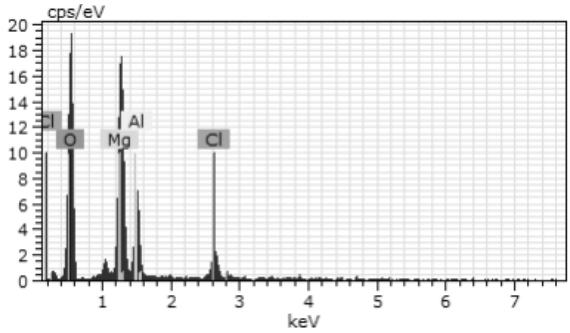

(c)

Fig. 4.13. EDS spectra identifying oxygen, aluminum and chlorine for the (a) PEO-AM60, and the (b) PEO-7FC and (c) PEO-MHNC-7F3NP composites respectively, which corresponds the SEM graphs in Figure 4.12.

4.4. Conclusions

The corrosion behaviors and microstructure of the PEO coated unreinforced AM60 alloy, 7 vol.% Al_2O_3 short fibers reinforced AM60 composites and AM60 hybrid composites with 7 vol.% Al_2O_3 short fibers and 3 vol.% Al_2O_3 nano-sized particles have been investigated. The following conclusions can be made based on the present study.

1. The top and cross-section microstructures of the PEO coated AM60 alloy and its composites (PEO-7FC and PEO-MHNC-7F3NP) were investigated. The primary α-Mg grains, eutectic β-$Mg_{17}Al_{12}$ phases and Al-Mn intermetallics were randomly distributed in the substrate of the PEO-AM60. The same types of phases were also present in the substrates of PEO-7FC and PEO-MHNC-7F3NP. The phases were likely to attach the fibers in the composites, which could be caused by the preheated fibers acting as a heat source to slow down the solidification of the surrounding molten matrix alloy solidification during the infiltration process under pressures.
2. A dense and inhomogeneous coating was produced on the AM60 alloy and its composites. The unreinforced AM60 alloy had thicker PEO coating than its composites. The addition of the reinforcement influenced the growth of coating during the PEO process, since the Al_2O_3 short fibers and nano-sized particles broke down the continuity of the matrix alloy, and were an insulator affecting the discharge and delayed the passivation of the matrix alloy.
3. The PEO coating process tremendously improved the corrosion resistance of the AM60 and its composites. The corrosion resistance of the AM60 alloy was increased from 4.072 $k\Omega \cdot cm^2$ to 342.811 $k\Omega \cdot cm^2$ by the PEO coating, which also increased the raised resistance of the 7FC and MHNC-7F3NP composites from 2.083 $k\Omega \cdot cm^2$ and 1.883 $k\Omega \cdot cm^2$ to 301.731 $k\Omega \cdot cm^2$ and 290.442 $k\Omega \cdot cm^2$ respectively.
4. The comparison of the coated and uncoated samples indicated that the difference in corrosion resistance between the unreinforced AM60 alloy and its composites was reduced significantly after applying PEO coating. The addition of reinforcements (Al_2O_3 short fibers and nano-sized particles) in the composites still had a negative

influence for their corrosion behaviors. The presence of 3 vol.% nano-sized particles had almost no effect on the corrosion resistance of the 7FC composite.

5. No deep pitting corrosion was observed on the PEO coated composites, and the corrosion evenly spread over the entire PEO coating surface after immersion in 3.5 wt.% NaCl aqueous solution for 1 hour. The major elements in the corroded areas of the PEO coatings on the AM60 alloy, 7FC and MHNC-7F3NP composites were identified to be oxygen, aluminum, chloride and magnesium.

4.5. References

[1] Gupta, M. & Wong, W. (2015). Magnesium-based nanocomposites: lightweight materials of the future. Mater. Charact. 105: 30– 46.

[2] Ye, H. & Liu, X. (2004). Review of recent studies in magnesium matrix composites, J. Mater. Sci. 39: 6135–6171.

[3] Zhou, J., Ren, Luyang., Geng, X., Fang, L.& Hu, H. (2019). As-cast magnesium AM60-based hybrid nanocomposite containing alumina fibres and nanoparticles: Microstructure and tensile behavior. Materials Science & Engineering A. 740-741: 305-314.

[4] Zhang, X., Fang, L., Xiong, B. & Hu, H. (2015). Microstructure and Tensile Properties of Mg (AM60)/Al_2O_3 Metal Matrix Composites with Varying Volume Fractions of Fiber Reinforcement. Journal of Materials Engineering and Performance. 24(12): 4601-4611.

[5] Zhang, X., Zhang, Q. & Hu, H. (2014). Tensile Behavior and Microstructure of Magnesium AM60-based Hybrid Composite Containing Al_2O_3 Fibres and Particles. Materials Science and Engineering A. 607: 269-276.

[6] H. Hu. (1998). Squeeze casting of magnesium alloys and their composites. J. Mater. Sci. 33: 1579–1589.

[7] Towle, D. & Friend, C. (1994). Effect of Reinforcement architecture on mechanical properties of a short fibre/magnesium RZ MMC manufactured by Preform Infiltration. Mater. Sci. Eng. A. 188: 153–158.

[8] Yerokhin, A., Nie, X., Leyland, A., Matthews, A. & Dowey, S. (1999). Plasma electrolysis for surface engineering. Surf. Coat Technol. 122: 73-93.

[9] Yerokhin, A., Lyubimov, V. & Ashitkov. R. (1998). Phase formation in ceramic coatings during plasma electrolytic oxidation of aluminium alloys. Ceramics International. 24: 1–6.

[10] Wang, Y., Wang, J. & Zhang, J. (2005). Characteristics of anodic coatings oxidized to different voltage on AZ91D Mg alloy by micro-arc oxidization technique. Mater. Corros. 56: 88–92.

[11] Hsiao, H. & Tsai, W. (2005). Characterization of anodic films formed on AZ91D magnesium alloy. Surf. Coat Technol. 190: 299-308.

[12] Zhang, Y., Yan, C., Wang, F., Lou, H. & Cao, C. (2002). Study on the environmentally friendly anodizing of AZ91D magnesium alloy. Surf Coat Technol. 161: 36-43.

[13] Khaselev, O., Weiss, D. & Yahalom, J. (2001). Structure and composition of anodic films formed on binary Mg-Al alloys in KOH-aluminate solutions under continuous sparking. Corros. Sci. 43: 1295-1307.

[14] Yerokhin, A., Ahatrov, A., Samsonov, V., Shashkov, P., Leyland, A. & Matthews, A. (2004). Fatigue properties of Keronite® coatings on a magnesium alloy. Surf.

Coat Technol. 182: 78–84.

[15] Guo, X., Ding W., Lu, C. & Zhai, C. (2004). Influence of ultrasonic power on the structure and composition of anodizing coatings formed on Mg alloys. Surf. Coat. Technol. 183: 359–368.

[16] Zhang, P., Nie, X., Han, L. & Hu, H. (2010). Wear protection of Al383/SiO_2 Metal Matrix Composites by Plasma Electrolytic Oxidation (PEO) Process. Inter. J. Mat. Manuf. 3(1): 55-62.

[17] Zhang, P., Nie, X., Hu, H. & Zhang, J. (2010). Preparation and tribological properties of thin oxide coatings on an Al383/SiO_2 metallic matrix composite. Surf Coat Technol. 205(6): 1689-1696.

[18] Xue, W., Jin, Q., Zhu, Q., Hua, M. & Ma, Y. (2009). Anti-corrosion microarc oxidation coatings on SiCP/AZ31 magnesium matrix composite, Journal of Alloys and Compounds, 482: 208-212.

[19] Hussein, R., Zhang, P., Northwood, D., & Nie, X. (2011). Improving the corrosion resistance of magnesium alloy AJ62 by a plasma electrolytic oxidation (PEO) coating process. Corrosion and Materials, 36(3), 38-49.

[20] Zhang, Q., Hu, H. & Lo, J. (2011). Solidification of discontinuous Al_2O_3 fiber reinforced magnesium (AM60) matrix composite. Defect and Diffusion Forum. 312-315: 277-282.

[21] Bakkar, A., & Neubert, V. (2007). Corrosion characterization of alumina–magnesium metal matrix composites. Corrosion science, 49(3), 1110-1130.

[22] John, W. & Sons. (2000). R.W. Revie, Uhlig's Corrosion Handbook, 2nd ed. New York.

[23] Mondal, A., Blawert, C., & Kumar, S. (2015). Corrosion behaviour of creep-resistant AE42 magnesium alloy-based hybrid composites developed for powertrain applications. Materials and Corrosion, 66(10), 1150-1158.

[24] Shi, Z. & Atrens, A. (2011). An innovative specimen configuration for the study of Mg Corrosion, Corrosion Science, 53, 226-246.

[25] Shi, Z., Liu, M. & Atrens, A. (2010). Measurement of the corrosion rate of magnesium alloys using Tafel extrapolation, Corrosion Science 52, 579–588.

CHAPTER 5
Conclusions

The objectives of this study are to analyze the microstructures of the developed magnesium-based hybrid composite containing micron sized fibres and nano sized particles in comparison with the only micron sized fibres reinforced composite, and evaluate the corrosion resistance of magnesium alloy-based micron sized fibre reinforced composite and micron sized fibre and nano sized particle reinforced hybrid composite in comparison with the unreinforced magnesium matrix alloy. Meanwhile, another goal of this study is to investigate the plasma electrolytic oxidation process for improving the corrosion resistance of magnesium alloy-based composites and evaluate the corrosion resistance of PEO coated magnesium alloy and its composites and compare the corrosion resistance between the PEO coated materials and uncoated materials. The conclusions drawn from this study are summarized as follows:

1. The microstructure of the matrix alloy AM60 consisted of primary α-Mg grains, eutectic β-$Mg_{17}Al_{12}$ phases, and Al-Mn intermetallics. The eutectic β-$Mg_{17}Al_{12}$ phases, and Al-Mn intermetallics were present in the form of isolated fine particles surrounding the boundaries of the primary α-Mg grains. But, in the 7FC and MHNC-7F3NP composites, the eutectic β-$Mg_{17}Al_{12}$ phases, and Al-Mn intermetallics attached to the surface of the fibres and particles.
2. The introduction of the micron-sized fibres and nano-sized particles refined grain structure in the composites. The grain size decreased from 65 μm for the matrix alloy

AM60 to 37 μm for the 7FC composite by 43%. The introduction of the nano particles (3 vol.%) resulted in a minor reduction in the grain size from 37 to 26 μm.

3. The unreinforced as-cast AM60 performed the best corrosion resistance, and the micron-sized Al_2O_3 fibres and nano-sized Al_2O_3 particles reinforcement deteriorates its corrosion resistance. The addition of the micron-sized fibres at 7 vol.% as reinforcement significantly reduced the corrosion resistance of the matrix alloy AM60 from 4.07 to 2.08 $k\Omega \cdot cm^2$ by almost 50%. The presence of the nano-sized particles resulted in a reduction of the corrosion resistance of the 7FC composite from 2.08 to 1.88 $k\Omega \cdot cm^2$ by 0.20 $k\Omega \cdot cm^2$. This observation indicated that the introduction of the nano-sized particles up to 3 vol.% had almost no effect on the corrosion resistance of the FC composite.
4. The formation of the surface morphology on the corroded unreinforced alloy AM60 resulted from a combined effect of galvanic corrosion, and pitting corrosion. The presence of different phases in the microstructure of the unreinforced alloy AM60 should be responsible for these types of corrosion mechanisms. The eutectic β-$Mg_{17}Al_{12}$ and Al-Mn intermetallic phases in the Mg-Al alloy could serve as cathodic sites, and the primary α-Mg matrix would be anodic.
5. No galvanic interaction between the alloy matrix and reinforcing fibres and particles could take place since the Al_2O_3 fibres and particles are an insulator. In the composites, the lack of such relatively more noble precipitates such as β-$Mg_{17}Al_{12}$ phases and Al-Mn intermetallics at the grain boundaries could result in a low corrosion resistance, although the high density of grain boundaries might not be the main mechanism of decreasing in corrosion resistance.

6. The introduction of the fibres and particles in the 7FC and MHNC-7F3NP composites generated new interfaces between the matrix alloy and reinforcements, which broke the continuity of the matrix and formed preferential spots for corrosion attack. The poor corrosion resistance of the composites should be attributed to the irregular and less adherent film on their surface.
7. The top and cross-section microstructures of the PEO coated AM60 alloy and its composites (PEO-7FC and PEO-MHNC-7F3NP) were investigated. The primary α-Mg grains, eutectic β-$Mg_{17}Al_{12}$ phases and Al-Mn intermetallics were randomly distributed in the substrate of the PEO-AM60. The same types of phases were also present in the substrates of PEO-7FC and PEO-MHNC-7F3NP. The phases were likely to attach the fibers in the composites, which could be caused by the preheated fibers acting as a heat source to slow down the solidification of the surrounding molten matrix alloy solidification during the infiltration process under pressures.
8. A dense and inhomogeneous coating was produced on the AM60 alloy and its composites. The unreinforced AM60 alloy had thicker PEO coating than its composites. The addition of the reinforcement influenced the growth of coating during the PEO process, since the Al_2O_3 short fibers and nano-sized particles broke down the continuity of the matrix alloy, and were an insulator affecting the discharge and delayed the passivation of the matrix alloy.
9. The PEO coating process tremendously improved the corrosion resistance of the AM60 and its composites. The corrosion resistance of the AM60 alloy was increased from 4.072 $k\Omega \cdot cm^2$ to 342.811 $k\Omega \cdot cm^2$ by the PEO coating, which also increased the raised resistance of the 7FC and MHNC-7F3NP composites from 2.083 $k\Omega \cdot cm^2$ and

1.883 kΩ·cm^2 to 301.731 kΩ·cm^2 and 290.442 kΩ·cm^2 respectively.

10. The comparison of the coated and uncoated samples indicated that the difference in corrosion resistance between the unreinforced AM60 alloy and its composites was reduced significantly after applying PEO coating. The addition of reinforcements (Al_2O_3 short fibers and nano-sized particles) in the composites still had a negative influence for their corrosion behaviors. The presence of 3 vol.% nano-sized particles had almost no effect on the corrosion resistance of the 7FC composite.
11. No deep pitting corrosion was observed on the PEO coated composites, and the corrosion evenly spread over the entire PEO coating surface after immersion in 3.5 wt.% NaCl aqueous solution for 1 hour. The major elements in the corroded areas of the PEO coatings on the AM60 alloy, 7FC and MHNC-7F3NP composites were identified to be oxygen, aluminum, chloride and magnesium.

CHAPTER 6
Future works

This study carried out the investigation of the corrosion behavior of the AM60 alloy and its composites with and without plasma electrolytic oxidation (PEO) coating which provides the foundation work to pursue further investigation in the future. The following are the suggestions for the future work:

- Study the different parameters of the plasma electrolytic oxidation process for optimization of the PEO coating on the magnesium-based composites, including different types of electrolytes and their concentrations, current mode and coating times.
- Investigate mechanical properties of PEO coated magnesium-based composites such as tensile properties and wear resistance.
- Analyze microstructure of PEO coatings on magnesium-based composites, which are to be produced with optimized coating process parameters.

APPENDICES

Appendix A

Chapter 3

AMPT 2018 submission 20 Inbox ×

AMPT 2018 <ampt2018@easychair.org> Sat, Mar 24, 2018, 9:42 PM

to me

Dear authors,

We received your paper:

Authors : Xinyu Geng, Luyang Ren, Zixi Sun and Henry Hu
Title : Corrosion Resistance of Magnesium Alloy AM60-based Hybrid Nanocomposite
Number : 20

The paper was submitted by Henry Hu <huh@uwindsor.ca>.

Thank you for submitting to AMPT 2018.

Best regards,
EasyChair for AMPT 2018.

AMPT abstract acceptance - AMPT2018, 4th - 7th September 2018, Dublin City University, Dublin, Ireland

Inbox ×

Dermot Brabazon <dermot.brabazon@dcu.ie> Tue, May 22, 2018, 5:39 PM

to Sithara, Shadi, Saleem

Dear Author,

After review of the submitted abstracts, we are delighted to confirm that your abstract has been accepted for presentation at AMPT2018.

A link for your registration at the conference is provided here: https://ampt2018.org/custom-registration-form/

The conference website link with further information is: https://ampt2018.org/

If you require a specific letter of acceptance for visa processing please let us know.

We are looking forward to a good conference and welcoming you to Dublin this coming September.

Best regards,

Prof. Dermot Brabazon, Chair of AMPT Conference

Prof. Saleem Hashmi, Chair of AMPT Steering Committee

Chapter 4

AMPT 2019 submission 4 Inbox ×

AMPT 2019 <ampt2019@easychair.org> Fri, Dec 14, 2018, 2:59 PM

to me

Dear authors,

We received your paper:

Authors : Xinyu Geng, Luyang Ren, Zixi Sun, Henry Hu and Xueyuan Nie
Title : Enhanced corrosion resistance of as-cast magnesium alloy AM60-based hybrid nanocomposite by a plasma electrolytic oxidation (PEO) coating process
Number : 4

The paper was submitted by Henry Hu <huh@uwindsor.ca>.

Thank you for submitting to AMPT 2019.

Best regards,
EasyChair for AMPT 2019.

The 22nd International Conference on Advances in Materials & Processing Technologies
Oct. 20-24, 2019,Taipei, Taiwan

Sponsored by the Chinese Society of Mechanical Engineers (CSME)
National Taiwan University of Science and Technology (NTUST)

Date: 22 Feb., 2019

Official Acceptance and Invitation Letter

Dear Henry Hu,

We are pleased to inform you that your abstract submitted to the 22nd International Conference on Advances in Materials & Processing Technologies (AMPT 2019) has been accepted. At least one of the authors is expected to register and attend the conference to present the paper with the following topic:

Paper ID: 4
Title: Enhanced corrosion resistance of as-cast magnesium alloy AM60-based hybrid nanocomposite by plasma electrolytic oxidation (PEO) coating
Authors: Xinyu Geng, Luyang Ren, Zixi Sun, Henry Hu, Xueyuan Nie and Li Fang

The conference will be held in Taipei, Taiwan on Oct. 20-24, 2019. All papers were rigorously reviewed by at least two experts in the relevant fields. The guidelines of attending AMPT 2019 are shown in http://www.ampt2019.org.

Your presence at the conference would be a great contribution to the event. We look forward to seeing you at the conference.

Best Regards

Prof. Zone-Ching Lin
Conference Chair, AMPT 2019
Department of Mechanical Engineering
National Taiwan University of Science and Technology

PS: This letter is being sent to you for possible financial support from your institute, and for VISA application if needed.

Appendix B

Microstructure Analysis Figures

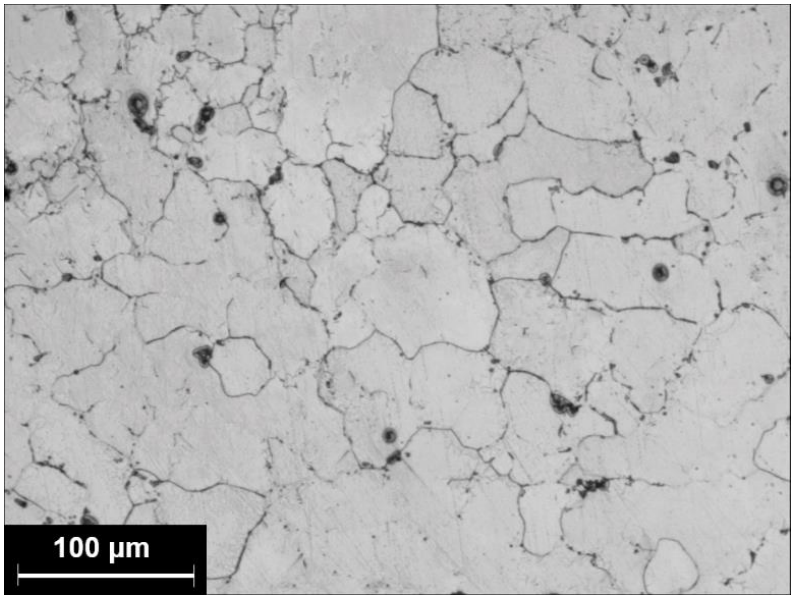

(a)

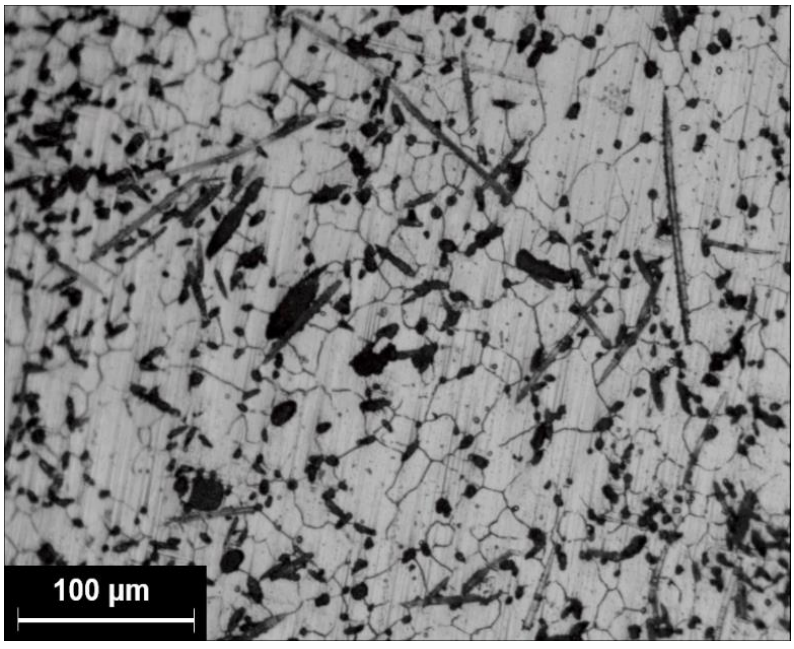

(b)

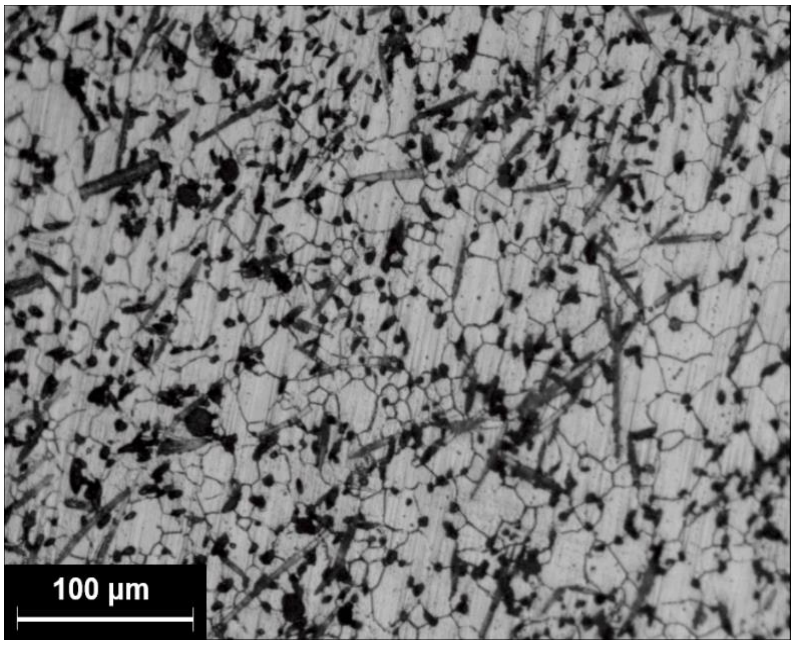

(c)

Fig. B.1. Optical micrographs showing grain structures of etched (a) unreinforced matrix alloy AM60, (b) 7FC, and (c) MHNC-7F3NP.

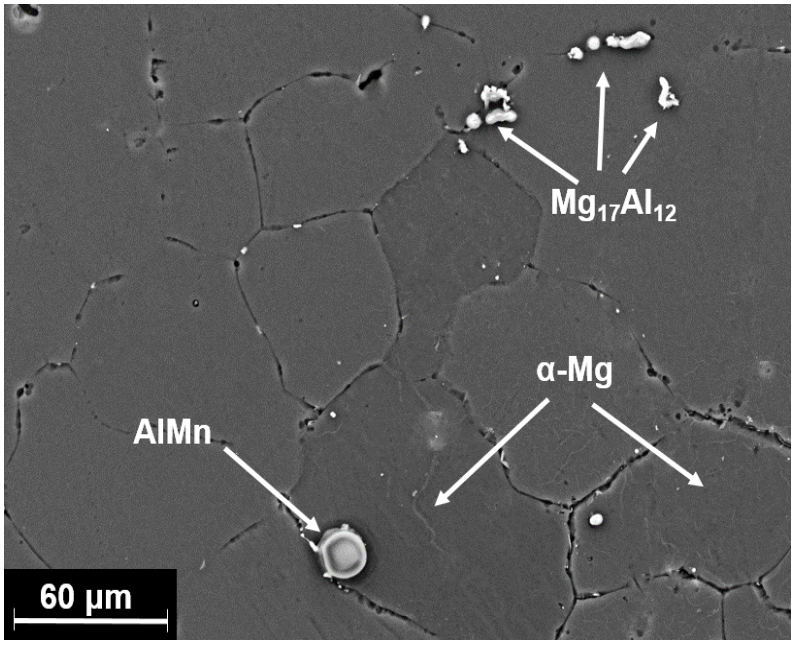

Fig. B.2. SEM micrographs in BSE mode showing constituent phases in microstructure of etched unreinforced matrix alloy AM60.

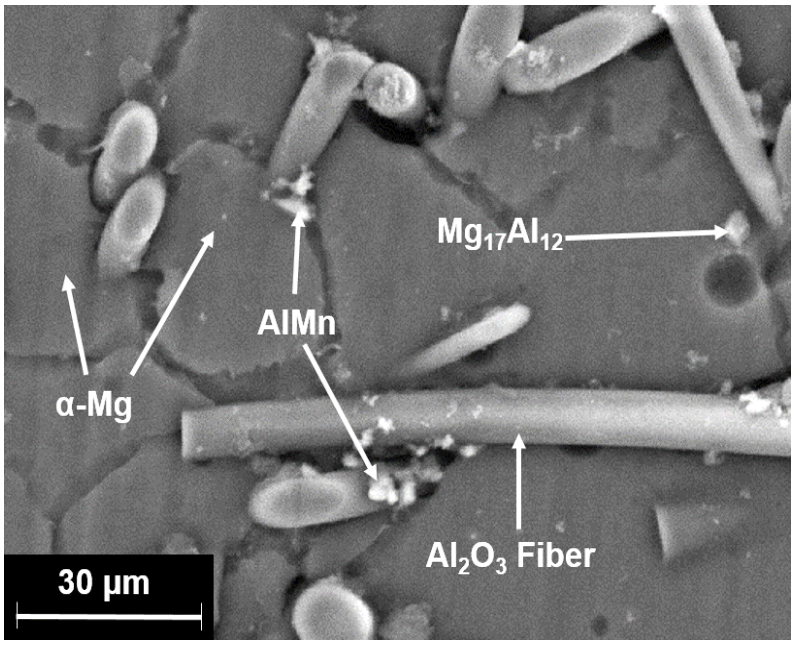

Fig. B.3. SEM micrographs in BSE mode showing constituent phases in microstructure of the 7FC composite

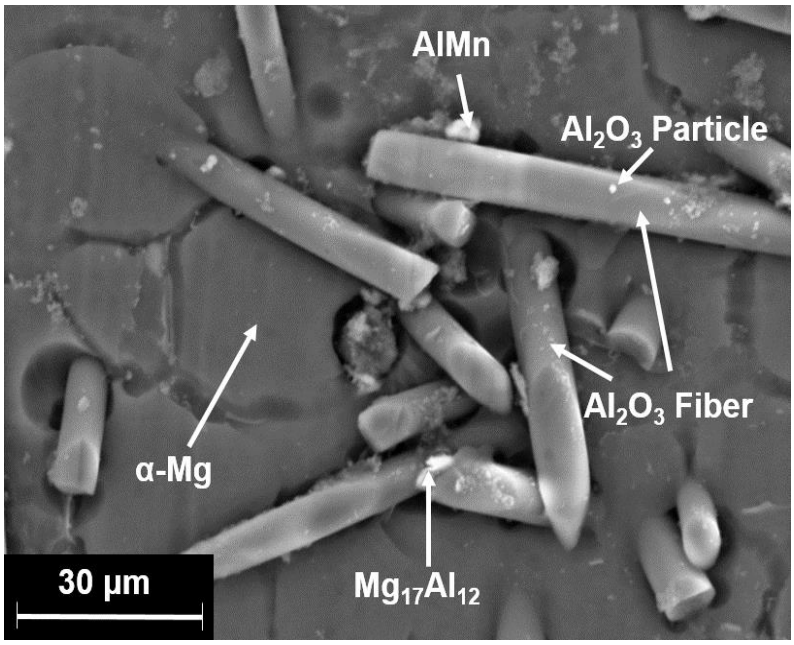

Fig. B.4. SEM micrographs in BSE mode showing constituent phases in microstructure of the MHNC-7F3NP composite

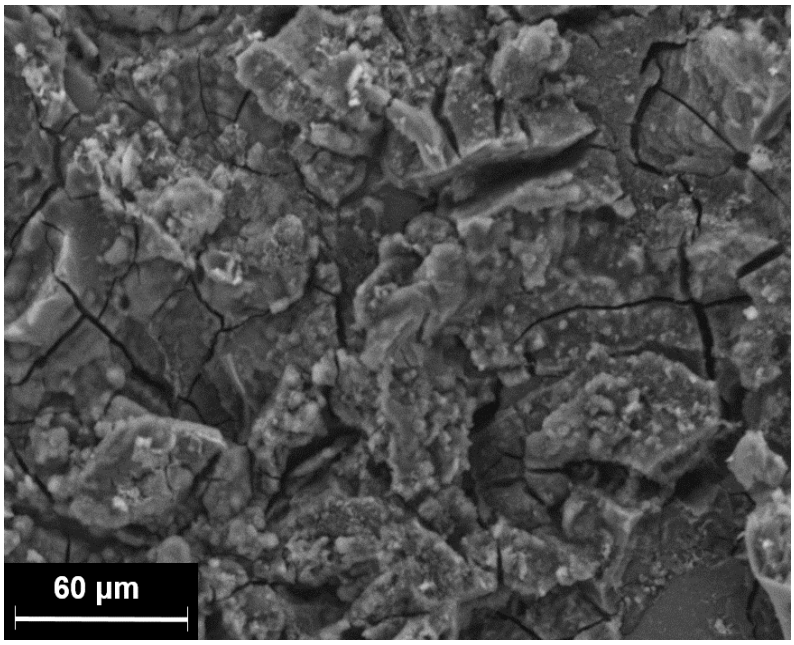

(a)

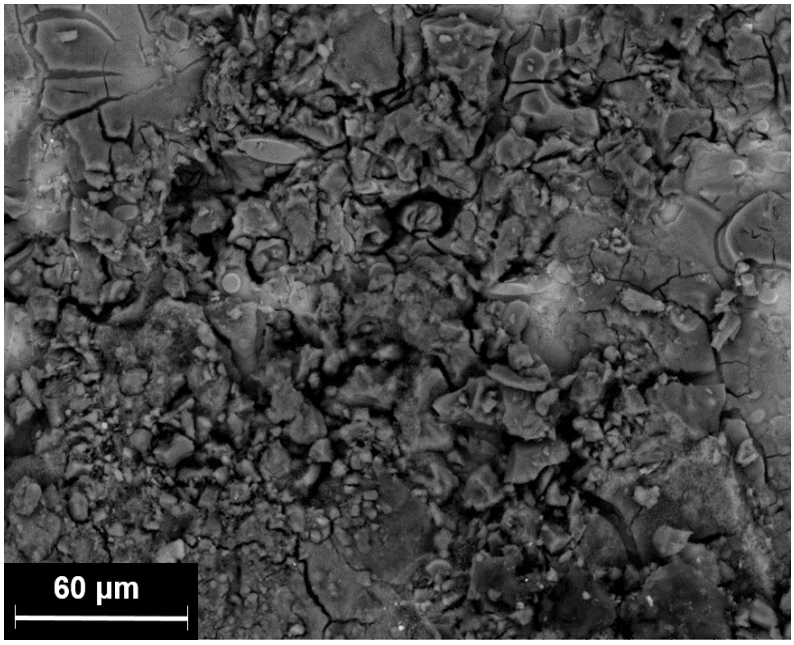

(b)

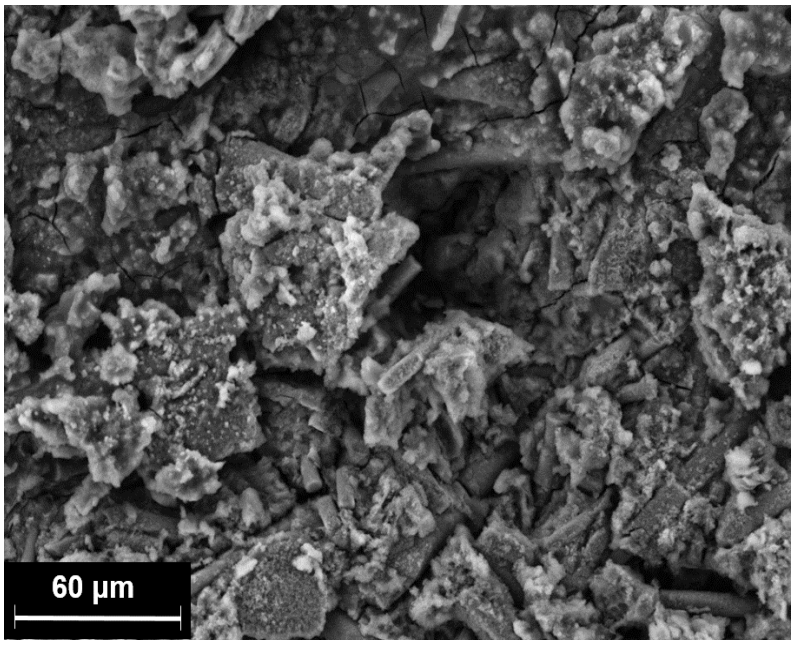

(c)

Fig. B.5. SEM micrographs in SE mode showing corroded surfaces of (a) the unreinforced alloy AM60, and the (b) 7FC and (c) MHNC-7F3NP composites.

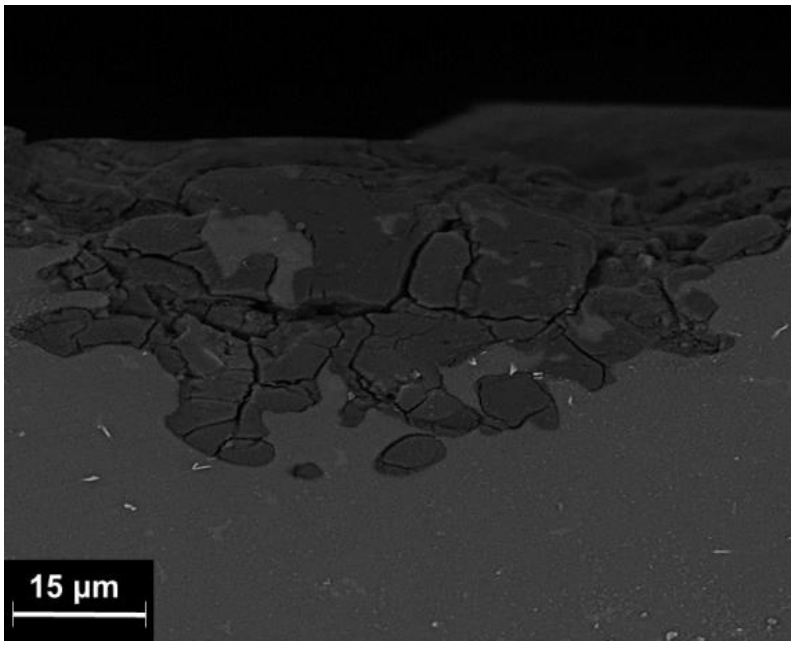

(a)

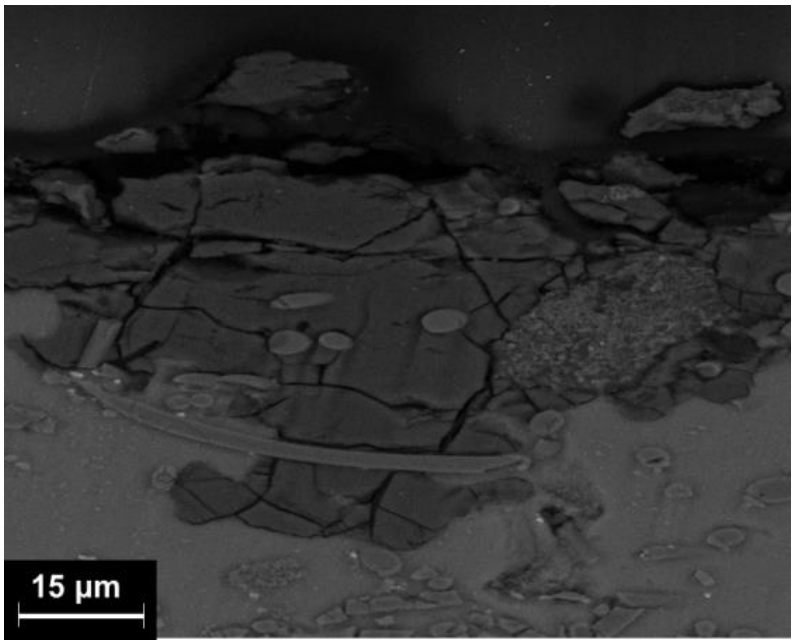

(b)

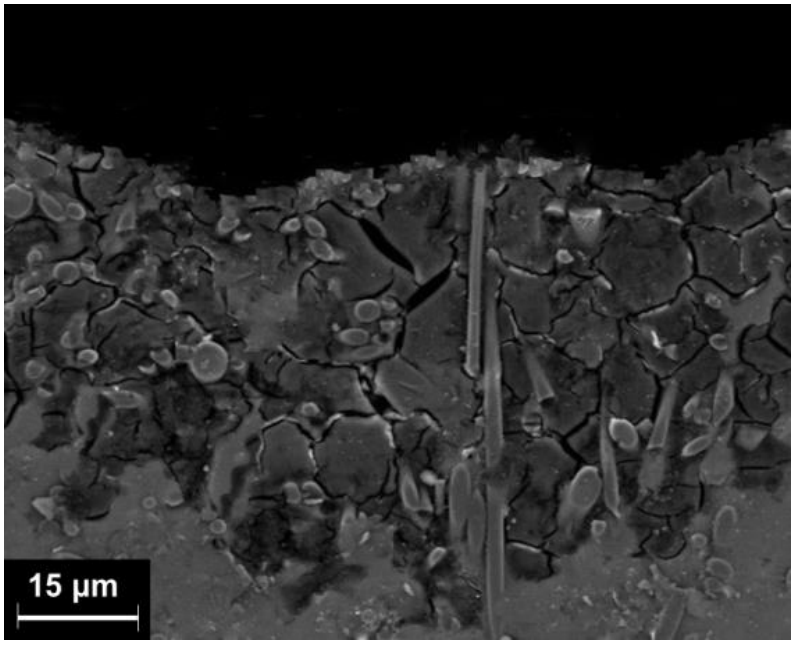

(c)

Fig. B.6. SEM micrographs in SE mode showing corroded sub surfaces in the cross-section of (a) the unreinforced alloy AM60, and the (b) 7FC and (c) MHNC-7F3NP composites.

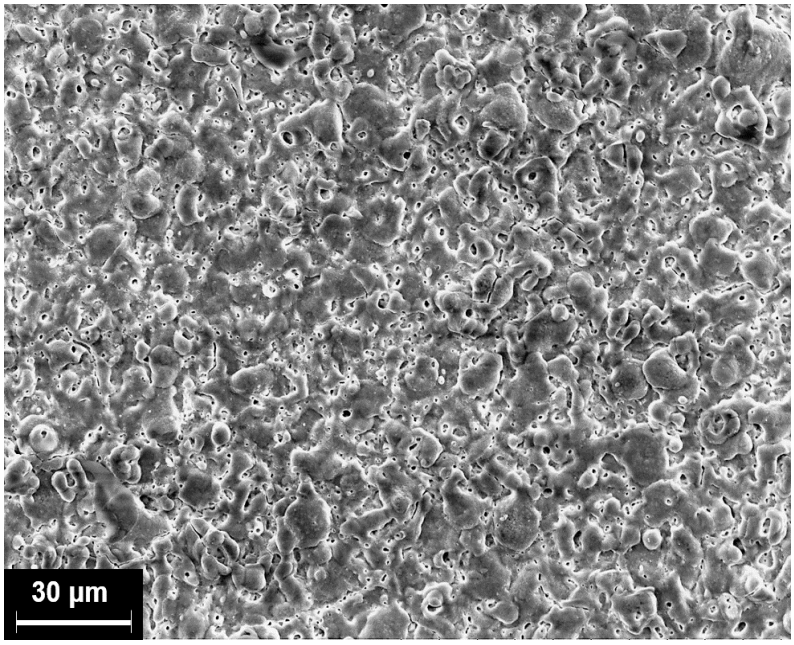

(a)

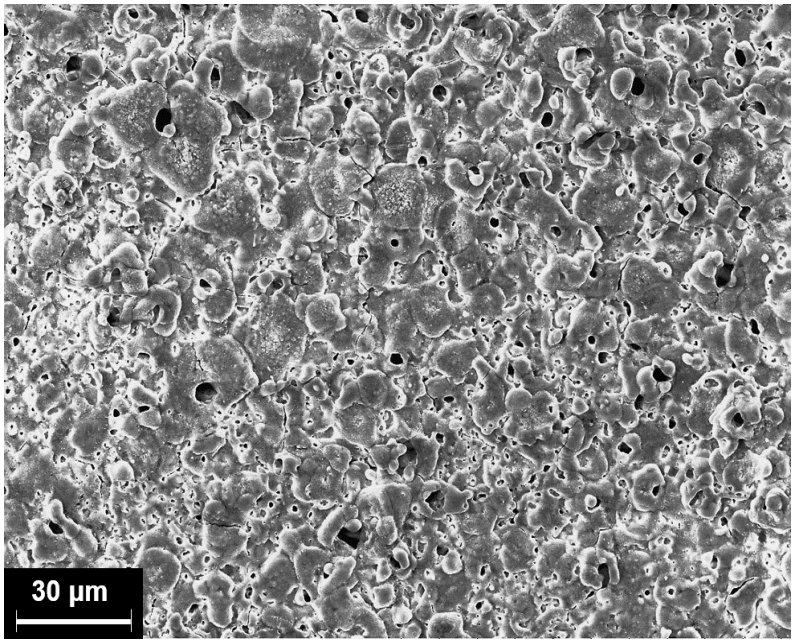

(b)

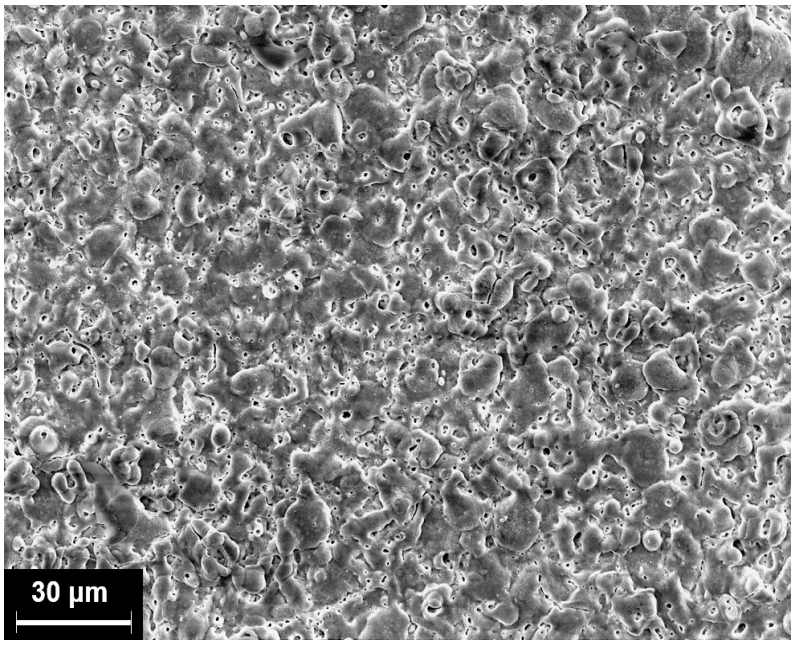

(c)

Fig. B.7. SEM micrographs in SE mode showing PEO coating surfaces of (a) PEO-AM60, (b) PEO-7FC and (c) PEO-MHNC-7F3NP, respectively.

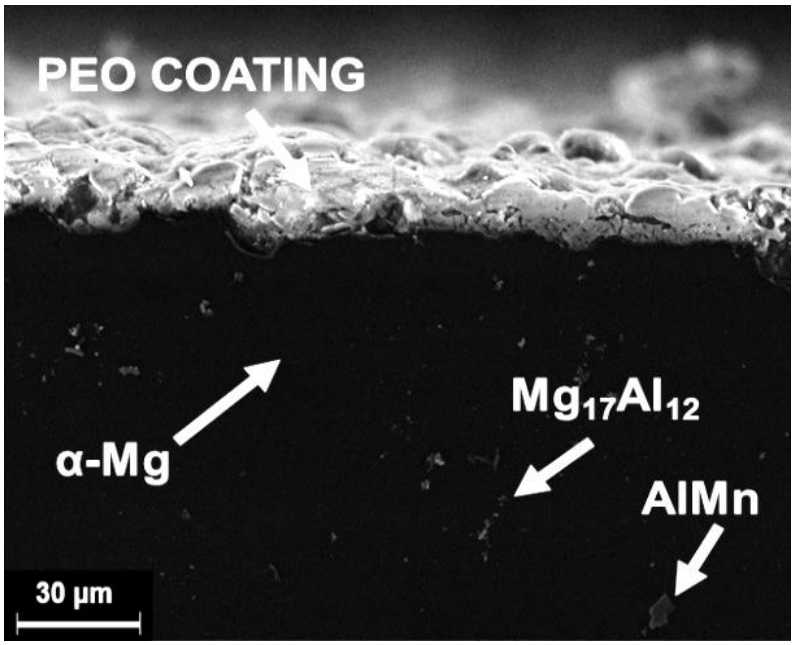

(a)

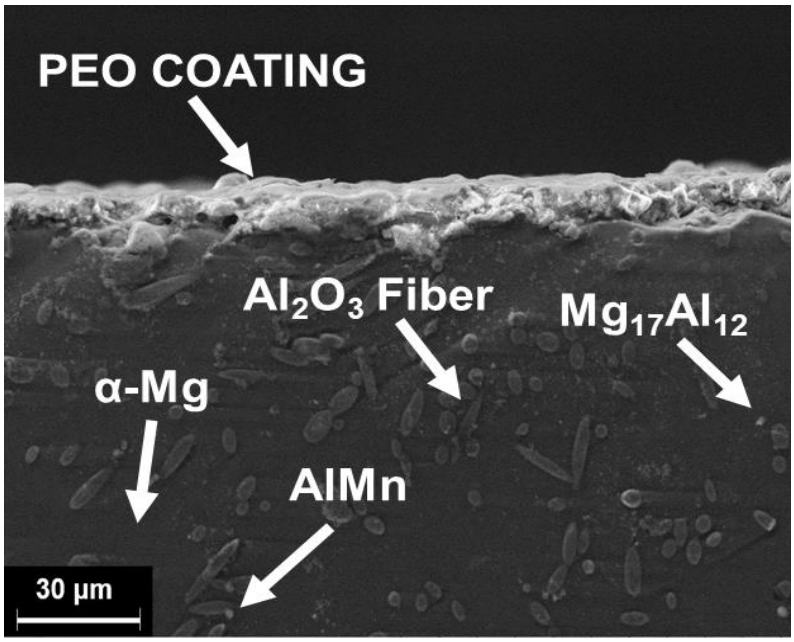

(b)

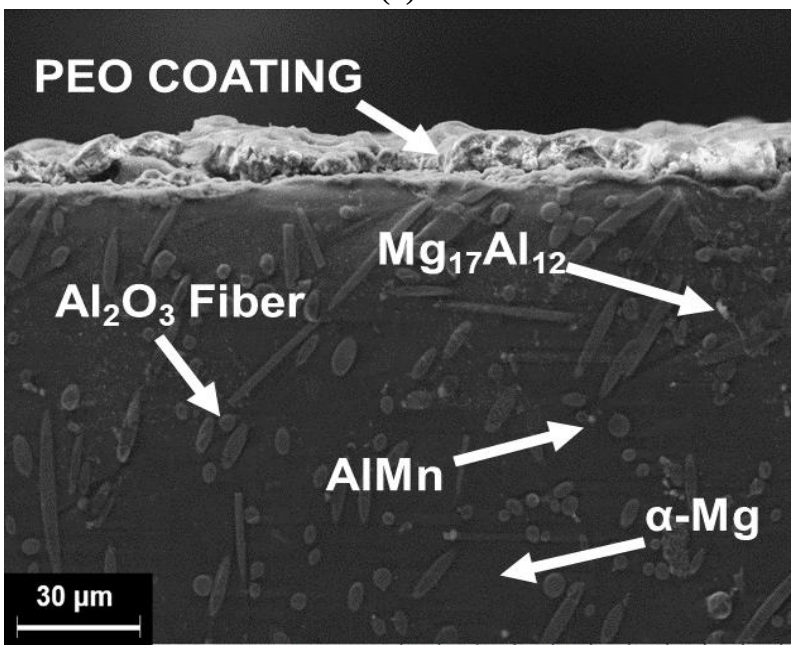

(c)

Fig. B.8. SEM micrographs in SE mode showing the PEO coating cross-sections of PEO coatings for (a) PEO-AM60, (b) PEO-7FC and (c) PEO-MHNC-7F3NP, respectively.

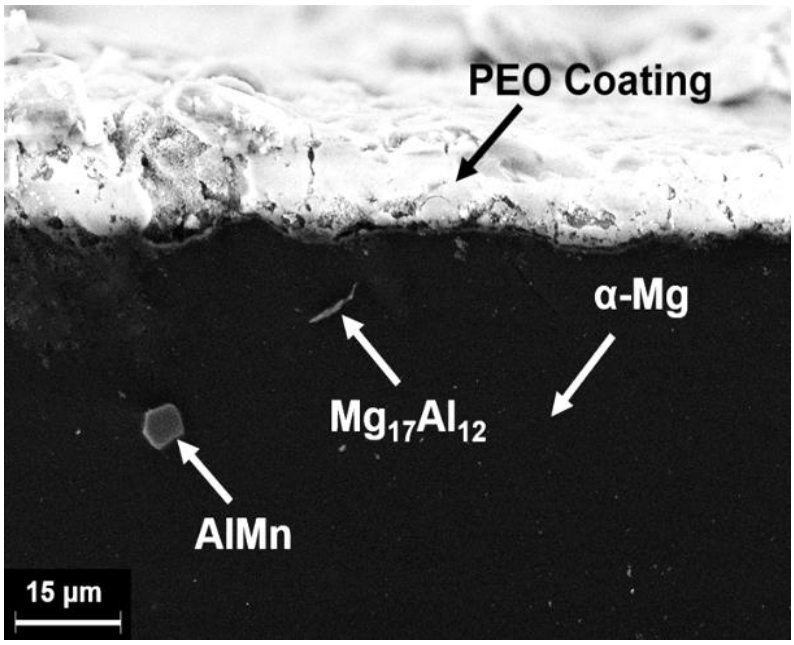

Fig. B.9. SEM micrograph in SE mode showing constituent phases in microstructure of the PEO-AM60

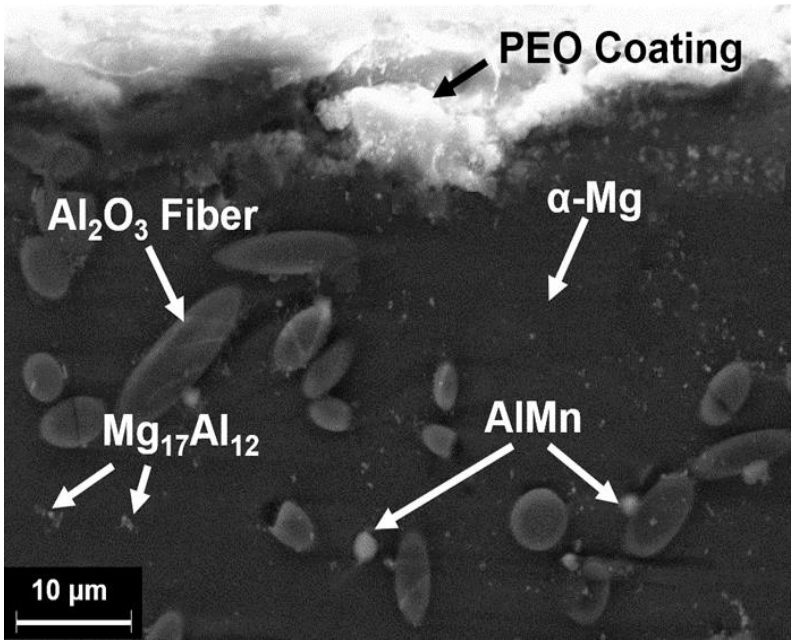

Fig. B.10. SEM micrograph in SE mode showing constituent phases in microstructure of the PEO-7FC

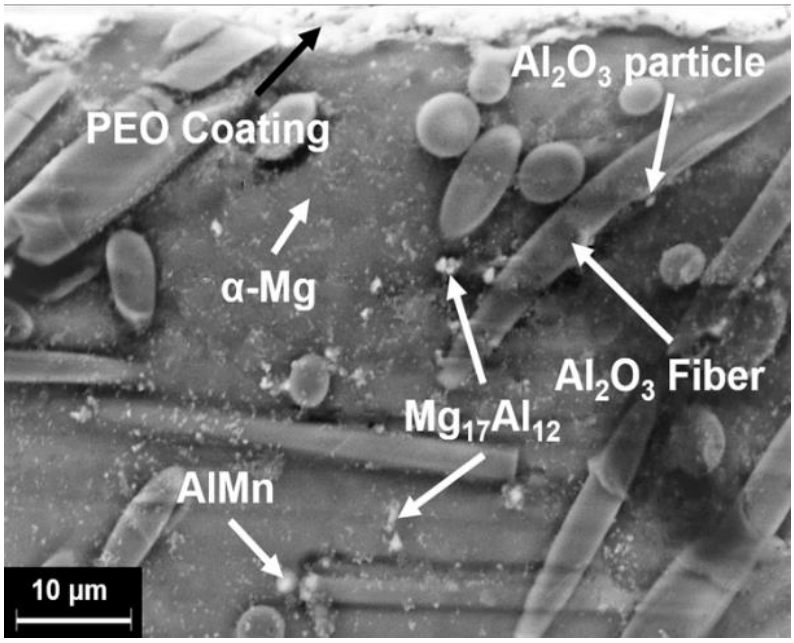

Fig. B.11. SEM micrograph in SE mode showing constituent phases in microstructure of the PEO-MHNC-7F3NP

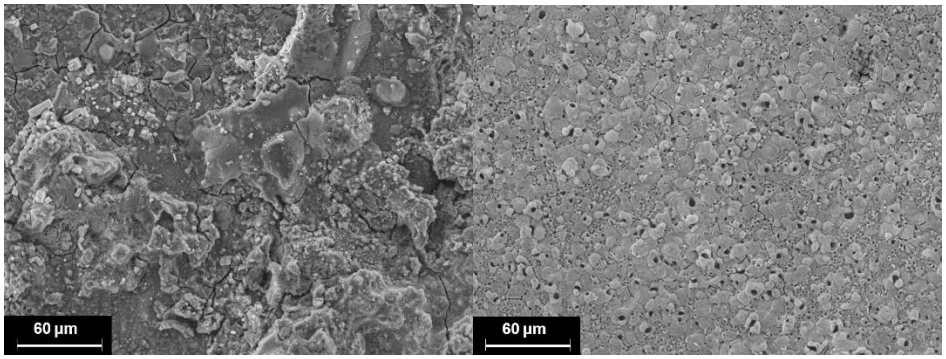

(a) (b)

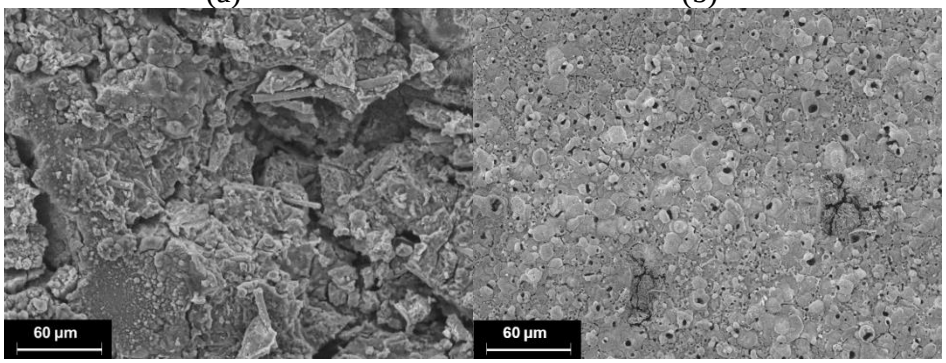

(c) (d)

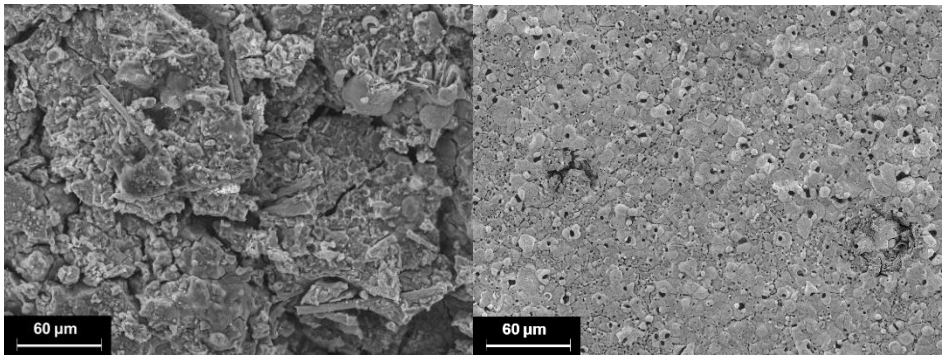

(e) (f)

Fig. B.12. SEM micrographs in SE mode showing corroded surfaces of (a) AM60, (b)PEO-AM60, (c) 7FC, (d) PEO-7FC, (e) MHNC-7F3NP and (f) PEO-MHNC-7F3NP composites.

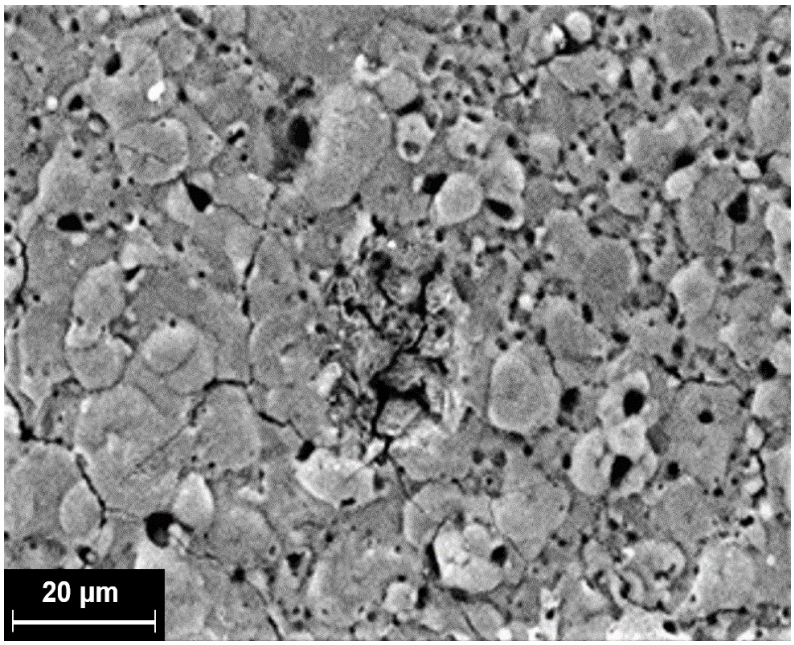

(a)

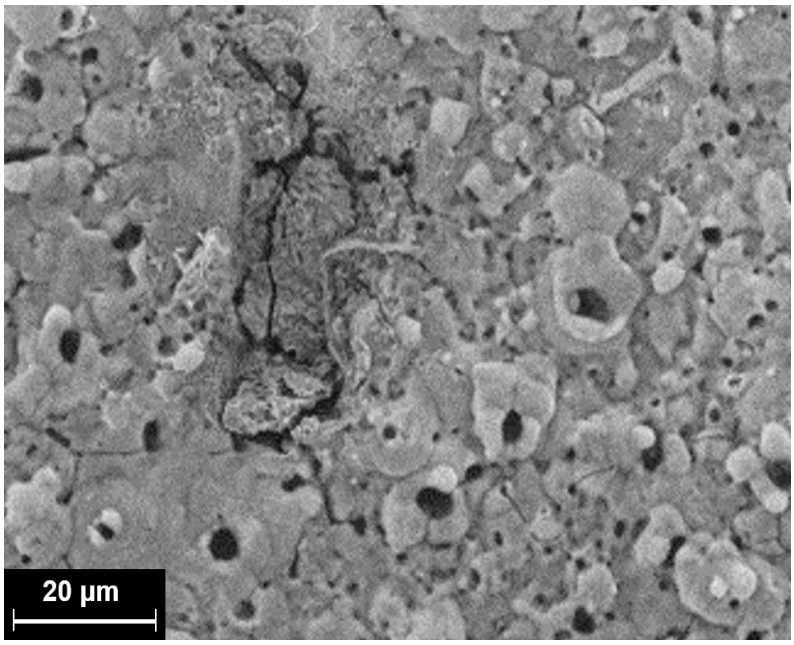

(b)

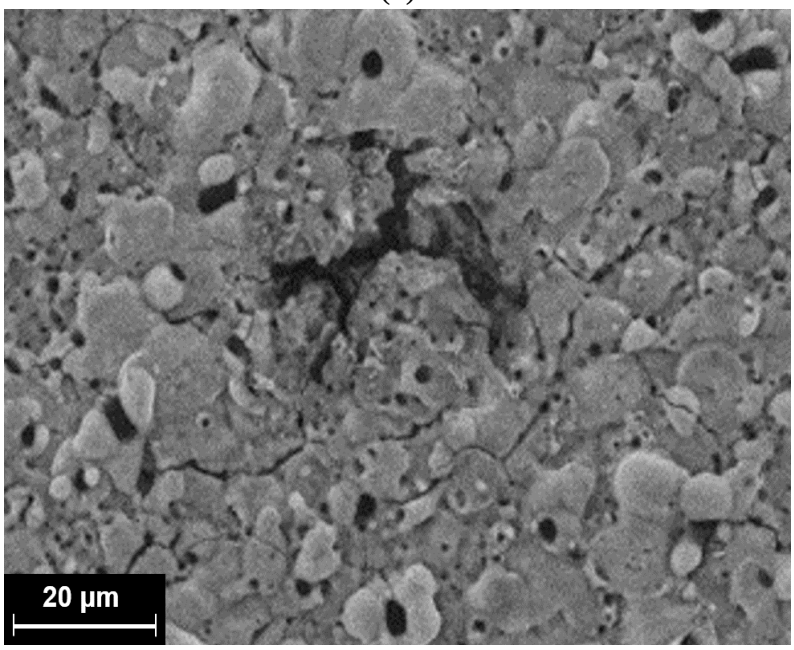

(c)

Fig. B.13. SEM micrographs in SE mode showing corroded surfaces of (a) PEO-AM60, and the (b) PEO-7FC and (c) PEO-MHNC-7F3NP composites.

VITA AUCTORIS

NAME:	Xinyu Geng
PLACE OF BIRTH:	Daqing, China
YEAR OF BIRTH:	1991
EDUCATION:	University of Windsor, B.Sc., Windsor, ON, 2015
	University of Windsor, M.Sc., Windsor, ON, 2019